University of Groningen
Discrete Technology & Production Automation

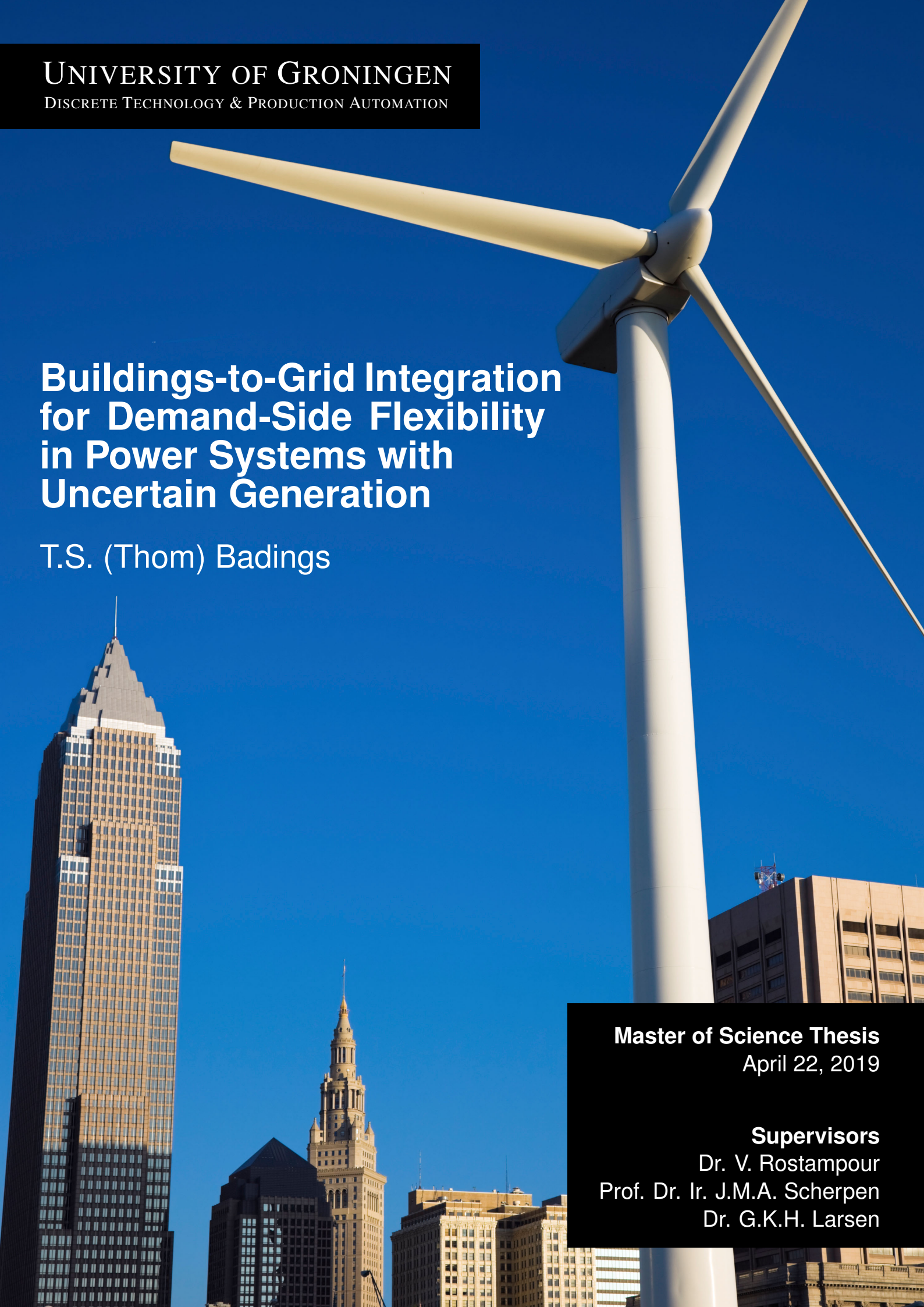

Buildings-to-Grid Integration for Demand-Side Flexibility in Power Systems with Uncertain Generation

T.S. (Thom) Badings

Master of Science Thesis
April 22, 2019

Supervisors
Dr. V. Rostampour
Prof. Dr. Ir. J.M.A. Scherpen
Dr. G.K.H. Larsen

Abstract

The increasing penetration of Renewable Energy Sources (RES) in power systems, such as wind and solar power, leads to uncertain behavior of the grid. The limited predictability of RES is traditionally compensated by scheduling reserves; deployment of electrical buffers to increase or decrease generator output. A promising alternative to reserve scheduling is the use of demand-side flexibility, or demand response. Advantages mentioned in literature include less environmental impact, lower costs, and increased building energy efficiency. Although demand response applications have been proposed widely before, almost no research has considered this problem explicitly, by integration of all dynamical systems within the scope of the power grid.

This work is, therefore, concerned with developing a unified framework with integrated grid and building dynamics, called Buildings-to-Grid (BtG) integration. The model integrates TSO, DSO and buildings with unified control decisions, and describes stakeholder interactions in the power system. Centralized, finite-horizon Model Predictive Control (MPC) problems are formulated, for holistic optimization of the BtG framework in three different simulation studies.

First of all, the potential role of individual buildings in frequency control of the power system is demonstrated, by utilizing their inherent thermal inertia, and introducing electrical storage units for demand-side flexibility. The simulation study shows that building-side storage flexibility has significant regulative capacity for the grid, and can decrease grid frequency deviations by up to 64.17%, by reducing power demand ramp up/down and minimizing load fluctuations.

Second, uncertain wind power generation is introduced in the BtG framework, and the deployment of demand-side flexibility is formulated explicitly. A method using the so-called randomization technique is employed to provide an approximated reformulation with probabilistic feasibility certificates for the proposed stochastic MPC. It is concluded that demand-side flexibility can substitute reserve scheduling in networks with wind power penetration of at least 20%. We successfully provide a-posteriori analyses based on Monte Carlo simulations, for a probabilistic certificate of the given solutions.

Finally, an operating model for consumer incentives for using solar power, and market model for consumer participation on the ancillary services market are developed, to capture the societal element in the BtG framework. Longer time simulations (7 days) are performed, and it is shown that societal elements can have a significant impact on the integration of RES and deployment of demand-side flexibility. However, it is stressed that the current model lacks a rigorous link with sociological or psychological theories, prohibiting the deduction of strong conclusions yet.

It is concluded that buildings can be a primary stakeholder in providing ancillary services to the future power grid. Demand-side flexibility can substitute traditional reserve scheduling, without losing stability of the grid and violating the building thermal comfort of occupants. Nevertheless, suggestions for further research include to embrace non-linear, AC grid modeling to increase accuracy, and a distributed MPC problem formulation to improve computational performance.

Table of Contents

Acknowledgements

This thesis is written for the Master of Science in Industrial Engineering and Management at the University of Groningen, and marks one of the final steps in completing the specialization of Smart Systems in Control and Automation.

First of all, I would like to express my gratitude to dr. Vahab Rostampour, who enthusiastically supervised and guided me throughout the whole project. His critical yet positive attitude, and the many, hours-long discussions that we have had really helped me in achieving the result that is currently in front of you. I look forward to continuing working with dr. Rostampour, in order to extend the results of the current thesis for the purpose of an academic journal article.

Furthermore, I would like to thank Prof. dr. ir. Jacquelien Scherpen for supervising me on my Master's thesis. Her guiding role as supervisor, and her extensive experience in the field of research helped me to structure my thesis, and often aided me in the research decisions that I have made.

Finally, special thanks go to dr. Gunn Larsen, for her role as secondary supervisor during the project. Her helpful feedback on intermediate presentations and reporting was very useful for improving both the content and coherence of my Master's thesis.

List of Figures

List of Tables

List of Acronyms

AC	Alternating Current
ADS	Active Distribution System
AGC	Automatic Generation Control
AGR	Aggregator
BLD	Building
BRP	Balance Responsible Party
BtG	Buildings-to-Grid
CCP	Chance Constrainted Program
CHP	Combined Heat and Power
DAE	Differential-Algebraic system of Equations
DC	Direct Current
DG	Distributed Generation
DNO	Distribution Network Operator
DSM	Demand Side Management
DSO	Distribution System Operator
GR	Generator
HVAC	Heating, Ventilation, and Air Conditioning
MPC	Model Predictive Control
OPF	Optimal Power Flow
PV	Photovoltaic
RES	Renewable Energy Sources
RCP	Robust Convex Program
SCP	Scenario Convex Program
TSO	Transmission System Operator

List of Symbols

α	Switching variable for sociological dynamics
$\mathbb{W}$	Bounded uncertainty set
β	Confidence level parameter
ΔP_w	Wind power error
δ	Bus voltage angle
$\dot{Q}$	Energy flow
ϵ	Violation level parameter
η	Electrical storage efficiency
Γ	Generator-TSO incidence matrix (entries γ)
$\hat{d}$	Frequency-sensitive uncontrollable load
$\hat{S}^{\text{id/dd}}_{\text{hvac/stor}}$	Estimated flexibility capacity
$\hat{S}^{\text{id/dd}}_{\text{potential}}$	Estimated potential flexibility capacity
$\mathcal{B}$	Set of buildings
$\mathcal{D}$	Set of DSO networks
$\mathcal{D}_i$	Set of DSO i nodes
$\mathcal{D}_l^{n,i}$	Neighborhood set of DSO i node l
$\mathcal{F}$	Set of wind farms
$\mathcal{G}$	Set of generators
$\mathcal{K}$	Set of MPC prediction time steps
$\mathcal{L}_d^i$	Set of DSO i transmission lines
$\mathcal{L}_t$	Set of TSO transmission lines
$\mathcal{N}$	Set of simulation time steps
$\mathcal{T}$	Set of TSO nodes
$\mathcal{T}_k^n$	Neighborhood set of TSO node k
$\mathcal{W}$	Unbounded uncertainty set
$\mathcal{X}$	Set of decision variables
P_{w_k}	Bounded vector of uncertainty over k steps
μ_{hvac}	HVAC coefficient of performance (COP)
ω	Bus angular velocity (frequency)
Φ	TSO-DSO i incidence matrix (entries ϕ)
Π^i	BLD-DSO i incidence matrix (entries π)
Ψ	Nonlinear swing equation term (entries ψ)
σ	Sociological weight of market model
τ	Sociological weight of operating model
PF	Power factor
Υ	Wind farm-TSO incidence matrix (entries υ)
ζ	Loss of power stored
B	Susceptance
C	Thermal capacity
c_h	Sociological model depletion factor
d	Damping coefficient
$d^{\text{up/down}}$	up/down-spinning distribution
G	Conductance
h	Simulation time step
J	Objective (cost) function
$L^{\text{min/max}}$	Transmission line limits
m	Moment of inertia
N^{MC}	Number of Monte Carlo tests
N^d	Number of decision variables
N_{sim}	Number of simulation time steps
n_b	Number of buildings
n_d^i	Number of DSO i nodes
n_g	Number of generators
N_s	Number of scenarios for scenario approach
N_s^j	Number of evaluations in estimated objective function
n_t	Number of TSO nodes
n_w	Number of wind farms
P	Active power flow
P^*	Optimal control power flow
P_{BD}	Building total power load
P^i_{BD}	Building power load from Distribution System Operator (DSO) i
P_{BL}	Base load
P_{GR}	Generator power production
P_{hvac}	HVAC power
P^i_{IMP}	TSO-DSO i power transmission matrix
P_{LD}	TSO power load

P^i_{LD}	DSO i power import
P_{misc}	Miscellaneous load
$P_{\text{pv,gen}}$	Solar power generation curve
P_{pv}	Solar power
P_{stor}	Power storage rate
P_{tot}	Total instantaneous building load
P_w	Actual wind power
P^f_w	Wind power forecast
Q	Reactive power flow (also cost matrix)
R	Reserve dispatch (also (thermal) resistance)
$R^{\text{us/ds}}$	Reserve scheduled (up-/down-spinning)
S	Flexibility dispatch (also apparent power)
s	Gear's method integration order
$S^{\text{id/dd}}$	Flexibility scheduled (increased-/decreased-demand)
S_{BD}	Building flexibility load
S_{hvac}	Building HVAC flexibility
S^i_{IMP}	TSO-DSO i flexibility transmission matrix
S_{LD}	TSO flexibility load
S^i_{LD}	DSO i flexibility import
S_{stor}	Building storage flexibility
T	Temperature
t	Time
T_{end}	MPC simulation end time
T_p	MPC prediction horizon
V	Voltage magnitude
X	Stacked state variable (also reactance)
x_b	Building state variable
x^i_d	DSO i state variable
x_h	Sociological state variable
x_s	Storage state variable
x_t	TSO state variable
Y	Admittance matrix
Z	Impedance matrix

1 Introduction

Cities attribute to approximately two-thirds of the global energy consumption, contributing to 71% of global direct energy-related greenhouse emissions (Swilling et al., 2013). In particular, buildings consume approximately 40% of the global energy, with half of this being directly related to building Heating, Ventilation, and Air Conditioning (HVAC) (Lawrence et al., 2016). According to Unicef (2012), by 2050, 70% of the world's population is bound to live in cities, with a yearly increase of the urban population by 60 million. It is, therefore, evident that energy demand in cities will further increase in the coming years, and that this transition can have big consequences for climate change.

At the same time, the United Nations (2015) has set sustainable development goals to combat climate change and its impacts, while simultaneously making cities resilient and sustainable. In particular, the European Union (2013) has set targets for its member states to achieve a 20% share of energy consumption from RES by 2020. Hence, accessibility and grid penetration of RES is a profound focus in achieving these goals. RES are found in centralized locations, such as industrial wind farms, but are also extensively generated in a distributed manner (Gill et al., 2014). As a result of the increasing deployment of this Distributed Generation (DG), distribution networks, being managed by Distribution Network Operators (DNOs), are becoming highly complex and active components of the power grid (Conte et al., 2017).

In their transition from passive networks to active components of the power systems, DNOs are rather referred to as DSOs (Saint-Pierre and Mancarella, 2017; USEF, 2015). Instead of passively managing a network with inflexible demand and only centralized supply, DSOs are expected to manage active distribution systems with high penetration of DG. Traditional DNOs use a 'fit-and-forget' strategy that resolves all issues upfront at the planning stage. However, the future DSO is expected to manage the system on-line on a rolling basis, as discussed by Saint-Pierre and Mancarella (2017). This requires the knowledge of DG forecasts, schedules and planned maintenance for the DSO. Today, DSOs miss a majority of this information, or are even bypassed by Transmission System Operator (TSO) at all (Eurelectric, 2013). For a resilient, sustainable power system, DSOs need monitoring, simulation tools and control strategies that allow them to act as active system operator of the future distribution network.

The 20/20/20 targets of the European Parliament (2012) have led to a notable increase in the share of RES in the European energy mix. For example in France, Photovoltaic (PV) and wind power installations have grown significantly, with average yearly growth rates of 58.8% and 12.4%, respectively, between 2010 and 2015 (Swaminathan, 2018). The majority of the new PV and wind power is generated in a decentralized manner, and the installations are connected to the distribution network, rather than the transmission network (Reinders et al., 2017). Voltage levels can vary significantly across a distribution network, and related problems are generally accentuated by the introduction of decentralized RES (Gill et al., 2014). In addition, the stochastic nature of PV and wind energy contributes to power imbalance in the power system, making

perfect control of the grid frequency difficult (Andersson, 2004). Consequently, DSOs have the inevitable task to engage in providing ancillary services to the power system, in order to secure grid frequency, voltage levels, and power balance (ENTSO-E, 2015).

One strategy to solve the aforementioned challenges posed by distribution grid constraints is the use of flexibility in the power system, for example by embedding Demand Side Management (DSM) (Eurelectric, 2013). DSM is defined as a wide array of methods to change the (consumer) energy demand profile in a beneficial way for the grid, while ensuring the same degree of customer satisfaction (Gellings, 2017). Embedding energy storage in the lower-level grid is one type of DSM that facilitates flexibility of the distribution network (Anwar et al., 2017a). La Bella et al. (2018) studied the design of aggregators in the management of the distribution system, consisting of an aggregated group of DG and consumers (buildings). Each aggregator is equipped with some type of energy storage, either at the level of the consumer or at the aggregated level. Aggregators can offer flexible ancillary services to both DSOs (for management of local constraints) and the TSO (for balancing of transmission line congestions) (Eurelectric, 2013).

As buildings are physically connected to the power grid, it is natural to develop a framework which explicitly couples buildings to the grid. Taha et al. (2019) developed a BtG integration framework, in which the power grid and building cluster control actions are explicitly coupled. Similarly, Anwar et al. (2017a) considered an integrated BtG model with thermal energy storage to allow for building participation in DSM. Both studies extend the research by La Bella et al. (2018) by further decomposing energy consumers into individual buildings, and explicitly coupling the building thermal model and its control actions to the power system.

To summarize, the increasing penetration of DG of RES requires a paradigm shift of the electrical power grid. Participation of DSOs as active system operators and involvement of aggregations of DG and consumers for offering flexibility can contribute significantly in the development of a resilient, sustainable power grid. This novel perspective on the power distribution network with increased TSO/DSOs/aggregator coordination is sometimes referred to as the Active Distribution System (ADS) (Eurelectric, 2013; Saint-Pierre and Mancarella, 2017). Finally, buildings can be coupled explicitly to the framework by embedding a BtG integration approach.

1.1 Research problem definition

As outlined in the previous section, various studies have addressed the future role of DSOs and more recently, authors have proposed BtG frameworks for more efficient power system control. However, little research has considered the complete future power system as a multi-layer hierarchical system, ranging from the TSO to explicit coupling of buildings.

In traditional power system models, the regulation of power grid frequency and voltage profile is achieved through scheduling and control of active and reactive power generation (Conejo and Baringo, 2018). On the contrary, buildings decisions are typically only optimized locally to minimize energy consumption (Rostampour and Keviczky, 2017, 2018), but not in the bigger scope of optimal control of the distribution system or even the general power system. The

exclusion of building dynamics in the decision-making makes it impossible to develop optimal control strategies that take full advantage of building-side flexibility and their inherent thermal inertia (Beil et al., 2016; Lymperopoulos et al., 2015). Traditionally, buildings decisions are only optimized locally to minimize energy consumption, but not in the bigger scope of optimal control of the distribution system or even the general power system. As a result, insight in the potential contribution of buildings to the regulation of the grid is limited, which leads to the following problem statement;

Problem definition: *Current insight in the potential role of buildings in the regulation and control of multi-layer power systems with high penetration of Renewable Energy Sources (RES), is limited.*

This research project aims to solve the problem introduced above. First of all, Section 1.2 provides a thorough literature study, extending the overview provided in the current chapter. The contributions and limitations of available case studies are discussed, revealing promising gaps in the current body of knowledge on the subject. The survey is concluded in Section 1.3 with a list of gaps in the current literature, which provides the basis for the research contributions and research goal. Corresponding research questions are posed in Section 1.4. Finally, the remainder of the thesis structure is outlined in Section 1.5.

1.2 Literature Review on Power System Analysis

In the current section, a review of the current literature on power system dynamics and the potential for building-integrated frameworks is provided, with the goal to highlight gaps in the current body of knowledge. First of all, a description of the general power system is provided in subsection 1.2.1, while the stakeholders participating in the power system market are discussed in subsection 1.2.2. General ancillary services provided in the power system industry are described in subsection 1.2.3. The interface between TSO and DSOs is introduced in subsection 1.2.4, to discuss the difference between both networks, and why it is relevant to model the two entities separately. The integration of building models in the power grid dynamics (the formerly introduced Buildings-to-Grid (BtG) approach) is discussed in subsection 1.2.5. Finally, an overview of related case studies is provided in subsection 1.2.6, which is used to provide current open issues in Section 1.3.

1.2.1 General structure of the power system

The physical layer of the power system consists of four subsystems, namely: (1) *generation*, (2) *transmission*, (3) *distribution*, and (4) *supply* (Conejo and Baringo, 2018). All layers are operated at different nominal voltage level, and are physically connected by means of transformers, as depicted in Figure 1.1. To minimize power losses, transmission networks in Europe are generally operated at voltages of 225 or $400\,\mathrm{kV}$ (Swaminathan, 2018). Continental transmission networks are almost universally operated at Alternating Current (AC), although a few oversea Direct Current (DC) transmission lines exist in Europe as well (Siemens, 2011). Power production is mostly done by synchronous generators (Machowski et al., 2008), that produce electrical

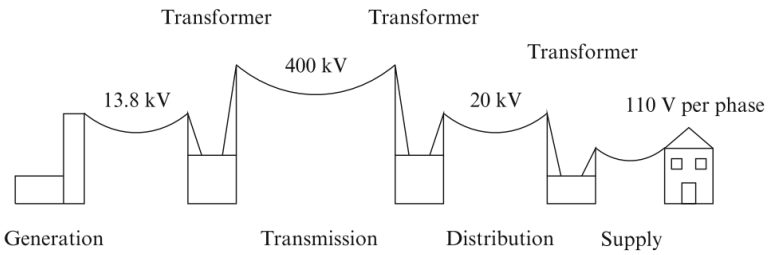

Figure 1.1: Physical layer of the power system (Conejo and Baringo, 2018).

energy at a voltage around 14 kV, which is directed to a step-up transformer to match the higher voltage of the transmission network (Conejo and Baringo, 2018). The transmission network is usually a meshed network, and is typically operated by one monopoly company in a country, referred to as the Transmission System Operator (TSO).

Contrary to the monopoly of the TSO, the distribution network of a country is generally operated by multiple Distribution System Operators (DSOs), typically operating around 20 kV (Conejo and Baringo, 2018). Typically, each DSO operates in a fixed geographical region of a country. Distribution networks are radially shaped for protection purposes, and were traditionally passive systems, as power flow was unidirectional towards the consumer (Machowski et al., 2008). However, emerging RES installations in the DSO network have led to fundamental changes in the network requirements (Swaminathan, 2018). Because RES, such as solar and wind power, are mainly generated decentralized, power flows from the distribution to the transmission networks will increase significantly in the near future (Reinders et al., 2017).

Power balance in each subsystem of the power system is a prerequisite to preserve the grid frequency (Trip et al., 2016). Due to the stochastic nature (Mirakhorli and Dong, 2016), exactly predicting consumer power demand and power generation by RES (such as wind and solar energy) is practically impossible. Furthermore, the current power system is primarily designed for downstream power flow, yielding network security issues if local generation by RES is too high. Consequently, providing frequency response services is an important operation in power system operations (Molder et al., 1996). As discussed in subsection 1.2.3, regulatory mechanisms like that of frequency response services in the power system are referred to as ancillary services.

1.2.2 Stakeholders in the power system market

According to Freeman (2010), a stakeholder is *"any group or individual who can affect or is affected by the achievement of the organization's objective."* In the scope of the power system, this *organization* entails the power system market. From the discussion above, it is evident that **TSO**, **DSO** and **consumers** are primary stakeholders in the power system market. In addition, USEF (2015) also identifies the Balance Responsible Party (BRP), and **aggregators** as stakeholders of the system. However, in the scope of the current study, the TSO also plays the role of the BRP, and thus, only the aggregator is adopted as additional stakeholder.

In an active distribution system, aggregators accumulate flexibility offered by individual pro-

sumers, and sell it to provide ancillary services to TSO, DSO and suppliers. Eurelectric (2014) considers flexibility as the modification of power generation and/or consumption in response to an external signal, with the main purpose to provide ancillary services within the power system. Aggregators can provide reliable flexibility to system operators because they do not rely on the resources of individual prosumers. At the same time, they protect individual participants from the risks and liabilities involved in the ancillary service market (USEF, 2015). The aggregator purchases flexibility from contracted prosumers and sells it on the electricity market, where they compete with each other (Swaminathan, 2018)

1.2.3 Ancillary services

The United States Federal Energy Regulatory Commission (FERC) defines ancillary as services necessary to support electricity transmission from seller to purchaser, while complying to obligations of control areas and transmitting utilities (FERC, 2018). Ancillary services are provided by the different stakeholders in the power system market, and are crucial to support the basic services of power delivery generating capacity (Kirby et al., 1995; Molder et al., 1996). Because they rely on active power contributions from a providing entity, some types of ancillary services can also be provided by consumers (Blum, 2016). In the following sections, the primary types of ancillary services are briefly introduced.

Active power supply and frequency response services

The grid frequency is regulated by the injection or withdrawal of active power in response to a control dispatch signal of the TSO or DSO (Papalexopoulos and Andrianesis, 2014). Although the TSO schedules power generation to secure grid stability, actual power dispatch can deviate, due to uncertainty or deviations in both demand and generation (BPA, 2014). Frequency response services are provided by certified partners, and pursue to maintain the grid frequency by instantaneously balancing power supply and demand (Macdonald et al., 2012). Resources that provide energy imbalance services charge a tariff for the product, incentifying the TSO to forecast the power demand more accurately (Wan et al., 2007). By providing the TSO with partial control over consumer loads via aggregators (typically by offering demand-side flexibility services), grid frequency can also be stabilized (Razmara et al., 2017a). Although similar to spinning reserve, frequency regulation is a faster response to grid frequency deviations (Corbin et al., 2016).

Spinning and supplemental reserve services

Spinning reserve is the unused capacity which can be activated by the TSO or DSO to affect the active power in the network (Rebours and Kirschen, 2005). Spinning reserve is already connected to the grid, but not loaded yet, and can be delivered within 10 minutes (Macdonald et al., 2012). Certain loads can stabilize the grid frequency around its nominal value, with the so-called *droop frequency* quantifying the strength of this effect (Andersson, 2004). To secure the grid frequency and quality of power supply, every entity in the power system should have adequate spinning reserve scheduled. If spinning reserve is not sufficient to restore the grid

frequency, supplemental reserves are required, e.g. at permanent outages. In general, supplemental reserves are to be delivered within 30 minutes, and are, in most countries, controlled automatically by the so-called Automatic Generation Control (AGC) (Macdonald et al., 2012).

Reactive power supply and voltage control services

In most countries, the reactive power market is embedded in an independent market, separated from that for active power (Rabiee et al., 2009). Active power flow itself typically causes losses of reactive power, and the reactive power market is responsible to compensate for these losses (Ahmadimanesh and Kalantar, 2017). Voltage regulation is closely related to reactive power management (Chung et al., 2004; Qin, 2018). Inductance of transmission lines (rather than resistance) is the primary cause of voltage drops, which can be prevented by supplying reactive power (Hirst and Kirby, 1996). Hence, appropriate balance between supply and demand of reactive power is required to secure voltage stability.

1.2.4 TSO/DSO interaction in power grid models

During the last decade, the TSO/DSO interface experienced significant changes, accentuating the need to redefine the responsibilities of both parties. However, based on interviews with grid operators and industry experts, the EAC (2018) concluded that there is no clear holistic definition for the future TSO/DSO interface, thus highlighting the relevance of the current discussion.

Traditionally, DSOs were passive network operators, whereas the TSO was primarily responsible for grid regulation, by procuring ancillary services from large power producers (Macdonald et al., 2012). However, the increasing penetration of RES in distribution networks tends to result in more extensive participation of DSOs on the ancillary services market (Eurelectric, 2013).

In most countries, the transformer at the TSO/DSO interface is still operated by the TSO, but Zegers and Brunner (2014) suggested that it is beneficial for future grid security to shift this responsibility to the DSO. By letting the DSO control the transformer, no ad hoc communication with the TSO is needed for every congestion, and the DSO can decide to take local measures itself. In addition, power generation is shifted from controllable centralized production in the TSO network, towards uncontrollable generation by RES at consumers or in the DSO network (Reinders et al., 2017). Giving DSOs more direct control over the distribution system and the TSO/DSO interface is important to optimally harvest these intermittent energy sources (ENTSO-E, 2015).

Although TSO and DSO are physically coupled in an interconnected system, they are often unwilling to share commercially sensitive data with each other in the scope of commercial incentives (Mohammadi et al., 2018). At the same time, it is recognized that increased data sharing is required to facilitate a resilient power system in the future (EAC, 2018; Reinders et al., 2017). Thus, it is important to consider not only the physical, but also the informational aspect towards the new definition of the TSO/DSO interface.

To summarize, multiple reasons are apparent why it is beneficial to distinguish between TSO and DSO in power dynamics. First of all, the TSO network tends to be meshed, whereas the dis-

tribution network is radially shaped. Furthermore, embedding the multi-level approach allows for explicit investigation of alternative approaches with increased TSO/DSOs/market coordination, and enhanced utilization of flexibility in the distribution network introduced by DG and other resources (Saint-Pierre and Mancarella, 2017). Finally, as DSOs tend to be commercial companies, they are generally unwilling to share sensitive data. Distinction between the two operators in research allows to model privacy-related issues appropriately.

1.2.5 Integration of building thermal dynamics in the power grid

Traditional power system research considered buildings power demand as deterministic loads, which are available through past experiences or other load models (Rene, 2016). However, adopting a holistic approach with interconnected decision-making between buildings and system operators, the so-called *Buildings-to-Grid (BtG) approach*, can open new potential ways to provide ancillary services to the grid from a bottom-up perspective.

Instead of treating the power demand as deterministic loads, BtG approaches aim to consider the control decisions of buildings in the optimization process (Taha et al., 2019). BtG approaches allow the development of control strategies that utilize all available flexibility and controllable resources in an optimal way (Short et al., 2007). Furthermore, it allows better utilization of distributed RES, as consumers can participate in providing ancillary services, which can even result in superior responses to conventional generators (Ma et al., 2013).

In the absence of active storage elements, the thermal inertia and the corresponding HVAC control decisions of a building provide a primary asset for demand response (Pavlak et al., 2014). Although constrained by allowable indoor temperature levels, the thermal mass of buildings can be used as temporary energy buffer that can be used for grid optimization purposes (Beil et al., 2016).

Traditional resistance and capacitor (RC) networks are widely used to model thermodynamics of building envelopes (Blum, 2016). The building to be modeled is divided in a number of lumped thermal zones (characterized by capacitors) surrounded by resistive elements (modeled as resistors), for which dynamics are provided. RC building models are typically represented in first order state-space representation, with inputs comprised of electrical or thermal interaction with the environment or power grid (Yahiaoui et al., 1996).

Taha et al. (2019) proposed a 3R-2C model to represent building dynamics as two distinct zones; one for the wall and one for the room temperature. In a follow-up study by the same authors, a similar model was utilized, adding occupancy-based constraints to enhance accuracy (Dong et al., 2018). Although a tight model formulation with small number of zones has computational benefits, it can also come at the cost of inaccurate results due to over-aggregation of the building dynamics.

More detailed building thermal models have been developed as well for similar purposes (Dong, 2010; Razmara et al., 2018). These detailed models result in highly accurate simulation results compared to reality (Danza et al., 2016), but also require significantly higher computational resources. It remains, therefore, questionable what level of detail is required to model building

thermodynamics with sufficient accuracy. In general, simple 3R-2C models are preferred if the purpose of the study is to simulate large clusters with hundreds or even thousands of building (Taha et al., 2019). On the contrary, more detailed models are adopted in case of specific simulation of an individual building.

1.2.6 Overview of modeling and simulation studies

In this section, simulation studies found in the current literature are listed. Classification criteria for the simulation studies are listed. Then, the complete overview of studies is provided in Table 1.1. A similar, but more detailed review of power flow studies applied to smart grids and microgrids was published by Abdi et al. (2017). The authors compared 29 case studies in great detail, on elements including the type of constraints, objective functions, grid modeling techniques, control strategies, and computational performance. Although such a detailed review is outside the scope of the current section, the interested reader is referred to the corresponding review article (Abdi et al., 2017).

Modeling perspective

First of all, studies are distinguished based on the main perspective that was adopted. From the preceding discussion, four main perspectives were identified. A research project is either focused on the **TSO**, **DSO**, **Buildings (BLDs)**, **Aggregator (AGR)**, or a **combination** of these perspectives. Generally, the specific perspective of a simulation study is closely related to its goal. TSO- and DSO-oriented studies typically focus on optimizing grid operations, whereas studies from the buildings perspective tend to minimize costs or energy imported from the grid.

Modeling elements

Secondly, studies are categorized according to the elements that the model comprises. Modeling elements can either be deterministic or stochastic. Deterministic elements include **thermal** and **electrical storage**, **μ-Combined Heat and Power (CHP)**, **HVAC** and other **appliances**. On the contrary, stochastic elements include most (distributed) RES, such as **wind** and **PV** power, and **uncertain loads** in general.

Optimization approach

A significant number of studies use a **MPC** approach to solve the optimization problem. More information about MPC is found in the preliminaries in Section 2.4. **Optimal Power Flow (OPF)** considers the optimal dispatch of power in a network, given certain boundary conditions, and is often used in combination with a MPC approach. **Direct optimization** entails one-step optimization of a problem, and is in fact the same as a MPC approach without the receding horizon. Some studies propose **multi-step optimization** procedures to solve the problem to be solved. Finally, some authors apply **multilevel optimization**, to optimize holistic models that span over multiple hierarchical levels.

Table 1.1: Overview of modeling and simulation studies

#	Authors	Perspective	Elements	Approach	Remarks
1	Taha et al. (2019)	TSO, BLD	HVAC	Centralized MPC	Considers OPF and frequency control in a BtG framework. Main contribution is the mathematical BtG framework, with explicit TSO-BLD integration.
2	Dong et al. (2018)	TSO, BLD	HVAC	Centralized MPC	Extends the previous study by integrating occupancy-based building dynamics in the BtG framework
3	Anwar et al. (2017b)	TSO, BLD	Thermal storage	Direct optimization	Considers thermal storage in a BtG framework to provide flexibility to the grid. However, perfect forecast is assumed, i.e. no uncertainty is modeled.
4	Mohammadi et al. (2018)	TSO, DSO		Decentralized OPF (TSO and DSO decoupled)	Focuses on the interface between TSO and DSO. Proposes decentralized solution for collaborative TSO-DSO OPF, based on a hierarchical model.
5	La Bella et al. (2018)	TSO, AGR	Electrical storage	Multi-step optimization	Focuses on aggregators for providing active and reactive ancillary services. Aggregators are proposed as alternative to generator reserves.
6	Trip et al. (2016)	TSO	Uncertain load	Internal model controller using incremental passivity	Studies analytical frequency regulation in microgrids, and how the OPF problem is solved for uncertain, time-varying power demand.
7	Jiang et al. (2018)	DSO, BLD, AGR	HVAC	Nonlinear OPF	Solves the OPF of a branch flow model distribution network with aggregated dynamics of 5 buildings. The OPF is solved by piecewise linearization and second order relaxation.
8	Nguyen et al. (2017)	DSO, BLD, AGR		Multilevel distributed control (aggregator and building level)	Uses explicit flexibility definitions for aggregated consumers to participate in providing ancillary services. Primary focus on distributed optimal control and congestion management for DSO

9	Razmara et al. (2017b)	DSO, BLD	HVAC, electrical storage, PV	Centralized MPC	Develops a BtG framework integrated with distributed PV power and electrical storage, to enable consumer participation in DSM, resulting in significantly reduced grid load ramp up and down.
10	Short et al. (2007)	DSO, BLD	Wind, Appliances	Dynamic control of refrigerator	Stabilization of local grid frequency through demand control of appliances. Models local grid frequency near the appliance using aggregate inertia, but excludes the rest of the distribution network.
11	Bharati et al. (2016)	DSO, BLD	HVAC	Multilevel control (grid and building level)	Distributed OPF is combined with integrated building dynamics to minimize losses in the distribution system, and minimize energy costs of building loads.
12	Liu et al. (2018)	BLD, DSO	HVAC	Multilevel optimization (Distributed MPC at building level, plus DSO network constraints)	Assesses the hierarchical relation of TSO, DSO and BLD. A bi-level approach to optimize building operations in a distributed manner, while satisfying DSO constraints, such as line limits and phase imbalance.
13	Gržanić et al. (2018)	DSO, AGR	Electrical storage	Multilevel control (grid and aggregator level)	Studies how distributed electrical storage owned by consumers or aggregators can be contracted by DSO as a source of flexible resources. Applies OPF bidding strategy for contracting the right to use the battery in case of potential grid constraint violation.
14	Saint-Pierre and Mancarella (2017)	DSO	Wind power, electrical storage	AC nonlinear OPF	A dual-horizon rolling scheduling model based on dynamic AC OPF is proposed to optimize distribution network operations. Energy import from TSO to DSO is minimized in the objective. Primary focus on integration of uncertainty from wind power.

15	Larsen et al. (2014a)	BLD	Thermal storage, μ-CHP	Distributed MPC	Has the main goal to balance heat demand locally, while balancing power balance for a larger network. The main contribution is the use of an information network, which enables a fully distributed MPC approach, which only required local information at the building level to solve the problem.
16	Lin et al. (2017)	BLD	HVAC	Multilevel control (building and ancillary service level)	Studies how demand scheduling of building HVAC can provide ancillary services to a power grid with significant power variations. Gives explicit definition of building ancillary service (flexibility) capacity, but does not include grid dynamics.
17	Pavlak et al. (2014)	BLD	HVAC	MPC (at individual building level)	Frequency regulation capacity of office buildings is estimated, and a MPC framework is applied to optimize building operations, considering energy costs, demand penalties, and regulation revenues (the latter two reflect building-side flexibility).

1.3 Open issues and research contributions

Using the literature review of the preceding section, open issues are highlighted, and the research motivation of the current study is positioned. Based on the literature review, it is evident that the following aspects, or combinations of them, deserve more attention in research:

- Development of a holistic BtG integrated framework with explicit TSO/DSOs/BLDs dynamics, and integrated building HVAC control decisions;
- Investigation of the effect of high penetration of uncertain RES (such as wind power) on the network stability of a BtG integrated framework;
- Study of alternative control strategies to deal with the stochastic nature of RES, by enabling consumers to deliver ancillary services in the form of building-side flexibility;
- Studying the sociological impact of enabling consumer participation on the ancillary services market.

As discussed in subsection 1.2.1, power systems are multi-layer systems, that need to be modelled in a holistic manner, in order to optimally exploit all flexibility and control freedom. Although some authors considered either TSO/BLDs or TSO/DSOs systems, none of the current studies have developed a fully dynamic TSO/DSOs/BLDs framework. Decision-making is further unified by explicitly defining HVAC control decisions. Although some studies incorporates explicit building dynamics in the BtG approach (Dong et al., 2018; Taha et al., 2019), none of these studies has considered uncertain generation from wind power in a holistic, multi-layer framework. Hence, the first main contribution of this thesis is to develop a holistic power system framework with integrated dynamics between TSO/DSOs/BLDs, with high wind power penetration.

The second contribution of the thesis is to deal with the stochastic nature of power systems with high penetration of RES. Based on discretized dynamics of the BtG framework, a centralized MPC procedure is developed to optimize decision variables over all layers of the system, while also dealing with highly uncertain generation. We use a method based on the so-called randomization technique to deal with the uncertainty of wind power in the MPC, and provide a-posteriori analyses based on Monte Carlo simulations, to provide a probabilistic certificate for the performance of the system.

Third, we propose the deployment of building-side flexibility as an alternative means of compensating for the uncertainty in the wind power forecast. As depicted in Figure 1.2a, generator reserves are traditionally deployed to account for uncertainty in power demand (Rostampour et al., 2019c). In systems with high penetration of RES, higher reserve buffers are required, to also account for the uncertainty of wind power (Halamay et al., 2011), as shown in Figure 1.2b. By deploying building-side (demand-side) flexibility, traditional reserve usage is minimized, as visualized in Figure 1.2c. Flexibility elements are controllable components that introduce flexibility in the power system, such as flexible appliances (e.g. HVAC systems and μ-CHP units) and storage systems. We study the potential role of individual buildings in providing ancillary services to the power system, by introducing distributed electrical energy storage units, and en-

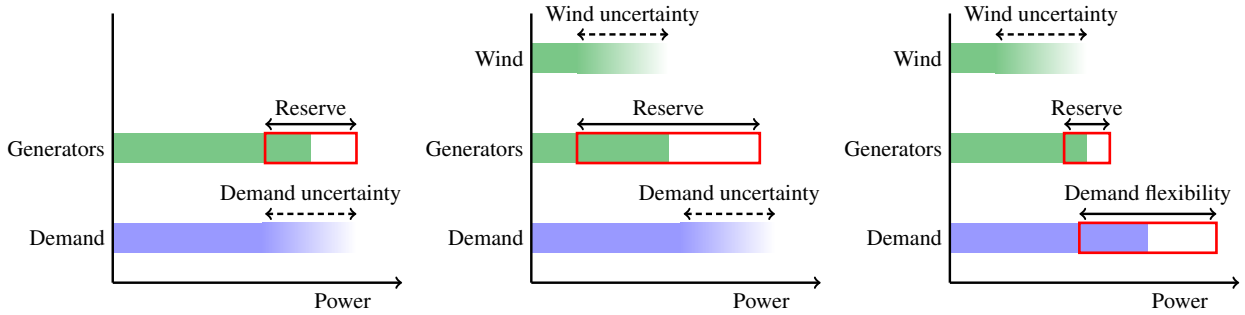

(a) Traditional reserve scheduling (b) High wind power penetration (c) Demand flexibility deployment

Figure 1.2: Power system with traditional reserve scheduling (a) compared to system with high wind power penetration (b) and power system with demand (building-side) flexibility deployment (c). Flexibility scheduling compensates for uncertainty in demand and wind power, resulting in lower reserve scheduling requirements.

abling holistic decision-making with grid operators. The electrification of transportation evokes a growing base of distributed storage in the coming years (Lamadrid et al., 2011). For example, in Futumata, Japan, a 34 MW electrical storage battery supports a 51 MW wind farm (NGK, 2008). Multiple simulation studies have also verified the benefits of coupling battery storage to PV and wind power (Bragard et al., 2010; Riffonneau et al., 2011). In general, advantages of demand-side flexibility may include less environmental impact (Lin et al., 2015), lower costs (Lymperopoulos et al., 2015), superior grid stabilization responses (Ma et al., 2013), and increased building energy efficiency (Kiliccote et al., 2011).

Finally, we discuss the sociological impact of enabling consumer participation on the ancillary services market. Current studies typically assume perfect collaboration between consumers (buildings) and grid operators. In reality, consumers are not readily intrinsically motivated to contributed to grid operation control. By introducing explicit dynamics for the sociological impact, we develop a basic framework that embeds the social factor of consumers as stakeholders, which allows research from a more socio-technical point of view.

The main objectives of the current study are summarized in the following research goal;

Research goal: *To develop a holistic power system framework with integrated TSO/DSOs/BLDs dynamics, and to use this framework to explore the potential role of buildings on the regulation and control of power systems with high penetration of Renewable Energy Sources (RES).*

1.4 Research questions

In order to achieve the research goal posed above in a structural manner, research objectives are developed. Within the class of research objectives, Wieringa (2014) distinguishes between design questions and knowledge questions. Design questions are in fact design problems that

aim to design or redesign an artifact (defined as *something created by people for some practical purpose*) so that it better contributes to the achievement of some goal. Knowledge questions aim to acquire knowledge about some field of research, without the need for improvement of an artifact. The design problems and knowledge questions to be answered in the remainder of this research project are as follows;

1. What are the mathematical tools required to develop the models in this thesis?
   This knowledge question provides the mathematical preliminaries required for the subsequent questions.
2. How will the framework with integrated TSO/DSOs/BLDs dynamics be modeled?
   This design question provides the mathematical power system framework with integrated BtG dynamics.
3. How will the optimization model of the developed power system framework be formulated?
   This design question provides the formulation of the optimization model of the developed power system framework.
4. How will the developed framework be extended with uncertain power generation of RES?
   This design question extends the power system framework with the stochastic element of uncertain power generation.
5. How will the optimization model of the framework with uncertain generation be formulated, and how will the stochastic aspect be embedded?
   This design question provides the optimization model for the framework with uncertain generation, and presents a method to deal with its stochastic nature.
6. How will the sociological impact of consumer participation on the ancillary services market be embedded in the developed framework?
   This design question integrates the social factor in the developed framework with uncertain generation.
7. What case studies will be used to validate the different optimization model formulations?
   This design question is applicable after any optimization model (re)formulation, and will therefore be answered at the end of every main chapter of the thesis.
8. What conclusions can be drawn from the results of the case studies?
   This knowledge question determines the main conclusions of the thesis, in order to add knowledge to the existing literature, while also discussing current limitations and potential areas for further work.

1.5 Thesis outline

The research questions posed above are generally answered in numerical order throughout the thesis. However, *research question 7* is relevant after each optimization model (re)formulation, and is therefore considered at the end of every main chapter.

First of all, Chapter 2 (addressing *research question 1*) provides the mathematical preliminaries for the remainder of the thesis. This chapter provides the mathematical tools and equations used in models developed in subsequent chapters, but could be skipped by the experienced reader.

In Chapter 3 (*research questions 2 and 3*), a dynamic BtG framework with fully deterministic power generation is developed, and used to formulate a discrete, centralized MPC optimization procedure. The centralized procedure, referred to as BtG-MPC, is proposed to optimize grid and building operations in the holistic power system framework, by combining the control actions at grid and building level.

In Chapter 4 (*research questions 4 and 5*), the developed BtG-MPC is extended, by considering uncertain generation from wind power. This modification accounts for the increasing penetration of RES in the sub-transmission network. A centralized controller, referred to as w-BtG-MPC, is proposed for holistic optimization of grid and building operations for the power system, while considering realistic wind power scenarios, and taking the wind power prediction error into account.

In Chapter 5 (*research questions 6*), the sociological aspect of consumer participation on the ancillary services market is discussed. An extended version of the optimization framework with uncertain generation is formulated, to model the intrinsic motivation of consumers.

The thesis is concluded by discussing limitations of the current research project and highlighting potential areas for further work in Chapter 6. Finally, *research question 8* is addressed in Chapter 7, in which concluding remarks are provided.

2 Preliminaries

In this chapter, a theoretical background on power system dynamics is presented, providing the required preliminaries to the subsequent chapters. The chapter could be skipped by the experienced reader, but describes the majority of theoretical concepts applied in the remainder of the thesis.

2.1 Notations

Throughout the thesis, $\mathbb{N}$ and $\mathbb{R}$ denote the set of natural and real numbers, respectively. Furthermore, $\mathbb{1}_n \in \mathbb{R}^{n\times 1}$ denotes a column vector of ones, I_n an identity matrix of size n, $\mathbb{0}_{n\times m}$ the n by m zeros matrix, and $\circ$ the Hadamard (entrywise) product. Calligraphic letters $\mathcal{A}$ are reserved for sets, and the corresponding cardinality of that set is denoted by $|\mathcal{A}|$.

2.2 Graph theory

In network theory, an undirected graph is defined as $\mathcal{G} = (\mathcal{V}, \mathcal{E})$ and consists of a set of $\mathcal{V} = \{1, ..., n_v\}$ nodes and $\mathcal{E} = \{1, ..., n_e\}$ edges (Mesbahi and Egerstedt, 2010). The neighborhood of node i is denoted by the set $\mathcal{V}_i^n \subseteq \mathcal{V}$, and consists of all nodes directly connected to that node i.

The positive incidence matrix of a graph consisting of $\mathcal{V} \in \mathbb{R}^n$ and $\mathcal{E} \in \mathbb{R}^m$ relates nodes to their connected edges (Bullo, 2018). The incidence matrix $D \in \mathbb{R}^{n\times m}$ with elements $D_{i,j}$ is defined as

$$d_{i,j} = \begin{cases} 1 & \text{if node } i \text{ is connected to edge } j \\ 0 & \text{otherwise.} \end{cases} \tag{2.1}$$

Similarly, the incidence matrix can relate two sets of nodes to each other, without explicitly defining the set of edges between them. Let $\mathcal{A} \in \mathbb{R}^n$ and $\mathcal{B} \in \mathbb{R}^m$ be two sets of nodes, and let $\Pi \in \mathbb{R}^{n\times m}$ be the incidence matrix, with entries $\pi_{i,j}$ defined by

$$\pi_{i,j} = \begin{cases} 1 & \text{if node } i \text{ of } \mathcal{A} \text{ is connected to node } j \text{ of } \mathcal{B} \\ 0 & \text{otherwise.} \end{cases} \tag{2.2}$$

In this research, the resulting incidence matrix Π is utilized to model power flows or communication between sets $\mathcal{A}$ and $\mathcal{B}$.

2.3 Power flow theory

In this section, a background in power flow theory is provided. First of all, the concepts of active and reactive power flow, and their relation to AC and DC power flow study, respectively, are discussed. The AC power flow equations are introduced, and the general DC power flow assumptions are derived. Finally, the DC swing equation for power flow analysis is introduced, which is extensively used in Chapter 3 - 5.

2.3.1 Active and reactive power flow

In DC systems, power transmission is denoted by the product of voltage and current. The instantaneous power flow between two nodes in a circuit is the actual power exchanged at that specific moment in time (Conejo and Baringo, 2018). Tellegen's theorem of power conservation states that the sum of the instantaneous power over all branches of a system is zero at any instant (Kwatny and Miu-Miller, 2016). As voltage in a DC circuit does not oscillate and is constant over time, instantaneous power flow is also constant, and is equal to the **active (or real) power** flow, indicated by P.

In AC systems, instantaneous power flow is not constant, because voltage oscillates over time with a specific frequency. In general, the DC relation between power, voltage and current does not hold for AC systems. Often, voltage and current in AC systems are not in phase, resulting in the generation of **reactive (or imaginary) power**, indicated by Q. Reactive power helps to establish and sustain the electric and magnetic field in AC circuits, but does not do electrical work (Kwatny and Miu-Miller, 2016). In AC systems, **complex power**, indicated by S, is defined as the sum of its real and imaginary parts:

$$S = P + jQ. \tag{2.3}$$

Similarly, the apparent power $|S|$ is defined as the absolute value of the complex power:

$$|S| = \sqrt{P^2 + Q^2}. \tag{2.4}$$

Finally, the power factor, PF, is defined as the ratio of active and apparent power:

$$\text{PF} = \cos\theta = \frac{P}{|S|}, \tag{2.5}$$

where θ is the angle between active and reactive power, as indicated in Figure 2.1. A power factor of one means that power flow is purely active, whereas a low value relates to a large portion of reactive power. The power factor is widely used to express how much of the apparent power contributes transfer of useful energy to the load (active power), and how much supports oscillations and system stability (reactive power) (Kirby et al., 1995).

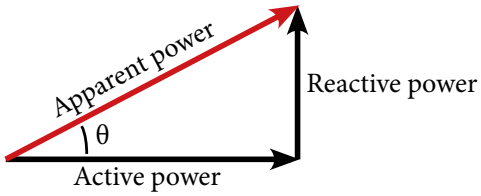

Figure 2.1: Geometric relation between active, reactive and apparent power.

In power system analysis, reactive power control is particularly important in long-distance transmission networks. As transmission lines and transformers generally exhibit high inductance, reactive power flow significantly more difficult through the network than active power does (Hirst and Kirby, 1996). Hence, reactive power ancillary services must be provided much closer to the source of problems than similar active power services. The transmission of reactive power results in increased demand in the grid branches, causing voltage violations and extra losses (Qin, 2018).

Although reactive power presents is highly relevant for power system stability, the current study is limited to active power. As discussed in subsection 2.3.3, power flow analysis in this study is, therefore, simplified through the DC power flow approximation.

2.3.2 AC power flow equations

Given a transmission line between two nodes k and j in a power grid, both the active and reactive power flow depend on the voltages V at the two ends, and the angle difference between the bus voltages. In particular, the power transmitted from node k to node j is given by the following equations (Qin, 2018; Saint-Pierre and Mancarella, 2017):

$$P_f(t) = V_k V_j \Big[G_{k,j} \cos(\delta_k(t) - \delta_j(t)) + B_{k,j} \sin(\delta_k(t) - \delta_j(t)) \Big] \tag{2.6a}$$

$$Q_f(t) = V_k V_j \Big[G_{k,j} \sin(\delta_k(t) - \delta_j(t)) - B_{k,j} \cos(\delta_k(t) - \delta_j(t)) \Big], \tag{2.6b}$$

where $P_f(t)$ and $Q_f(t)$ are the active and reactive power flow, V_k and V_j are the voltages at the ends of the transmission line, and δ_k and δ_j are the voltage angles. Furthermore, $G_{k,j}$ and $B_{k,j}$ are the conductance and susceptance values of the line, which are related to the admittance Y via

$$Y = G + jB, \tag{2.7}$$

i.e. conductance is the real part of admittance, and susceptance is the imaginary part. An interesting quantity in power transmission systems is the X/R ratio, defined as the ratio between the

system reactance X to the system resistance R. The impedance Z, which is the inverse of the admittance, is the sum of resistance R, and its imaginary part reactance X:

$$Z = R + jX = \frac{1}{Y}. \tag{2.8}$$

Conversely, this yields

$$Y = \frac{1}{R+jX} = \frac{R-jX}{R^2+X^2} = \frac{R}{R^2+X^2} - \frac{jX}{R^2+X^2} = G + jB, \tag{2.9a}$$

$$G = \frac{R}{R^2+X^2}, \qquad B = -\frac{X}{R^2+X^2}. \tag{2.9b}$$

For typical transmission lines, $X \gg R$, as they span relatively large distances, whereas for lines in a distribution network the opposite is true (McCalley, 2012). In distribution networks, resistance effects are more apparent than at the transmission level, changing the X/R ratio from typically 10 in transmission networks to 2 for distribution networks (Machowski et al., 2008).

2.3.3 DC power flow approximation

From Eq. (2.6), it is evident that applying the power flow equations to an optimization problem imposes a nonlinear equality constraint, generally making the resulting feasible set non-convex and the problem NP-hard to solve (Lee et al., 2018). Hence, solving AC OPF problems requires high computational resources, especially for larger networks.

In order to improve computational performance and simplify power system representation, engineers developed DC power flow approximations, which have been widely used in literature (Van Den Bergh et al., 2014; Frank and Rebennack, 2016; Zhu, 2009). The DC power flow approximation is a linearization of the AC power flow equations, and is based on the following four assumptions:

1. Line resistances are negligible compared to line reactances ($R \ll$X). As a result, grid losses are neglected, and the line parameters are simplified as follows:

$$\begin{aligned} G &\approx 0, \quad B \approx -\frac{1}{X}, \\ Z &\approx jX, \quad Y \approx jB. \end{aligned} \tag{2.10}$$

2. The differences between adjacent bus voltage angles are small. Thus, via the small angle approximation, the nonlinear terms in the power flow equations are linearized to

$$\begin{aligned} &\sin(\delta_k(t) - \delta_j(t)) \approx \delta_k(t) - \delta_j(t), \\ &\cos(\delta_k(t) - \delta_j(t)) \approx 1. \end{aligned} \tag{2.11}$$

3. The voltage profile in the system is flat, and the voltage at all buses is $V_k \approx 1.0$p.u.
4. Reactive power flow is neglected.

Applying these assumptions discards Eq. (2.6b) for the reactive power flow, and produces the simplified DC power flow equation

$$P_{trans} = B_{k,j}\big(\delta_k(t) - \delta_j(t)\big). \tag{2.12}$$

The DC power flow approximation has been used successfully in many OPF studies and applications, and can lead to robust solutions and improved computational performance (Frank and Rebennack, 2016). Under typical operating conditions, the voltage angle difference between two buses δ_k and δ_j is less than $15°$ (Zhu, 2009), justifying assumption 2 under normal circumstances. However, in stressed systems, voltage angle differences can increase up to $30°$, indicating that the assumptions are prone to errors for systems in extreme conditions, especially for distribution networks (where resistance effects are more apparent).

2.3.4 DC swing equation

The swing equation is a representation of the energy balance over the individual nodes (buses) of a power network, and is used profoundly throughout this thesis to model power system dynamics. It provides a means to analyze the power balance at a power grid bus, and explicitly models the influence of synchronous generators on the voltage angle and frequency of the system (Taha et al., 2019; Trip et al., 2016). Under the DC power flow assumptions, the swing equation for node k in a network $\mathcal{T}$ with neighborhood matrix $\mathcal{T}_k^n$ is given by

$$m_k\ddot{\delta}_k(t) + d_k\dot{\delta}_k(t) = P_{GR_k}(t) - P_{LD_k}(t) - \sum_{j\in\mathcal{T}_k^n} b_{kj}\big(\delta_k(t) - \delta_j(t)\big), \tag{2.13}$$

where δ_i and $\dot{\delta}$ are the voltage angle and frequency at bus i (Mallada et al., 2017). Furthermore, m_k and d_k are the moment of inertia and damping (droop) coefficient of the generator, P_{GR_k} and P_{LD_k} are the power generation and load, and the final term considers the power flow from node k to all neighboring nodes (Zhao et al., 2015). Balance of energy must always be preserved, since it can either be injected or withdrawn as electricity, or be converted from or to mechanical energy.

2.4 Model Predictive Control

Model Predictive Control (MPC) is a powerful control methodology which is widely used in power system analysis (Ilić et al., 2011a; Taha et al., 2019) and building HVAC studies (Pavlak et al., 2014; Rene, 2016). In MPC, an optimal control sequence u^* is calculated by optimizing an objective (or cost) function over a specific time horizon, while simulating the corresponding model of the system to determine its behavior over this horizon (Camacho and Bordons, 2007).

Only the first step in the optimal control sequence is applied to the controller of the system, and the rest is discarded. Afterwards, a new optimal control sequence is calculated, using the updated state of the system and shifting the time horizon with one step.

In the scope of this study, we are primarily interested in finite-horizon MPC for discretized linear systems, which is in general formulated as follows:

$$\begin{aligned}
\underset{\mathcal{X}}{\text{minimize}} \quad & \sum_{k \in \mathcal{K}} J(x,u) && \text{(2.14a)}\\
\text{subject to} \quad & x(k_0) = x_0 && \text{(2.14b)}\\
& x(k+1) = Ax(k) + Bu(k) && \text{(2.14c)}\\
& x(k+1) \in \mathcal{Z}, \quad u(k) \in \mathcal{U} && \text{(2.14d)}\\
& \forall k \in \mathcal{K},
\end{aligned}$$

where it is assumed that the feasible sets $\mathcal{Z}$ and $\mathcal{U}$ are convex (Simon, 2017). In this formulation, we want to choose the decision variables in $\mathcal{X}$ over a horizon of time steps $\mathcal{K}$ such that the sum of the cost function $J(x,u)$ is minimized. The state of the system is bounded by the initial state in Eq. (2.14b), is subject to the dynamics in Eq. (2.14c), and both the state and input must belong to the feasibility sets $\mathcal{Z}$ and $\mathcal{U}$. In its most common form, the (quadratic) cost function is formulated as

$$J(x,u) = x(k)^\top Q x(k) + u(k)^\top R u(k), \tag{2.15}$$

where cost matrices Q and R represent the relative penalties of deviations in $x(k)$ and $u(k)$. Note that Eq. (2.15) attempts to steer both the state and input to zero. In case a different state/input goal is desired, say $x(k) = \overline{x}$ and $u(k) = \overline{u}$, the cost function is modified to

$$J(x,u) = \big(x(k) - \overline{x}\big)^\top Q \big(x(k) - \overline{x}\big) + \big(u(k) - \overline{u}\big)^\top R \big(u(k) - \overline{u}\big). \tag{2.16}$$

Finally, the linear equivalent of Eq. (2.15) is formulated as follows:

$$J(x,u) = q^\top x(k) + r^\top u(k), \tag{2.17}$$

where q and r are cost vectors of appropriate size. Quadratic cost functions steer the elements to a desired value, which is, therefore, also called *reference tracking*. On the contrary, linear cost functions are used to minimize the corresponding elements, even if their value is allowed to be negative.

The inherent receding horizon of MPC efficiently steers the states of the system towards the optimal value, by generating predictions of future states (Rene, 2016). If the mathematical model

of the system is accurate, MPC is a powerful tool, due to its open methodology, and ability to determine optimal control options for future states of the system (Camacho and Bordons, 2007).

However, a large drawback of MPC is that it requires an accurate model of the system, which can be time consuming and costly to generate (Camacho and Bordons, 2007). Furthermore, the computational complexity of a centralized MPC with a large number of constraints and control inputs quickly becomes excessive (Ilić et al., 2011b).

Despite the drawbacks of MPC, it is adopted as the primary methodology for this study. Although basic MPC usually relies on a centralized approach, various authors proposed distributed procedures to relieve the computational burden of solving large-scale networks (Nguyen et al., 2017; Lampropoulos et al., 2013). As mathematical models of power networks are widely described in literature, accurate models of the physical network can be developed, to ensure that the actual process is effectively steered to its desired state (Maciejowski, 2002; Taha et al., 2019). Finally, as MPC is easily implemented and open for improvement, the underlying optimization model can readily be modified if the system is changed or the accuracy of its mathematical description is improved.

2.5 Stochastic optimization models

A general deterministic optimization model is formulated as minimizing (or maximizing) a cost function $J(x) : \mathbb{R}^d \to \mathbb{R}$ over a set of variables $x \in \mathbb{R}^d$ in a feasible set $\mathcal{D}$ defined by a vector of constraints g (Prékopa, 1970):

$$\begin{aligned} &\underset{x}{\text{minimize}} \;\; J(x) \\ &\text{subject to} \;\; g(x) \leq 0. \end{aligned} \tag{2.18}$$

This problem is well defined if the cost function and constraints depend only on deterministic values. However, when the cost function or any of the constraints also depends on a random input $\mathsf{P} \in \mathcal{W}$, with $\mathcal{W}$ an unbounded uncertainty set, the formulation of the optimization becomes unclear. The most conservative way of dealing with the uncertainty is to force the solution to satisfy the union of feasible sets for all elements in $\mathcal{W}$. The resulting problem is called a Robust Convex Program (RCP) (Boyd and Vandenberghe, 2004), and is formulated as

$$\text{RCP} \begin{cases} \underset{x}{\text{minimize}} & J(x, \mathsf{P}) \\ \text{subject to} & \Big\{ g(x, \mathsf{P}) \leq 0 \Big\} \quad \forall \mathsf{P} \in \mathcal{W}. \end{cases} \tag{2.19}$$

As the uncertainty set $\mathcal{W}$ is typically a continuous set of an infinite number of instances (Campi et al., 2009), it is impossible to consider all elements of the uncertainty set in the constraints. Instead, a more sophisticated way to deal with the uncertainty is to define the new feasible

set by imposing constraints on the probability function (Dentcheva, 2006), as in the following formulation:

$$\begin{aligned} &\text{minimize} \;\; \mathbb{E}\big[J(x,\mathsf{P})\big] \\ &\text{subject to} \;\; \mathbb{P}\big[g(x,\mathsf{P}) \leq 0\big] \geq 1-\epsilon, \end{aligned} \tag{2.20}$$

where we estimate the objective function based on the random input P, and we require that all constraints are satisfied for all realizations of P, expect for a probability mass of ϵ. The random input P does not have to be a constant value, but can also be a trajectory over the time horizon of the optimization problem. In case of a random trajectory, we use the set notation $\{\mathsf{P}\}_{t=1}^{t_{\text{end}}}$, where the span of t to t_{end} reflects the time horizon of the optimization problem.

Elements in $\mathcal{W}$ are drawn according to the probability distribution $\mathbb{P}$. Hence, we can reformulate Eq. (2.20) by stating that the constraints $g_i(x,\mathsf{P})$ need to be satisfied for all realizations of P over the optimization time horizon, except for a set with probability to be drawn of ϵ (Rostampour, 2012). This yields the following formulation of the stochastic optimization model, called Chance Constrainted Program (CCP):

$$\text{CCP} \begin{cases} \underset{x}{\text{minimize}} & \mathbb{E}\big[J(x,\mathsf{P})\big] \\ \text{subject to} & \mathbb{P}\Big(\; \{\mathsf{P}\}_{t=1}^{t_{end}} \in \mathcal{W} \;\Big|\; g(x,\mathsf{P}) \leq 0 \; \Big) \geq 1-\epsilon. \end{cases} \tag{2.21}$$

Although historical data can be used to predict likely trajectories, the actual random input P is unknown, and the uncertainty set contains infinite elements. As the problem contains a finite number of decision variables and infinite constraints, it is called *semi-infinite*, and is, in many cases, NP-hard to solve (Ben-Tal and Nemirovski, 1998).

In the scope of this study, we follow a randomized methodology based on the *scenario approach*, which samples at random N_s instances of the uncertainty set $\mathcal{W}$, and explicitly considers the corresponding constraints related to these instances in the optimization problem (Margellos et al., 2014). The corresponding problem is a Scenario Convex Program (SCP), and is formulated as follows:

$$\text{SCP} \begin{cases} \underset{x}{\text{minimize}} & \hat{J}(x) \\ \text{subject to} & \Big\{ g(x,\mathsf{P}) \leq 0 \Big\} \quad \forall \mathsf{P} \in \mathbb{W} \\ & \mathbb{W} = \{P^1, \ldots, P^{N_s}\}, \end{cases} \tag{2.22}$$

where $\mathbb{W}$ is a set of independent and identically distributed realizations of the uncertainty set $\mathcal{W}$, and where cost function $\hat{J}(x)$ is generally an estimation, based on N_s^j evaluations of the random input P, i.e.

$$\hat{J}(x) = \sum_{j=1}^{N_s^j} \frac{1}{N_s^j} J(x, \mathsf{P}^j). \tag{2.23}$$

The SCP is very similar to the RCP, but instead of satisfying all possible elements in $\mathcal{W}$, a finite number of N_s elements, contained in the set $\mathbb{W} \subset \mathcal{W}$ are considered. Although the set of extractions $\mathbb{W}$ is a random variable, the SCP itself is convex and no longer chance constrained, making it efficient to solve if N_s is not too large. On the contrary, N_s should be chosen large enough such that it is representative for $\mathcal{W}$, with a minimal probability $1 - \beta$. In particular, according to Campi et al. (2009), if the number of instances for a problem with N^d decision variables is at least

$$N_s \geq \frac{2}{\epsilon}\big(\ln \frac{1}{\beta} + N^d\big), \tag{2.24}$$

then, with probability no smaller than $1-\beta$, the solution x^* of the SCP satisfies all constraints in the uncertainty set $\mathcal{W}$ but at most a fraction of ϵ. As the scenario approach imposes a relaxation on the original problem, the corresponding optimal cost function $J(x^*, Z) \leq J(\overline{x}, Z)$, with $\overline{x}$ being the optimal solution to the original problem. Although there is a small probability that this approach results in an infeasible solution to the original problem, it allows convex optimization of the model, and is therefore used to optimize problems with uncertain generations in this study.

3 Building Energy Storage Units for Centralized Optimal Frequency Control

3.1 Introduction

In this chapter, we propose a dynamical BtG framework with explicit hierarchical interactions between TSO, DSO, and BLD, which allows to realistically model the future power system as a multi-level framework, as visualized in Figure 3.1. Such a framework yields the possibility of modeling multiple DSOs connected to a centralized TSO, to represent the interaction between different stakeholders in the power system. A centralized MPC is proposed to optimize BLD, DSO, and TSO control variables simultaneously over a common time horizon. The potential role of individual buildings in frequency control of the power system is studied, by introducing dedicated electrical energy storage units for individual buildings in the BtG framework. By coupling BLD, DSO, and TSO control decisions and solving the corresponding MPC procedure, the grid regulative capacity of building storage flexibility is demonstrated.

The remainder of the chapter is organized as follows. First of all, we justify why we only consider distributed electrical energy storage systems, and not other types of energy storage. Then, dynamical models for the TSO, DSOs and buildings are proposed. The models are explicitly coupled by defining the energy transmission at the interfaces. Buildings are equipped with distributed electrical energy storage to provide flexibility to the system. Finally, we develop a centralized MPC procedure, to solve the optimization problem as a finite-horizon optimal control problem. The proposed MPC is used to demonstrate the grid regulative capacity of building HVAC and storage flexibility.

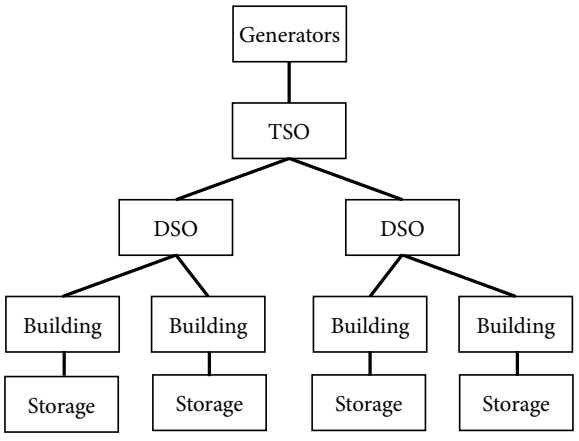

Figure 3.1: Hierarchy of the power system framework with integrated TSO/DSO/BLD dynamics.

3.2 Types of energy storage

In the current study, we introduce demand-side flexibility by integrating distributed electrical energy storage systems (batteries). Batteries have near-instantaneous response times (Breeze, 2014), and are modular in size (Tuohy et al., 2014), making them valuable resources for improving network stability of the power grid. Electrical storage systems are mainly used for reducing short-term supply/demand mismatches and load fluctuations (NERC, 2010).

Due to the fast response times, versatility, and general availability, we limit the scope of the current study to electrical storage. In particular, we do not focus on a specific battery, but develop dynamics for electrical storage buffers in general. Although the storage dynamics developed in subsection 3.5.2 are specifically for electrical batteries, other types of storage can be embedded in the power network as well, for similar purposes. Furthermore, we stress that the electrical storage can also be embodied by batteries of electric vehicles (Kempton et al., 2008; Wang et al., 2011), although such integration also requires suitable equipment and the assistance of aggregators (NERC, 2010). Other mature storage technologies are pumped hydro (Deane et al., 2010) and compressed air (Pimm et al., 2011), and recently technologies such as flywheels, hydrogen, and super-capacitors have gained attention (Ferreira et al., 2013). Pumped hydro energy storage is by far the largest storage technology, accounting for 99% of the global storage capacity, but is also inflexible and less controllable (Tuohy et al., 2014). In general, most technologies do not exhibit the flexible and versatile characteristics of electrical storage systems, and are less suitable for distributed integration by consumers.

Based on their chemical properties, many different electrical storage technologies are available (Lund et al., 2015). Although detailed discussion of the different technologies is outside the scope of the current study, some disadvantages of battery storage are briefly discussed. First of all, as most electrical storage systems are subject to self-discharge losses, they are primarily used for short-term storage. Furthermore, capital cost of batteries dominates the cost of batteries compared to operation and maintenance costs, and performance decreases with the number of cycles (Poonpun and Jewell, 2008).

3.3 TSO model dynamics

Let $\mathcal{T} = \{1, \dots, n_t\}$ and $\mathcal{G} = \{1, \dots, n_g\}$ be the sets of TSO buses (represented by nodes) and generators in the upper level power network. Denote by $\mathcal{T}_k^n$ the set of neighboring nodes of TSO node k. TSO nodes and generators are respectively indexed by $k \in \mathcal{T}$ and $m \in \mathcal{G}$.

Generators are connected to TSO buses according to the incidence matrix $\Gamma \in \mathbb{R}^{n_t \times n_g}$, with entries given by

$$\gamma_{k,m} = \begin{cases} 1 & \text{if generator } m \text{ is attached to bus } k, \\ 0 & \text{otherwise.} \end{cases} \tag{3.1}$$

The TSO network is modeled by the swing equation introduced in subsection 2.3.4, relating the rotor angle δ with the angular velocity $\dot{\delta}$ and angular acceleration $\ddot{\delta}$. To this end, we define m_k

and d_k as the inertia and damping coefficients at bus k. In case no generator is present at bus k, $m_k = 0$ and $d_k = 0$. In addition, we consider $\hat{d}_k$ as the frequency-sensitive portion of the uncontrollable load at bus k. Similar to Taha et al. (2019), the active power swing equation for bus k in the TSO network is written as

$$\begin{aligned} m_k\ddot{\delta}_k(t) + (d_k + \hat{d}_k)\dot{\delta}_k(t) = &\sum_{m=1}^{n_g} \gamma_{k,m} P_{\text{GR}_m}(t) - P_{\text{BL}_k}(t) - P_{\text{LD}_k}(t) \\ &- \sum_{j \in \mathcal{T}_k^n} b_{kj} \sin(\delta_k(t) - \delta_j(t)). \end{aligned} \tag{3.2}$$

The first term in Eq. (3.2) represents the total generator input at bus k, with P_{GR_m} the power generated by generator m. P_{BL_k} is the frequency-insensitive uncontrollable base load, and P_{LD_k} is the controllable external load at node k, which is to be defined explicitly in Eq. (3.8). The last term relates node k to the state of its neighborhood nodes in set $\mathcal{T}_k^n$. The parameter b_{kj} is the susceptance coefficient of the transmission line connecting bus k and j.

The second order differential equation in Eq. (3.2) can be rewritten as two first order differential equations for the dynamics of bus $k \in \mathcal{T}$ in the TSO network as follows:

$$\dot{\delta}_k(t) = \omega_k(t) = \omega_k^{true}(t) - \omega_0 \tag{3.3}$$

$$\begin{aligned} m_k\dot{\omega}_k(t) = &- (d_k + \hat{d}_k)\omega_k(t) + \sum_{m=1}^{n_g} \gamma_{k,m} P_{\text{GR}_m}(t) - P_{\text{BL}_k}(t) - P_{\text{LD}_k}(t) \\ &- \sum_{j \in \mathcal{T}_k^n} b_{kj} \sin(\delta_k(t) - \delta_j(t)), \quad k \in \mathcal{T}, \end{aligned} \tag{3.4}$$

where ω_k is the angular velocity deviation, with ω_k^{true} the actual frequency of bus k, and ω_0 the synchronous frequency. The equivalent nonlinear state-space model is formulated as

$$E_t\dot{x}_t(t) = A_t x_t(t) + B_{\text{GR}} P_{\text{GR}}(t) - B_t\big(P_{\text{LD}}(t) + P_{\text{BL}}(t) + \Psi(\delta(t))\big), \tag{3.5}$$

with state variable $x_t(t) = [\delta_1, \ldots, \delta_{n_t} \quad \omega_1, \ldots, \omega_{n_t}]^\top$, and the state-space matrices defined as follows:

$$E_t = \begin{bmatrix} \mathbf{I}_{n_t} & \mathbb{0}_{n_t \times n_t} \\ \mathbb{0}_{n_t \times n_t} & M \end{bmatrix}, \quad A_t = \begin{bmatrix} \mathbb{0}_{n_t \times n_t} & \mathbf{I}_{n_t} \\ \mathbb{0}_{n_t \times n_t} & -D \end{bmatrix}, \quad B_{\text{GR}} = \begin{bmatrix} \mathbb{0}_{n_t \times n_g} \\ \Gamma \end{bmatrix},$$
$$B_t = \begin{bmatrix} \mathbb{0}_{n_t \times n_t} \\ \mathbf{I}_{n_t} \end{bmatrix}.$$

$M = \text{diag}(m_1, \ldots, m_{n_t})$ and $D = \text{diag}(d_1 + \hat{d}_1, \ldots, d_{n_t} + \hat{d}_{n_t})$ are the equivalent matrices of the individual inertia and damping coefficients. Similarly, $P_{\text{GR}}(t) = [P_{\text{GR}_1}, \ldots, P_{\text{GR}_{n_g}}]^\top$, $P_{\text{BL}}(t) = [P_{\text{BL}_1}, \ldots, P_{\text{BL}_{n_t}}]^\top$ and $P_{\text{LD}}(t) = [P_{\text{LD}_1}, \ldots, P_{\text{LD}_{n_t}}]^\top$ are the column vectors of the power generation, base load, and controllable load, respectively. Finally, matrix $\Psi(\delta(t)) = [\psi_1, \ldots, \psi_{n_t}]^\top$ takes into account the nonlinear part of the swing equations, having its elements defined by

$$\psi_k = \sum_{j \in \mathcal{T}_k^n} b_{kj} \sin(\delta_k(t) - \delta_j(t)). \tag{3.6}$$

3.4 DSO model dynamics

Consider a TSO power network such that it is physically connected to n_d DSO networks in a hierarchical manner, with the set of DSO networks given by $\mathcal{D} = \{1, ..., n_d\}$. Let $\mathcal{D}_i = \{1, ..., n_d^i\}$ denote the set of buses (nodes) of DSO i. Denote by $\mathcal{D}_l^{n,i}$ the neighborhood set of node l of DSO i. Each DSO network is connected to the parent TSO network through one or multiple border buses. The interface of DSO i with the TSO is represented by incidence matrix $\Phi^i \in \mathbb{R}^{n_t \times n_d^i}$, with entries given by

$$\phi_{k,l}^i = \begin{cases} 1 & \text{if bus } l \text{ of DSO } i \text{ is attached to TSO bus } k, \\ 0 & \text{otherwise.} \end{cases} \tag{3.7}$$

The active power transmitted between TSO bus k and bus j of DSO i is denoted by $P_{k,j}^i$. The transmission matrix for DSO i is denoted by $P_{\text{IMP}}^i \in \mathbb{R}^{n_t \times n_d^i}$ and consists of all elements $P_{k,j}^i$. If positive, the power transmitted at the interface is modeled as load for the TSO network, and generation for the DSO. Physically, $\mathbb{1}_{n_t}^\top P_{\text{IMP}}^i \mathbb{1}_{n_d^i} > 0$ (the sum of transmission at border buses) for DSO i means that power is requested from the TSO, whereas a negative value implies an surplus at the DSO. The term $P_{\text{LD}} \in \mathbb{R}^{n_t}$ in Eq. (3.5) is now defined as

$$P_{\text{LD}}(t) = \sum_{i=1}^{n_d} \left[\left(\Phi^i \circ P_{\text{IMP}}^i(t) \right) \mathbb{1}_{n_d^i} \right], \tag{3.8}$$

adding a term for the DSO power import from the individual buses of the TSO network. From DSO point of view, let $P_{\text{LD}}^i \in \mathbb{R}^{n_d^i}$ denote the power flow vector from the TSO network to DSO i:

$$P_{\text{LD}}^i(t) = \left(\Phi^i \circ P_{\text{IMP}}^i(t) \right)^\top \mathbb{1}_{n_t} . \tag{3.9}$$

Since it is assumed that there are no generators connected to DSO buses[1], we consider $m = 0$ and $d = 0$ in the DSO swing equations. The dynamics at bus j of DSO i are described as

$$\begin{aligned}\hat{d}^i_j \dot{\delta}^i_j(t) = &- P^i_{\mathrm{BD}_j}(t) + \sum_{k=1}^{n_t} \left(\phi^i_{k,j} P^i_{k,j}(t)\right) \\ &- \sum_{q \in \mathcal{D}^{n,i}_j} \Big[g^i_{qj} \cos\left(\delta^i_j(t) - \delta^i_q(t)\right) + b^i_{qj} \sin\left(\delta^i_j(t) - \delta^i_q(t)\right) \Big],\end{aligned} \tag{3.10}$$

where $P^i_{\mathrm{BD}_j}(t)$ denotes the total building load at bus j of DSO i, which is to be defined explicitly in Eq. (3.18). Similar as for TSO dynamics, $\hat{d}^i_j$ is the frequency sensitive portion-sensitive uncontrollable load at bus j, and $P^i_{k,j}(t)$ is the entry of P^i_{IMP} corresponding to TSO bus k and bus j of DSO i. Furthermore, g^i_{qj} and b^i_{qj} are the conductance and susceptance of the line between bus q and j of DSO i. In distribution networks, conductance g of power lines cannot be neglected (Saint-Pierre and Mancarella, 2017). However, in line with the DC power flow approximation introduced in subsection 2.3.3, we assume that voltage across the network is constant and that the sum of each row in the conductance matrix is zero. This leads to have the conductance term in the linearization around operating point, $\delta^i_l - \delta^i_j = 0$, drop out. The resulting state-space model for DSO i is given by:

$$E^i_d \dot{x}^i_d(t) = A^i_d x^i_d(t) + B^i_d \big(P^i_{\mathrm{LD}}(t) - P^i_{\mathrm{BD}}(t) - P^i_{\mathrm{BL}}(t) - \Psi^i(\delta^i(t))\big), \tag{3.11}$$

where the state variable $x^i_d(t) = [\delta^i_1, \ldots, \delta^i_{n^i_d} \quad \omega^i_1, \ldots, \omega^i_{n^i_d}]^\top$, and with the state-space matrices defined as follows:

$$E^i_d = \begin{bmatrix} \mathrm{I}_{n^i_d} & \mathbb{0}_{n^i_d \times n^i_d} \\ \mathbb{0}_{n^i_d \times n^i_d} & \mathbb{0}_{n^i_d \times n^i_d} \end{bmatrix}, \quad A^i_d = \begin{bmatrix} \mathbb{0}_{n^i_d \times n^i_d} & \mathrm{I}_{n^i_d} \\ \mathbb{0}_{n^i_d \times n^i_d} & -\hat{D}^i \end{bmatrix}, \quad B^i_d = \begin{bmatrix} \mathbb{0}_{n^i_d \times n^i_d} \\ \mathrm{I}_{n^i_d} \end{bmatrix},$$

where $\hat{D}^i = \mathrm{diag}(\hat{d}^i_1, ..., \hat{d}^i_{n^i_d})$. The variables $P^i_{\mathrm{BL}}(t)$ and $P^i_{\mathrm{BD}}(t)$ are the column vectors of the uncontrollable base load and the controllable building load of the buses of DSO i, respectively, and $\Psi^i(\delta^i(t)) = [\psi^i_1, ..., \psi^i_{n^i_d}]^\top$ takes into account the nonlinear term of Eq. (3.11), having its elements defined by

$$\psi^i_l = \sum_{j \in \mathcal{D}^{n,i}_l} b^i_{lj} \sin\left(\delta^i_l(t) - \delta^i_j(t)\right) \tag{3.12}$$

[1]Note that this not a restriction of the modeling framework, and is easily modified to different network topology without loss of generality.

3.5 Building and storage model dynamics

The model developed in this research explicitly couples building's decision variables to the power grid. Furthermore, it provides flexibility to the grid by equipping individual buildings with electrical energy storage. Developing the storage-integrated building model consists of three parts. First, a building modeling framework based on 3R-2C circuits is proposed. Second, a general energy storage model is proposed, which is then integrated to the building energy load to the grid. Finally, the connection point of the building problem to the DSO problem is discussed in more detail.

3.5.1 Building thermal comfort model

Based on the model proposed in Taha et al. (2019), using a 3R-2C circuits model for each building, consider the following first-order continuous-time equations as the building thermal dynamics:

$$\dot{T}_{\text{wall}} = \frac{T_{\text{amb}} - T_{\text{wall}}}{C_{\text{wall}} R_2} + \frac{T_{\text{zone}} - T_{\text{wall}}}{C_{\text{wall}} R_1} + \frac{\dot{Q}_{\text{sol}}}{C_{\text{wall}}} \tag{3.13a}$$

$$\dot{T}_{\text{zone}} = \frac{T_{\text{wall}} - T_{\text{zone}}}{C_{\text{zone}} R_1} + \frac{T_{\text{amb}} - T_{\text{zone}}}{C_{\text{zone}} R_{\text{win}}} + \frac{\dot{Q}_{\text{int}} - \dot{Q}_{\text{hvac}}}{C_{\text{zone}}}, \tag{3.13b}$$

where $T_{\text{zone}}(t)$ and $T_{\text{wall}}(t)$ are the zone (building interior) and wall temperatures, respectively, $T_{\text{amb}}(t)$ is the ambient temperature, and C_{zone} and C_{wall} are the lumped thermal capacities of the zone and the walls plus roof, respectively. The parameters R_1, R_2 and R_{win} are resistance parameters of the external wall, internal wall, and windows, respectively. The variable $\dot{Q}_{\text{sol}}(t)$ is the sum of the absorbed solar radiation on the external wall, $\dot{Q}_{\text{int}}(t)$ the total internal heat gain from internal heat sources, and $\dot{Q}_{\text{hvac}}(t)$ the cooling/heating load. The room temperature variation is associated with cooling load $\dot{Q}_{\text{hvac}}$ term and the consumed HVAC power is proportional to the load via $\dot{Q}_{\text{hvac}}(t) = \mu_{\text{hvac}} P_{\text{hvac}}(t)$. The building dynamics of Eq. (3.13) for one building l are described using the following state space model:

$$\dot{x}_b^l(t) = A_b^l x_b^l(t) + B_p^l P_{\text{hvac}}^l(t) + B_{w_b}^l w_b^l(t), \tag{3.14}$$

where $x_b^l(t) = [T_{\text{wall}}^l \quad T_{\text{zone}}^l]^\top$, $w_b^l = [T_{\text{amb}}^l \quad \dot{Q}_{\text{sol}}^l \quad \dot{Q}_{\text{int}}^l]^\top$, and the system matrices are defined as

$$A_b^l = \begin{bmatrix} -\frac{1}{C_{\text{wall}}}\left(\frac{1}{R_1} + \frac{1}{R_2}\right) & \frac{1}{C_{\text{wall}} R_1} \\ \frac{1}{C_{\text{zone}} R_1} & -\frac{1}{C_{\text{zone}}}\left(\frac{1}{R_1} + \frac{1}{R_{\text{win}}}\right) \end{bmatrix}^l,$$

$$B_p^l = \begin{bmatrix} 0 \\ -\frac{\mu_{\text{hvac}}}{C_{\text{zone}}} \end{bmatrix}^l, \quad B_{w_b}^l = \begin{bmatrix} \frac{1}{C_{\text{wall}} R_2} & \frac{1}{C_{\text{wall}}} & 0 \\ \frac{1}{C_{\text{zone}} R_{\text{win}}} & 0 & \frac{1}{C_{\text{zone}}} \end{bmatrix}^l.$$

The superscript $[\cdot]^l$ refers to the dynamics and RC parameters for a specific building l. To describe the complete dynamics of buildings, let $\mathcal{B} = \{1, \ldots, n_b\}$ be the set of all buildings in the network, with n_b the total number of buildings. The building dynamics of Eq. (3.13) for the full set of buildings in $\mathcal{B}$ are described by the state space model

$$\dot{x}_b(t) = A_b x_b(t) + B_p P_{\text{hvac}}(t) + B_{w_b} w_b(t), \tag{3.15}$$

where (in the absence of communication between buildings) block diagonal system matrices are defined as $A_b = \text{diag}(A_b^l)_{l\in\mathcal{B}}$, $B_p = \text{diag}(B_p^l)_{l\in\mathcal{B}}$, and $B_{w_b} = \text{diag}(B_{w_b}^l)_{l\in\mathcal{B}}$. The model has state variables $x_b = [x_b^1, \ldots, x_b^{n_b}]^\top \in \mathbb{R}^{2n_b}$ with x_b^l the two state variables of an individual building l. The inputs $P_{\text{hvac}} \in \mathbb{R}^{n_b}$ are the cooling load set points of the individual buildings, and is the variable to be solved for (Patel et al., 2016). Finally, $w_b = [T_{\text{amb}} \quad \dot{Q}_{\text{sol}} \quad \dot{Q}_{\text{int}}]^\top \in \mathbb{R}^{3n_b}$ contains the ambient temperature, solar radiation, and internal heat gain of buildings. Although buildings can be connected to different DSOs, Eq. (3.15) is sufficient to describe the dynamics of all buildings in the network.

3.5.2 Electrical energy storage model

Define $x_s^l(t)$ to be the state variable (buffer level) and $P_{\text{stor}}^l(t)$ the input rate variable for the storage unit of building l. As each building is connected to a dedicated storage unit, we use the same set $\mathcal{B}$ and index l for buildings as for storage units. Consider now the discretized storage dynamical model for unit l for all $k \in \mathcal{N}$ given by

$$x_s^l(k+1) = \zeta^l x_s^l(k) + h\eta^l P_{\text{stor}}^l(k+1), \tag{3.16}$$

where $x_s^l(0) = x_s^{l,0}$ (initial storage level) is given, h is the simulation time resolution, and the parameters ζ^l and η^l are efficiency coefficients of the storage unit. The dynamics of all storage units in vector form are formed by $x_s(k) = [x_s^1(k), \ldots, x_s^{n_b}(k)]^\top$ and $P_{\text{stor}} = [P_{\text{stor}}^1(k), \ldots, P_{\text{stor}}^{n_b}(k)]^\top$. Note that if $\zeta < 1$ means that there is a loss of stored energy over time. Although the current equation models energy loss proportionally, higher order equations for losses can be modeled as well. Physical limitations on the storage rate and buffer level are imposed in the MPC constraints. If desired, disabling the storage unit of specific buildings is easily done by setting $x_s^{j,\min} = x_s^{j,\max}$, automatically forcing $P_{\text{stor}}^j(t)$ to zero.

3.5.3 Integrating BLD into DSO setting

Buildings with storage unit dynamics are coupled to the DSO model by considering a BLD-to-DSO incidence matrix $\Pi^i \in \mathbb{R}^{n_d^i \times n_b}$ for every DSO i, with entries given by

$$\pi_{l,n}^i = \begin{cases} 1 & \text{if building } n \text{ is attached to bus } l \text{ of DSO } i, \\ 0 & \text{otherwise.} \end{cases} \tag{3.17}$$

Using such an incidence matrix Π^i, we can now determine P^i_{BD} (the total building load vector for DSO i) in Eq. (3.11) as follows:

$$P^i_{\text{BD}}(t) = [P^i_{\text{BD}_1}, ..., P^i_{\text{BD}_{n^i_d}}]^\top = \Pi^i \big(P_{\text{stor}}(t) + P_{\text{hvac}}(t) + P_{\text{misc}}(t)\big) \tag{3.18}$$

where $P^i_{\text{BD}_l}$ is the load of building l requested from DSO i, and P_{stor}, P_{hvac}, $P_{\text{misc}} \in \mathbb{R}^{n_b}$ are the column vectors for building power storage, HVAC power demand, and uncontrollable miscellaneous power consumption, respectively. Eq. (3.18) can easily be extended with additional terms to account for the injection of distributed generation at the building level, e.g. from CHP systems (Larsen et al., 2014a) and PV cells (Gill et al., 2014). The power balance at the building level described in Eq. (3.18) is depicted in Figure 3.2.

Finally, the total building load vector (for all DSOs) is defined as the sum of its contributions, such that

$$P_{\text{BD}}(t) = \sum_i^{n_d} P^i_{\text{BD}}(t). \tag{3.19}$$

3.6 BtG-MPC optimal frequency control framework

Using the developed model for the integrated TSO, DSO, and BLD systems dynamics, we now formulate an optimal frequency control framework based on the traditional MPC paradigm, which we may refer to as Buildings-to-Grid (BtG)-MPC in the proceeding section. We define T_p as the MPC prediction time horizon, h as the simulation time step, and the set of prediction time steps $\mathcal{K} = \{k_0, k_0 + 1, \ldots, k_0 + \frac{T_p}{h} - 1\}$, where k_0 is the MPC starting time step. Finally, we define the set of simulation study time steps $\mathcal{N} = \{0, 1, \ldots, \frac{T_{\text{end}}}{h} - 1\}$, where T_{end} is the end time of the simulation study, and define the number of simulation time steps $N_{\text{sim}} = |\mathcal{N}| = \frac{T_{\text{end}}}{h}$.

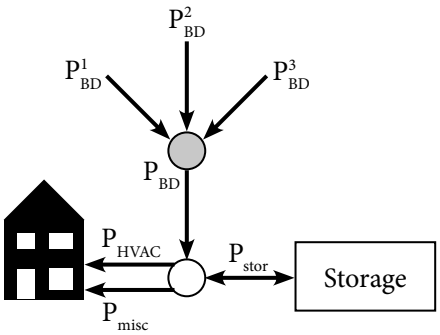

Figure 3.2: Nodal power balance at the building level, with arrows pointing in the positive value of a variable.

The proposed TSO, DSO and BLD dynamics are discretized using the so-called *first-order Gear's method*, which reduces to a backward Euler implicit method (Sincovec et al., 1981). A similar approach was used by Taha et al. (2019) to discretize TSO and building dynamics. A full derivation of the discretization technique is presented in Appendix A. To render the problem convex, we follow the general DC power flow approximation (as introduced in Section 2.3), and estimate power flow between buses in Eqs. (3.2) and (3.4) with $\sin(\delta_k(t)-\delta_j(t)) \approx (\delta_k(t)-\delta_j(t))$. Denote the discretized functions in the three physical network areas (TSO, DSO and buildings, respectively) by

$$\begin{aligned} x_t(k+1) &= f_t\big(x_t(k), P_{\text{GR}}(k+1), P_{\text{IMP}}(k+1), P_{\text{BL}}(k+1)\big) \\ &= \big(E_t - hA_t'\big)^{-1}\Big[E_t x_t(k) + h\big(B_{\text{GR}}P_{\text{GR}}(k+1) - B_t(P_{\text{LD}}(k+1) + P_{\text{BL}}(k+1))\big)\Big], \end{aligned} \tag{3.20a}$$

$$\begin{aligned} x_d^i(k+1) &= f_d^i\big(x_d^i(k), P_{\text{IMP}}^i(k+1), P_{\text{BD}}^i(k+1), P_{\text{BL}}^i(k+1)\big) \\ &= \big(E_d^i - hA_d'^i\big)^{-1}\Big[E_d^i x_d^i(k) + hB_d^i\big(P_{\text{LD}}^i(k+1) - P_{\text{BD}}^i(k+1) - P_{\text{BL}}^i(k+1)\big)\Big], \end{aligned} \tag{3.20b}$$

$$\begin{aligned} x_b(k+1) &= f_b\big(x_b(k), P_{\text{hvac}}(k+1), w_b(k+1)\big) \\ &= \big(I_{2n_b} - hA_b\big)^{-1}\Big[x_b(k) + h\big(B_p P_{\text{hvac}}(k+1) + B_{w_b} w_b(k+1)\big)\Big], \end{aligned} \tag{3.20c}$$

for all time steps $k \in \mathcal{N}$. Define the set of decision variables to be

$$\mathcal{X} = \{P_{\text{GR}}(k), P_{\text{IMP}}(k), P_{\text{BD}}(k), P_{\text{hvac}}(k), P_{\text{stor}}(k)\}_{k\in\mathcal{K}}, \tag{3.21}$$

such that $P_{\text{IMP}} = \{P_{\text{IMP}}^1, \dots, P_{\text{IMP}}^{n_d}\}$, $P_{\text{BD}} = \{P_{\text{BD}}^1, \dots, P_{\text{BD}}^{n_d}\}$. At each sampling time, we consider the objective function of BtG-MPC to be the holistic minimization of the frequency deviation, power generation, and total building load in the network for all time steps within the MPC prediction horizon, $k \in \mathcal{K}$:

$$\begin{aligned} J\big(x_t, \{x_d^i\}_{i\in\mathcal{D}}, \mathcal{X}\big) = \sum_{k\in\mathcal{K}} \Big[& x_t^\top(k) Q_t x_t(k) + \sum_{i=1}^{n_d} x_d^{i\top}(k) Q_d^i x_d^i(k) \\ & + P_{\text{GR}}^\top(k) Q_{\text{GR}} P_{\text{GR}}(k) + q_{\text{BD}}^\top P_{\text{BD}}(k)\Big], \end{aligned} \tag{3.22}$$

where Q_t and $\{Q_d^i\}_{i\in\mathcal{D}}$ are diagonal cost matrices of appropriate size for TSO and DSO frequency deviations, such that only the frequency entries are considered (i.e. voltage angle is left out). Furthermore, Q_{GR} is the diagonal cost matrix for power generation, and $q_{\text{BD}} \in \mathbb{R}^{n_b}$ is the vector of electricity costs. We are in a position to formulate the following optimization problem as a finite-horizon optimal control problem for each sampling time:

$$\underset{\mathcal{X}}{\text{minimize}} \qquad J\big(x_t, \{x_d^i\}_{i\in\mathcal{D}}, \mathcal{X}\big) \tag{3.23a}$$

Subject to, $\forall k \in \mathcal{K}$:

1. **TSO/DSO/BLD/storage Dynamics.** The system is subjected to the discretized dynamics of all physical areas of the network:

$$x_t(k+1) = f_t\big(x_t(k), P_{\text{GR}}(k+1), P_{\text{IMP}}(k+1), P_{\text{BL}}(k+1)\big), \tag{3.23b}$$
$$x_d^i(k+1) = f_d^i\big(x_d^i(k), P_{\text{IMP}}^i(k+1), P_{\text{BD}}^i(k+1), P_{\text{BL}}^i(k+1)\big), \qquad \forall i \in \mathcal{D} \tag{3.23c}$$
$$x_b(k+1) = f_b(x_b(k), P_{\text{hvac}}(k+1), w_g(k+1)) \tag{3.23d}$$
$$x_s(k+1) = \zeta x_s(k) + h\eta P_{\text{stor}}(k+1). \tag{3.23e}$$

2. **Generation power and ramp limits.** The generator power production is bounded by the upper and lower limits, $P_{\text{GR}}^{\min}$ and $P_{\text{GR}}^{\max}$, such that

$$P_{\text{GR}}^{\min} \leq P_{\text{GR}}(k+1) \leq P_{\text{GR}}^{\max}. \tag{3.23f}$$

Furthermore, the generators are bounded by the ramp-up and -down limits:

$$P_{\text{GR}}^{\text{down}} \leq P_{\text{GR}}(k+1) - P_{\text{k}}(k) \leq P_{\text{GR}}^{\text{up}}. \tag{3.23g}$$

3. **TSO network balance.** To achieve power balance in the TSO network, the following constraint is imposed:

$$\Big[\Gamma P_{\text{GR}}(k+1) - P_{\text{LD}}(k+1) - P_{\text{BL}}(k+1)\Big]^\top \mathbb{1}_{n_t} = 0 \tag{3.23h}$$

4. **DSO network balance.** Similarly, power balance in each DSO network $i \in \mathcal{D}$ is achieved through

$$\Big[P_{\text{LD}}^i(k+1) - \Pi^i P_{\text{BD}}^i(k+1) - P_{\text{BL}}^i(k+1)\Big]^\top \mathbb{1}_{n_d^i} = 0. \tag{3.23i}$$

5. **Building nodal power balance.** To achieve power balance in every building, all power injected should equal the HVAC, storage and miscellaneous load:

$$\sum_{i=1}^{n_d} P_{\text{BD}}^i(k+1) = P_{\text{hvac}}(k+1) + P_{\text{stor}}(k+1) + P_{\text{misc}}(k+1). \tag{3.23j}$$

6. **Building comfort limits.** The building zone temperature is bounded by predefined comfort limits, such that

$$x_b^{\min}(k+1) \leq x_b(k+1) \leq x_b^{\max}(k+1). \tag{3.23k}$$

7. **HVAC power and ramp limits.** The HVAC systems are bounded by power limits and ramp-up and -down limits, by imposing the following constraints:

$$P_{\text{hvac}}^{\min} \leq P_{\text{hvac}}(k+1) \leq P_{\text{hvac}}^{\max}, \tag{3.23l}$$

$$P_{\text{hvac}}^{\text{down}} \leq P_{\text{hvac}}(k+1) - P_{\text{hvac}}(k) \leq P_{\text{hvac}}^{\text{up}} \tag{3.23m}$$

8. **Buffer level and power storage limits.** The buffer level of the electrical storage and power stored are bounded by limit values, such that:

$$x_s^{\min} \leq x_s(k+1) \leq x_s^{\max} \tag{3.23n}$$

$$P_{\text{stor}}^{\min} \leq P_{\text{stor}}(k+1) \leq P_{\text{stor}}^{\max} \tag{3.23o}$$

The solution of the proposed BtG-MPC formulation is the optimal input sequence $\mathcal{X}^*$. Based on an MPC paradigm, the current input at time step k is implemented in the integrated system dynamics using the first element of the optimal solutions as

$$P_{\text{GR}}^*(k), P_{\text{IMP}}^*(k), P_{\text{BD}}^*(k), P_{\text{hvac}}^*(k), P_{\text{stor}}^*(k), \tag{3.24}$$

and we proceed in a receding horizon fashion with step width h. This means the BtG- acMPC formulation is solved at each time step $\hat{k} \in \mathcal{N}$ using the current measurement of the state variables $\{x_t, x_d, x_b, x_s\}$, and with the MPC prediction horizon set $\mathcal{K}$ starting at $k_0 = \hat{k}$.

3.7 Simulation study and test results

3.7.1 Simulation setup

To illustrate the functionality of the proposed integrated model dynamics for TSO-DSO-BLD setting and to demonstrate the grid regulative capacity of building HVAC and storage flexibility, we consider the following two possible scenarios as the test for our case study:

1. BtG-MPC optimization problem, with building storage flexibility *disabled*. This is achieved by letting the storage power limits be $P_{\text{stor}}^{\min} = P_{\text{stor}}^{\max} = 0$. Hence, the BtG-MPC is solved, without the constraints related to the building storage units.

2. BtG-MPC optimization problem, with building storage flexibility *enabled*. Each building is equipped with the equivalent of four Tesla Model S batteries (Tesla, 2018), i.e. $x_s^{\min} = 2\text{kWh}$ and $x_s^{\max} = 400\text{kWh}$, constrained by $P_{\text{stor}}^{\min} = -0.2\text{MW}$ and $P_{\text{stor}}^{\max} = 2\text{MW}$. Furthermore, the initial storage level is constrained by $x_s(t_0) = 50\text{kWh}$.

The BtG-MPC is formulated in an iterative manner with respect to the prediction time steps $k \in \mathcal{K}$. However, to improve computational performance of the code, a stacked formulation was implemented in the MATLAB code. Instead of calculating the state of the system iteratively over time, the trajectory is directly calculated over the complete prediction horizon. The full derivation of the stacked MPC implementation is provided in Appendix B.

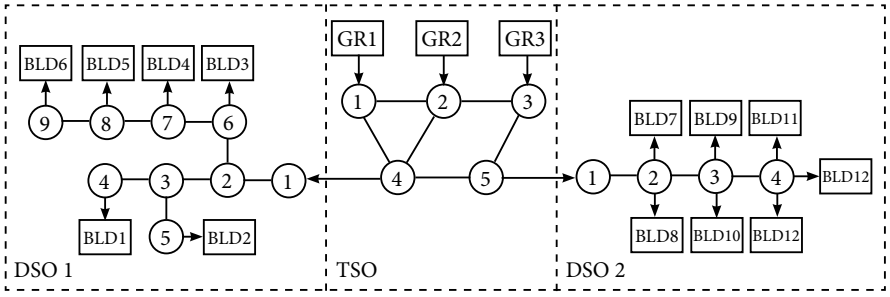

Figure 3.3: Network topology of the MPC problem.

Appropriate cost values are determined qualitatively such that all respective elements are reflected in the outcomes of the simulation study. Costs for both scenarios are valued at $Q_t = Q_d^i = 1000\,\$/\mathrm{rad}^2$, $Q_{\mathrm{GR}} = 50\,\$/\mathrm{kW}^2$, and $q_{\mathrm{BD}} = 50\,\$/\mathrm{kW}$. All scenarios were simulated for 24 hours ($T_{\mathrm{end}} = 86\,400\,\mathrm{s}$) with prediction horizon $T_p = 1$ hours and step width $h = 5$ minutes, on the case study network given in Figure 3.3, consisting of 1 TSO, 3 Generators (GRs), 2 DSOs, and 13 Buildings (BLDs).

Simulations were implemented in MATLAB, with Yalmip as interface (Lofberg, 2004) and Gurobi as solver (Gurobi Optimization, LLC, 2019). Building parameters and non-controllable loads were adopted from Taha et al. (2019), and grid parameters were obtained from MatPower IEEE 5-bus power system (Zimmerman et al., 2011). The full overview of simulation parameters is listed in Appendix C.

3.7.2 Simulation results

Computational time of the simulation codes averaged around 3 minutes. The resulting network frequency deviations, building storage state, and average building power load for both scenarios over the 24 hour simulation horizon are presented in Figure 3.4. In general, grid frequency deviations are caused by sudden changes in power loads and flows, as reflected in the swing equations in Eqs. (3.2) and (3.10). For Scenario 2, a reduction in grid frequency deviation is observed compared to Scenario 1, as reflected between Figure 3.4a and Figure 3.4b. As shown in Figure 3.4d, the scenario with storage employs the flexibility to decrease the ramp up/down in building grid load, when HVAC power is required or miscellaneous loads are increased. In particular, the storage flexibility is used to compensate for variations in building-side loads, resulting in a smoother building load to the grid. Consequently, grid frequency deviations spike significantly (e.g. between 4:00 and 9:00) for Scenario 1 (Figure 3.4a, especially in the DSO networks), whereas they appear more smooth for Scenario 2 (Figure 3.4b).

Around 20:00, the maximum allowable building temperature ($x_b^{\max}$) increases from 23 to 25 °C. As no cooling power is required anymore, building HVAC load is reduced, and spikes in the frequency deviation for Scenario 1 are apparent. For Scenario 2, the storage buffer damps the ramp down in building load, as depicted in Figure 3.4d. This leads to improved stability of the frequency, as reflected in the swing equation, and verified by inspection from the results.

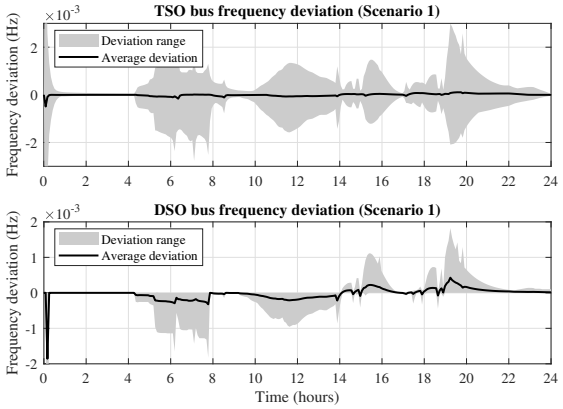

(a) Scenario 1 - Bus frequencies in the TSO and DSO networks

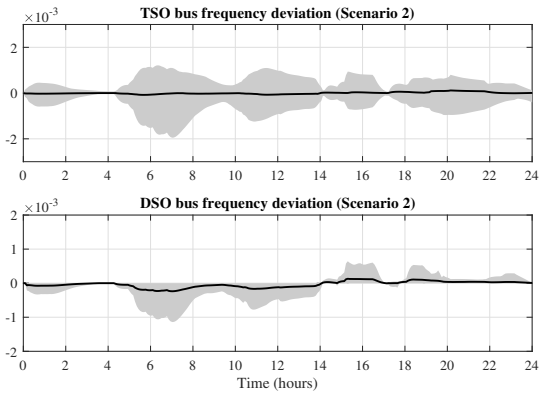

(b) Scenario 2 - Bus frequencies in the TSO and DSO networks

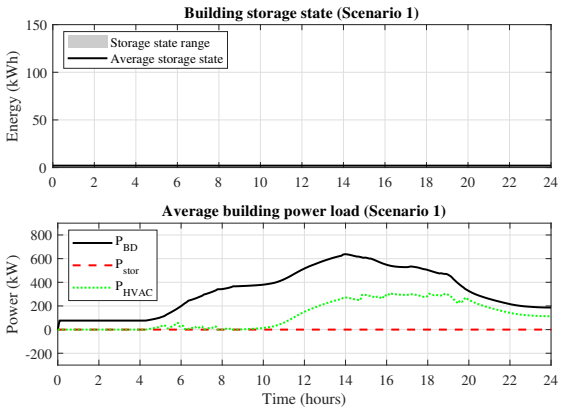

(c) Scenario 1 - Building storage state and average building power injections

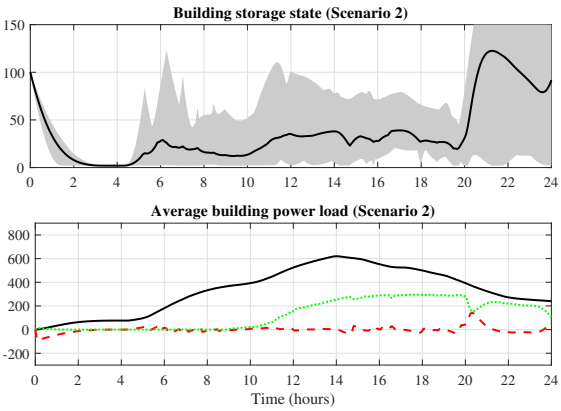

(d) Scenario 2 - Building storage state and average building power injections

Figure 3.4: Results of the case study for both BtG-MPC scenarios. Figures show the frequency deviation in the TSO and DSO networks, storage state, and average building power injections over the simulation time of 24 hours.

The dampening effect of the building storage units on the ramp up and down of building flexibility P_{BD} is particularly visible when isolating the nodal power balance of an individual building, as in Figure 3.5 for building 2. The miscellaneous load P_{misc} increases significantly around 8:30. In Case 1, this results in a step-function increase of the building load P_{BD}, instantaneously increasing the power demand from 100 kW to around 330 kW, as depicted in Figure 3.5a. However, in Case 2, the storage units are exploited to avoid this instantaneous increase in building load, as visualized in Figure 3.5b. By charging the battery before the step increase of P_{misc}, and discharging it shortly after, P_{BD} increases smoothly over the course of about 2 hours. Although the HVAC system contributes to a small regulative capability as well in the case of reducing load ramp up, it cannot deal with ramp down if $P_{\mathrm{HVAC}} = 0$, because is cannot be negative.

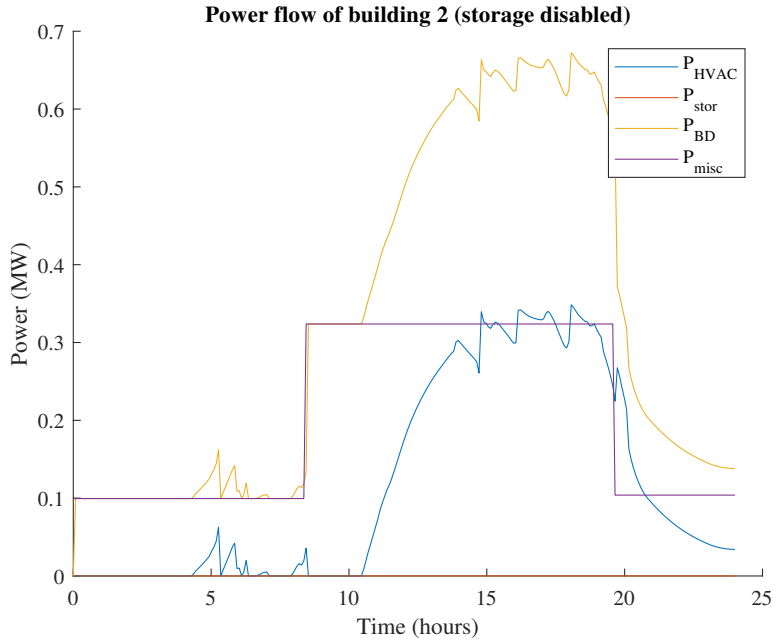

(a) Scenario 1 - Power balance of building 2 with storage units disabled

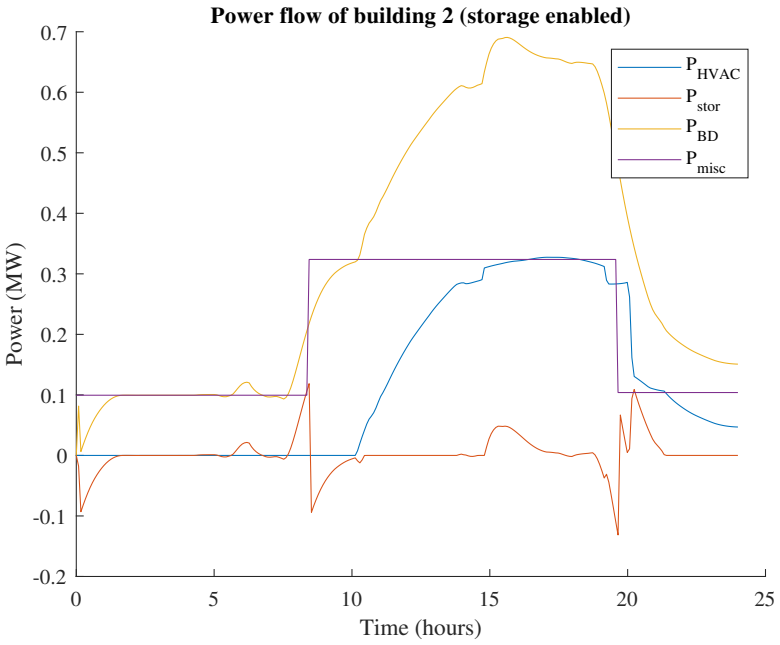

(b) Scenario 2 - Power balance of building 2 with storage units enabled

Figure 3.5: Nodal power balance of building 2 for BtG-MPC scenarios, indicating the balance between building load to the grid (P_{BD}), HVAC power (P_{HVAC}), storage power (P_{stor}) and the miscellaneous load (P_{misc}).

The obtained value of the closed-loop cost function over the simulation time for Scenario 1 is $3165.10\$$ and $2681.41\$$ for Scenario 2, yielding a reduction of 15.3% in cumulative cost function. Total grid frequency deviations were calculated as follows:

$$\omega_{\text{dev}} = \sum_{k \in \mathcal{N}} \left[x_t^\top(k) Z_t x_t(k) + \sum_{i=1}^{n_d} x_d^{i\top}(k) Z_d^i x_d^i(k) \right], \tag{3.25}$$

where Z_t and Z_d^i are diagonal matrices such that only voltage angle is considered. Compared to Scenario 1, total grid frequency deviations for Scenario 2 are reduced by 49.87% in the full network, and by 64.17% in the DSO networks alone.

3.8 Conclusion

In this chapter, we addressed *research questions 2 and 3*, and developed a dynamical BtG framework with explicit hierarchical interactions between TSO, DSO, and buildings with dedicated energy storage units. Using such a developed model, we proposed a centralized MPC framework to demonstrate the potential role of individual buildings in frequency control of the power system, by introducing electrical energy storage units in the BtG framework. We would like to stress the flexibility of the developed framework, as that it can easily be extended to other settings, without loss of generality. Based on the results obtained for the IEEE benchmark case study, we showed that building-side storage flexibility has significant regulative capacity for the grid (grid frequency deviations are decreased by 49.87% in the full network, and by 64.17% for the DSO specifically) when building and grid decision-making is coupled.

The contents of this chapter of the thesis are to be published in Badings et al. (2019), and will be presented during the Workshop on Control of Smart Grids and Renewable Energy Sources (CSGRES2019), organized by the International Federation of Automatic Control (IFAC) in June 2019, Korea (IFAC, 2019).

4 Buildings-to-Grid Integration with High Wind Power Penetration

4.1 Introduction

The centralized BtG-MPC developed in Chapter 3 can be applied for optimal frequency control in fully deterministic systems, in which power generation and loads are both exactly known beforehand. However, a different approach is required to drive the system to stability if uncertain power generation is apparent. In this chapter, we address this issue by extending the BtG framework proposed in the previous chapter with uncertain generation from wind farms. Demand-side flexibility is proposed as an alternative form of short-term operating reserve to compensate for the uncertain generation, without losing stability properties of the power grid and violating the buildings desired thermal comfort. In the long run, demand-side flexibility may have less environmental impact (Lin et al., 2015) and lower costs (Lymperopoulos et al., 2015) than traditional reserve.

In the remainder of this chapter, the corresponding extended control problem is referred to as w-BtG-MPC, to indicate the wind-integrated system. The remainder of this chapter is organized as follows. First of all, we integrate wind power in the TSO dynamics, and introduce a wind power model to generate realistic scenarios, while taking its temporal correlation into account. We discuss the common practice of deploying reserve power to compensate for wind power errors. Thereafter, we present a novel formulation for demand-side flexibility of buildings to be deployed as an ancillary service to handle uncertain wind power in the network. Finally, the w-BtG-MPC framework is developed, which utilizes reserve scheduling and distributed building flexibility power to compensate for highly fluctuating wind power in the network.

4.2 Wind-integrated TSO dynamics

In this section, the framework developed in Chapter 3 is extended to allow injection of distributed wind power in the TSO network. Most wind power generation is geographically distributed (Larsen, 2014). Depending on its magnitude of generation, wind generation is typically connected to the sub-transmission grid, or to the distribution network (Cabadag et al., 2015; Stock et al., 2018). In the scope of this study, we consider wind power generation in one location, which is connected to the lower TSO network, near the TSO-DSO interface, instead of directly to the same location as the synchronous generators.

Similar to the set of generators, define $\mathcal{F} = \{1, ..., n_w\}$ as the set of wind farms, and let the power generated be denoted by the vector $P_w(t) \in \mathbb{R}^{n_w}$. Without loss of generality, it is assumed that P_w is a realization of an unknown stochastic process defined on some probability space $(\mathcal{W}, \mathfrak{B}(\mathcal{W}), \mathbb{P})$. It is important to note that we do note require the sample space $\mathcal{W}$ and the probability measure $\mathbb{P}$ to be known explicitly, as will be explained later. We only need a

finite number of realizations of the uncertainty P_w, and it is sufficient to consider that they are independent and identically distributed. In the current study, we limit ourselves to **integration of one wind farm**. As explained in Section 4.5, this is a necessary condition for the scenario approach, which is used to formulate a tractable MPC program. However, we stress the fact that the modeling framework itself is easily extended to integration of multiple wind farms.

Wind farms are connected to TSO nodes through incidence matrix $\Upsilon \in \mathbb{R}^{n_t \times n_w}$, with entries given by

$$\upsilon_{l,n} = \begin{cases} 1 & \text{if wind farm } n \text{ is attached to TSO node } l, \\ 0 & \text{otherwise.} \end{cases} \tag{4.1}$$

As wind is variable, the wind power generation suffers from uncertainty and limited predictability (Kargarian et al., 2016). To account for this, define a separate variable $P_w^f(t) \in \mathbb{R}^{n_w}$ for the forecast value of the wind power, and denote the error between the two by

$$\Delta P_w(t) = P_w(t) - P_w^f(t). \tag{4.2}$$

Since solidifying power dispatch is done on a *day-ahead* basis (Doddema, 2015), only the wind forecast value, $P_w^f(t)$, is available in the scheduling process. To account for wind power forecast in the power dispatch, we modify the discrete TSO predicted dynamics in Eq. (3.20a) and network balance constraint in Eq. (3.23j) as follows:

$$\begin{aligned} x_{t_f}(k+1) = &\big(E_t - hA_t'\big)^{-1}\Big[E_t x_{t_f}(k) + h\big(B_{\text{GR}} P_{\text{GR}}(k+1) \\ &+ B_t\big(\underbrace{\Upsilon P_w^f(k+1)}_{\text{wind power forecast}} - P_{\text{LD}}(k+1) - P_{\text{BL}}(k+1)\big)\big)\Big], \end{aligned} \tag{4.3}$$

$$\Big[\Gamma P_{\text{GR}}(k+1) + \underbrace{\Upsilon P_w^f(k+1)}_{\text{wind power forecast}} - P_{\text{LD}}(k+1) - P_{\text{BL}}(k+1)\Big]^\top \mathbb{1}_{n_t} = 0, \tag{4.4}$$

where we inserted the term $\Upsilon P_w^f(k+1)$ for the forecasted wind power injection. We slightly renamed the TSO state variable to x_{t_f} to indicate that it is the expected trajectory, based on the wind forecast P_w^f. The new balance constraint, Eq. (4.4), takes the wind power forecast into consideration, and enforces network balance in the TSO power dispatch.

In the case of perfect wind power forecast, $\Delta P_w(t) = 0$, and no intervention is needed to compensate for any wind forecast error. However, if $\Delta P_w(t) \neq 0$, additional intervention is required to compensate for errors in the power dispatch. In such a case, compensation is required from other assets in the system, called ancillary services. As explained in the next section, the two types of ancillary services considered in this study are **reserve scheduling**, and **building-side flexibility**.

4.3 Ancillary service deployment

In order to maximize stability and minimize frequency deviations in the TSO network, operators always strive to satisfy the general power balance:

$$\sum_{i\in\mathcal{G}} P_{\text{GR}_i}(k)+\sum_{m\in\mathcal{F}} P_{w_m}(k) = \sum_{i\in\mathcal{G}} P_{\text{GR}_i}(k)+\sum_{m\in\mathcal{F}} \big(P^f_{w_m}(k)+\Delta P_{w_i}(k)\big) = \sum_{l\in\mathcal{B}} P_{\text{BD}_l}(k), \quad (4.5)$$

where $P_{\text{GR}}(k)$, $P_w(k)$, and $P_{\text{BD}}(k)$ are the power generation from generators, generation from wind power, and power demand, respectively at time step k. The TSO schedules its power dispatch according to the wind power forecast, P^f_w. In the case of any wind power forecast error, $\Delta P_w(t) \neq 0$, and balance in the network is not anymore satisfied. In the remainder of this section, we first describe the common practice in the TSO network to deal with highly fluctuating wind power integration, the so-called reserve scheduling service, and then present a novel formulation for buildings demand flexibility to be deployed as an ancillary service to handle uncertain wind power in the system.

4.3.1 Reserve scheduling formulation

In the case of wind power errors, the common practice to restore power balance is to deploy so-called reserve power. By adjusting the generator power output, deviations from P^f_w can be compensated with altered generation. Reserve power dispatch in the power flow equations is indicated with the letter $R \in \mathbb{R}^{n_g}$. Increasing the generator output is called *up-spinning* reserve ($R^{\text{us}} > 0$), and decreasing the output is *down-spinning* reserve ($R^{\text{ds}} > 0$).

In this section, we follow an approach similar to Rostampour et al. (2019c), for formulation of reserve scheduling in the BtG framework. Consider the following definition to determine the reserve power required to compensate for the wind power error:

$$-\sum_{i\in\mathcal{G}} R_i(k) = \max\Big(\sum_{m\in\mathcal{F}} \Delta P_{w_m}(k), 0\Big) + \min\Big(\sum_{m\in\mathcal{F}} \Delta P_{w_m}(k), 0\Big). \quad (4.6)$$

Then, the reserve power scheduling bounds, $R^{\text{ds}}(k)$ and $R^{\text{us}}(k)$ at each time step k are given by

$$-R^{\text{ds}}(k) \leq R(k) \leq R^{\text{us}}(k). \quad (4.7)$$

Note that the new scheduled power should also satisfy the generation limits, i.e.,

$$P^{\min}_{\text{GR}} \leq P_{\text{GR}}(k) + R(k) \leq P^{\max}_{\text{GR}}. \quad (4.8)$$

It is important to note the difference between reserve *scheduling* and the actual *dispatch* (or *deployment*). Reserve scheduling (R^{ds} and R^{us}) relates to the back-up plan that is made to

schedule an appropriate buffer to counteract possible wind power deviations. Reserve dispatch (R) is the actual portion of the schedule that is injected in the power grid.

4.3.2 Building flexibility formulation

Flexibility is defined as the capability of shifting production or consumption of energy in time, while satisfying end-user comfort requirements, and without changing the total energy production or consumption (Roossien, 2011). For example, a smart washing machine can provide flexibility by delaying operation, but only within a given time frame to ensure user comfort requirements (Kramer, 2015). By adjusting the power demand, deviations from P_w^f can be compensated with flexible loads (MacDougall et al., 2013). Flexibility power dispatch in the power flow equations is indicated with the letter $S \in \mathbb{R}^{n_b}$. Increasing power load is called *increased-demand* flexibility ($S^{\text{id}} > 0$), and decreasing load is *decreased-demand* flexibility ($S^{\text{dd}} > 0$).

Similar to the reserve scheduling formulation in Eq. (4.6), we define the building flexibility to be

$$\sum_{i \in \mathcal{B}} S_l(k) = \max\Big(\sum_{m \in \mathcal{F}} \Delta P_{w_m}(k), 0\Big) + \min\Big(\sum_{m \in \mathcal{F}} \Delta P_{w_m}(k), 0\Big), \tag{4.9}$$

while determining $S^{\text{dd}}(k)$ and $S^{\text{id}}(k)$ at each time step k by

$$-S^{\text{dd}}(k) \leq S(k) \leq S^{\text{id}}(k). \tag{4.10}$$

In the scope of this study, we consider the flexibility contribution to the grid of individual buildings in the network, via two sources: (1) *building storage systems*, and (2) *building HVAC loads*, which yields the following bounds on flexibility at time step k:

$$-S^{\text{dd}}_{\text{stor}}(k) - S^{\text{dd}}_{\text{hvac}}(k) \leq S(k) \leq S^{\text{id}}_{\text{stor}}(k) + S^{\text{id}}_{\text{hvac}}(k), \tag{4.11}$$

where $S^{\text{dd}}_{\text{stor}}(k)$, $S^{\text{dd}}_{\text{hvac}}(k)$, $S^{\text{id}}_{\text{stor}}(k)$, and $S^{\text{id}}_{\text{hvac}}(k)$ represent the increased- and decreased-demand flexibility using the storage unit and HVAC load, respectively.

4.3.3 Reserve scheduling together with building flexibility

Including reserve together with flexibility in the TSO power balance yields

$$\sum_{i \in \mathcal{G}} \big(P_{\text{GR}_i}(k) + R_i(k)\big) + \sum_{m \in \mathcal{F}} \big(P^f_{w_m}(k) + \Delta P_{w_m}(k)\big) = \sum_{l \in \mathcal{B}} \big(P_{\text{BD}_l}(k) + S_l(k)\big), \tag{4.12}$$

where the sum of reserve and flexibility should compensate the total wind power mismatch:

$$\sum_{i\in\mathcal{G}} R_i(k) - \sum_{i\in\mathcal{B}} S(k) = \max\Big(\sum_{m\in\mathcal{F}} \Delta P_{w_m}(k), 0\Big) + \min\Big(\sum_{m\in\mathcal{F}} \Delta P_{w_m}(k), 0\Big). \tag{4.13}$$

Taking into consideration Eq. (4.11), the following constraint encodes that the scheduled reserve and flexibility is always sufficient to compensate the wind power error:

$$-\sum_{i\in\mathcal{G}} R_i^{\text{us}}(k) - \sum_{l\in\mathcal{B}} S_l^{\text{dd}}(k) \leq \max\Big(\sum_{m\in\mathcal{F}} (P_{w_m}(k) - P_{w_m}^f(k)), 0\Big) + \tag{4.14}$$
$$\min\Big(\sum_{m\in\mathcal{F}} (P_{w_m}(k) - P_{w_m}^f(k)), 0\Big) \leq \sum_{i\in\mathcal{G}} R_i^{\text{ds}}(k) + \sum_{l\in\mathcal{B}} S_l^{\text{id}}(k)$$

4.3.4 Reserve and flexibility dispatch dynamics

To account for reserve and flexibility power dispatch in the TSO network, we modify the discrete TSO dynamics in Eq. (3.20a) as follows:

$$\begin{aligned} x_t(k+1) = \big(E_t - hA_t'\big)^{-1}\Big[E_t x_t(k) + h\big(B_{\text{GR}}(P_{\text{GR}}(k+1) + \overbrace{R(k+1)}^{\text{reserve dispatch}}) \\ + B_t\big(\underbrace{\Upsilon P_w(k+1)}_{\text{wind power injection}} - P_{\text{LD}}(k+1) - \underbrace{S_{\text{LD}}(k+1)}_{\text{flexibility dispatch}} - P_{\text{BL}}(k+1)\big)\big)\Big], \end{aligned} \tag{4.15}$$

where we introduced the flexibility power exchange term, $S_{\text{LD}}(k)$, which accounts for the portion of the power exchange with DSO related with building flexibility. Similar to the conventional TSO-DSO power exchange $P_{\text{LD}}(k)$, we define the following expressions for flexibility power exchange in both directions:

$$S_{\text{LD}}(k+1) = \sum_{i=1}^{n_d} \Big[\big(\Phi^i \circ S_{\text{IMP}}^i(k+1)\big)\mathbb{1}_{n_d^i}\Big], \tag{4.16}$$

$$S_{\text{LD}}^i(k+1) = \big(\Phi^i \circ S_{\text{IMP}}^i(k+1)\big)^\top \mathbb{1}_{n_t}, \tag{4.17}$$

where $S_{\text{IMP}}^i \in \mathbb{R}^{n_t \times n_d^i}$ is the flexibility power exchange matrix between TSO and DSO i, with entry $S_{k,l}^i$ representing the power transmission from TSO node k to node l of DSO i. The addition of this flexibility exchange term is necessary, because $P_{\text{LD}}(k)$ is already utilized to enforce TSO network balance in Eq. (4.4).

In order to integrate building flexibility power in the model, we introduce a new building power flow variable $S_{\text{BD}}^i(k)$ for each DSO i, which is positioned in parallel with the conventional

building demand variable $P^i_{\text{BD}}(k)$. Then, the discrete DSO dynamics in Eq. (3.20b) are extended as follows:

$$x^i_d(k+1) = \big(E^i_d - hA'^i_d\big)^{-1}\Big[E^i_d x^i_d(k) + hB^i_d\big(P^i_{\text{LD}}(k+1) + \overbrace{S^i_{\text{LD}}(k+1)}^{\text{flexibility dispatch}} - P^i_{\text{BD}}(k+1) - \underbrace{S^i_{\text{BD}}(k+1)}_{\text{building flexibility}} - P^i_{\text{BL}}(k+1)\big)\Big], \tag{4.18}$$

and the DSO-to-building power exchange interface is defined as follows to distribute the contributions of flexibility power at the building level:

$$\overbrace{S^i_{\text{BD}}(k+1)}^{\text{building flexibility}} = \big[S^i_{\text{BD}_1}(k+1), \ldots, S^i_{\text{BD}_{n^i_d}}(k+1)\big]^\top = \Pi^i\big(\underbrace{S_{\text{stor}}(k+1)}_{\text{storage flexibility}} + \underbrace{S_{\text{hvac}}(k+1)}_{\text{HVAC flexibility}}\big),$$

where $S^i_{\text{BD}_l}$ is the flexibility contribution of building l. As we need to consider the impact of flexibility power on the building dynamics, the building dynamics in Eq. (3.20c) are modified as

$$x_b(k+1) = \big(I_{2n_b} - hA_b\big)^{-1}\Big[x_b(k) + h\big(B_p(P_{\text{hvac}}(k+1) + S_{\text{hvac}}(k+1)) + B_{w_b}w_b(k+1)\big)\Big]. \tag{4.19}$$

Finally, the storage dynamics in Eq. (3.16) are modified as follows:

$$x_s(k+1) = \zeta x_s(k) + h\eta\big[P_{\text{stor}}(k+1) + S_{\text{stor}}(k+1)\big]. \tag{4.20}$$

4.4 w-BtG-MPC optimal control framework

In this section, the extended w-BtG-MPC optimization problem is formulated, in which reserve and building flexibility power are utilized to compensate for wind power forecast errors in the wind-integrated BtG framework. The scenario approach is proposed to deal with the wind power uncertainty in the optimization problem, and the corresponding Scenario Convex Program (SCP) is formulated. The theoretical background of the scenario approach is provided in the preliminaries in Section 2.5.

Similar to the BtG-MPC in Chapter 3, we follow the set of prediction time steps $\mathcal{K} = \{k_0, k_0 + 1, \ldots, k_0 + \frac{T_p}{h} - 1\}$, where k_0 is the MPC starting time step, T_p is the MPC prediction time horizon, and h the simulation time step. Similarly, define the set of simulation study time steps $\mathcal{N} = \{0, 1, \ldots, \frac{T_{\text{end}}}{h} - 1\}$, where T_{end} is the end time of the simulation study, and denote the

number of simulation time steps by $N_{\text{sim}} = |\mathcal{N}| = \frac{T_{\text{end}}}{h}$. To render the problem convex, we also follow the power flow approximations as discussed in subsection 2.3.3, and discretize the modified TSO, DSO and BLD dynamics for all time steps $k \in \mathcal{N}$ using the same technique as in Chapter 3. Define the set of decision variables to be

$$\begin{aligned}\mathcal{X}_w = \big\{ & P_{\text{GR}}(k), P_{\text{IMP}}(k), P_{\text{BD}}(k), P_{\text{hvac}}(k), P_{\text{stor}}(k), R^{\text{us}}(k), R^{\text{ds}}(k), \\ & S^{\text{id}}_{\text{hvac}}(k), S^{\text{dd}}_{\text{hvac}}(k), S^{\text{id}}_{\text{stor}}(k), S^{\text{dd}}_{\text{stor}}(k) \big\}_{k \in \mathcal{K}},\end{aligned} \tag{4.21}$$

The first five terms (P_{GR} to P_{stor}) are equivalent as in the optimization in Chapter 3, whereas the other terms represent the scheduling and dispatch of reserves and flexibility. In the next section, a realistic wind power model is introduced, which is used to generate different wind power trajectories based on historical data. Finally, the BtG-MPC developed in Chapter 3 is reformulated into the w-BtG-MPC, by modifying the cost function and imposing additional constraints.

4.4.1 Wind power model

In the scope of this study, we only consider the random variable *wind power*, instead of the random variable *wind speed*. The wind turbine static power curves that relate wind speed and power are nonlinear, and mapping is only achieved within the standard working range of the wind speed (Papaefthymiou and Klöckl, 2008). For wind speeds above this range, the power is curtailed to the nominal power, and below the minimum wind speed, no power is generated at all. Consequently, the distribution of the wind power has higher probability mass at the upper and lower ends on the power axis, corresponding to the nominal (curtailed) and zero output power (Papaefthymiou et al., 2006). As we are mainly interested in the generated power, the wind power data presents a simpler model with less states than the wind speed, because the latter contains unnecessary information in both extreme conditions.

Based on the work of Rostampour (2012), we use a wind power model that generates scenarios of the wind power and the corresponding error, $\Delta P_w(t)$, while taking its temporal correlation into account. The wind power forecast, actual wind power, and error between the two were discretized, to construct a Markov Chain model, which is capable of generating realistic wind power trajectories based on different error realizations, as depicted in Figure 4.1. The model was successfully used to integrate stochastic generation in power systems (Margellos et al., 2012). However, the authors explicitly mentioned that no frequency control action was considered, whereas this is in fact one of the key aspects of the current research. The Markov Chain transition matrix corresponding to this wind power model is utilized to generate appropriate wind power data to be used in the w-BtG-MPC developed in this chapter.

4.4.2 Expected cost function

At each sampling time, we consider the objective function of w-BtG-MPC to be the holistic minimization of the frequency deviation, power generation, HVAC usage, and reserve and flexibility in the network, for all time steps within the MPC prediction horizon, $k \in \mathcal{K}$. Consider the

vector of uncertainty within the MPC prediction horizon to be $\mathsf{P}_{w_k} := [P_w(k)_{k\in\mathcal{K}}]$. Define Q_t, $\{Q_d^i\}_{i\in\mathcal{D}}$, Q_{GR}, and Q_{hvac} as diagonal matrices with elements to be costs associated for the TSO and DSO states, power generation, and HVAC power usage, respectively. Furthermore, q_{S}^{id}, q_{S}^{dd}, q_{R}^{us}, and q_{R}^{ds} are the vector of costs related to increased- and decreased-demand, up- and down-spinning reserves, respectively. The cost function is then formulated for all time steps within the MPC prediction horizon, $k \in \mathcal{K}$, as follows:

$$\begin{aligned}\tilde{J}_w\big(x_t, x_d^i, \mathcal{X}_w, \mathsf{P}_{w_k}\big) = \sum_{k\in\mathcal{K}} \Big[& x_t^\top(k) Q_t x_t(k) + \sum_{i=1}^{n_d} x_d^{i\top}(k) Q_d^i x_d^i(k) \\ & + P_{\text{GR}}^\top(k) Q_{\text{GR}} P_{\text{GR}}(k) + P_{\text{hvac}}^\top(k) Q_{\text{hvac}} P_{\text{hvac}}(k) \\ & + (q_S^{\text{id}})^\top (S_{\text{stor}}^{\text{id}}(k) + S_{\text{hvac}}^{\text{id}}(k)) + (q_S^{\text{dd}})^\top (S_{\text{stor}}^{\text{dd}}(k) + S_{\text{hvac}}^{\text{dd}}(k)) \\ & + (q_R^{\text{us}})^\top R^{\text{us}}(k) + (q_R^{\text{ds}})^\top R^{\text{ds}}(k) \Big]\end{aligned} \tag{4.22}$$

As discussed in Section 2.5, the cost function $\tilde{J}_w(x_t, x_d^i, \mathcal{X}_w, \mathsf{P}_{w_k})$ is a random variable due to the uncertain TSO and DSO state variables, and thus, we consider the following estimation of the cost function:

$$J_w\big(x_t, \{x_d^i\}_{i\in\mathcal{D}}, \mathcal{X}_w\big) := \mathbb{E}\Big[\tilde{J}_w\big(x_t, \{x_d^i\}_{i\in\mathcal{D}}, \mathcal{X}_w, \mathsf{P}_{w_k}\big)\Big]. \tag{4.23}$$

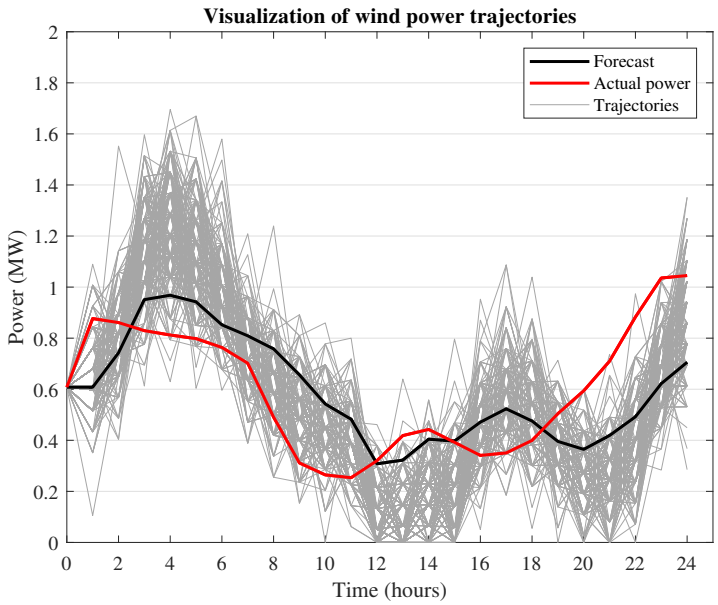

Figure 4.1: The forecasted and actual wind power, and 300 wind power trajectories, generated by the Markov Chain-based wind power model.

The new objective is a deterministic cost function, which can be approximated empirically using a set $\mathbb{W}^J \in \mathbb{R}^{N_s^j \times |\mathcal{K}|}$ of wind power trajectories extracted from the Markov Chain model, which is defined as follows:

$$\begin{aligned} \mathbb{W}^J &= \{P_w^{j,1}, P_w^{j,2}, \dots, P_w^{j,N_s^j}\}, \\ P_w^{j,1} &= P_w^f, \end{aligned} \tag{4.24}$$

where $P_w^{j,i}$ are wind power realizations from the Markov Chain model. Hence, set $\mathbb{W}^J$ contains N_s^j wind trajectories, which all span the full MPC prediction time, containing $|\mathcal{K}| = \frac{T_p}{h}$ time steps (wind power values). Furthermore, the wind power forecast P_w^f is always enclosed in $\mathbb{W}^J$. By averaging the value of Eq. (4.22) for different realizations of the uncertain variable, N_s^j plays a tuning parameter role in Eq. (4.23).

4.4.3 Line limit constraints

In order to prevent congestion of lines, we are also interested in TSO and DSO line limit constraints[1]. As power flow between two buses is characterized by the difference in voltage angle and the susceptance of the line, we need to impose a constraint that relates these variables to the line limits. To this end, let $\mathcal{L}_t$ and $\mathcal{L}_d^i$ be the sets of lines in the TSO and DSO i network. Define the Laplacian matrices $L^{\text{TSO}} \in \mathbb{R}^{|\mathcal{L}_t| \times n_t}$ for the TSO network and $L^{\text{DSO},i} \in \mathbb{R}^{|\mathcal{L}_d^i| \times n_d^i}$ for DSO network i, with entries defined by:

$$L_{kj}^{\text{TSO}} = \begin{cases} \sum_{m \in \mathcal{T}_k^n} [-b_{km}] & \text{if } k = j, \\ b_{kj} & \text{if } k \neq j \text{ and } j \in \mathcal{T}_k^n, \\ 0 & \text{otherwise.} \end{cases} \tag{4.25}$$

$$L_{lj}^{\text{DSO},i} = \begin{cases} \sum_{m \in \mathcal{D}_l^{n,i}} [-b_{lm}^i] & \text{if } l = j, \\ b_{lj}^i & \text{if } l \neq j \text{ and } j \in \mathcal{T}_l^n, \\ 0 & \text{otherwise.} \end{cases} \tag{4.26}$$

As we are only interested in the voltage angles, we can now construct the augmented matrices $\tilde{L}^{\text{TSO}}$ and $\tilde{L}^{\text{DSO},i}$ which are used to obtain the power flow in the TSO and DSO network lines:

$$\tilde{L}^{\text{TSO}} = \begin{bmatrix} \mathrm{L}^{\text{TSO}} & \mathbb{0}_{n_t \times n_t} \\ \mathbb{0}_{n_t \times n_t} & \mathbb{0}_{n_t \times n_t} \end{bmatrix}, \qquad \tilde{L}^{\text{DSO},i} = \begin{bmatrix} \mathrm{L}^{\text{DSO},i} & \mathbb{0}_{n_d^i \times n_d^i} \\ \mathbb{0}_{n_d^i \times n_d^i} & \mathbb{0}_{n_d^i \times n_d^i} \end{bmatrix} \tag{4.27}$$

[1]Note that line limit constraints were not imposed for the BtG-MPC in Chapter 3.

4.4.4 Probabilistic constraints

To capture the uncertain wind power generation in the w-BtG-MPC, we formulate the Chance Constrainted Program (CCP) of the stochastic optimization model, as defined in Section 2.5. As both reserve and flexibility power are related to the uncertain wind power generation, the probabilistic constraint is formulated as (DSO constraints are imposed for all $i \in \mathcal{D}$, and for brevity, time variables are partially omitted):

$$
\begin{aligned}
\mathbb{P}\Bigg(\; \mathsf{P}_{w_k} \in \mathcal{W} \;\Big|\; & x_t(k+1) = f_t\big(x_t, \Delta P_w, P_{\text{GR}}, R, P_{\text{IMP}}, S_{\text{IMP}}, P_{\text{BL}}\big), && \text{(4.28a)}\\
& x_d^i(k+1) = f_d^i\big(x_d^i, P_{\text{IMP}}^i, S_{\text{IMP}}^i, P_{\text{BD}}^i, S_{\text{BD}}^i, P_{\text{BL}}^i\big), && \text{(4.28b)}\\
& x_b(k+1) = f_b(x_b, P_{\text{hvac}}, S_{\text{hvac}}, w_g), && \text{(4.28c)}\\
& x_s(k+1) = \zeta x_s(k) + h\eta\big[P_{\text{stor}}(k+1) + S_{\text{stor}}(k+1)\big], && \text{(4.28d)}\\
& P_{\text{GR}}^{\min} \leq P_{\text{GR}}(k+1) + R(k+1) \leq P_{\text{GR}}^{\max}, && \text{(4.28e)}\\
& P_{\text{GR}}^{\text{down}} \leq P_{\text{GR}}(k+1) + R(k+1) - \big[P_{\text{GR}}(k) + R(k)\big] \leq P_{\text{GR}}^{\text{up}}, && \text{(4.28f)}\\
& L^{\min} \leq \tilde{L}^{\text{TSO}}\big[x_t(k+1)\big] \leq L^{\max}, && \text{(4.28g)}\\
& L^{i,\min} \leq \tilde{L}^{\text{DSO},i}\big[x_d^i(k+1)\big] \leq L^{i,\max}, && \text{(4.28h)}\\
& x_b^{\min} \leq x_b(k+1) \leq x_b^{\max}, && \text{(4.28i)}\\
& \sum_{i=1}^{n_d} \Big[S_{\text{BD}}^i(k+1)\Big] = S_{\text{hvac}}(k+1) + S_{\text{stor}}(k+1), && \text{(4.28j)}\\
& P_{\text{hvac}}^{\min} \leq P_{\text{hvac}}(k+1) + S_{\text{hvac}}(k+1) \leq P_{\text{hvac}}^{\max}, && \text{(4.28k)}\\
& P_{\text{hvac}}^{\text{down}} \leq P_{\text{hvac}}(k+1) + S_{\text{hvac}}(k+1) - \big[P_{\text{hvac}}(k) + S_{\text{hvac}}(k)\big] \leq P_{\text{hvac}}^{\text{up}}, && \text{(4.28l)}\\
& x_s^{\min} \leq x_s(k+1) \leq x_s^{\max}, && \text{(4.28m)}\\
& P_{\text{stor}}^{\min} \leq P_{\text{stor}}(k+1) + S_{\text{stor}}(k+1) \leq P_{\text{stor}}^{\max} && \text{(4.28n)}\\
& \text{Constraint in Eq. (4.14)} \Bigg) \leq 1-\epsilon && \text{(4.28o)}
\end{aligned}
$$

The probability constraints imply that all constraints, expect for the network balance, of the system should be satisfied for all possible wind power trajectories in $\mathcal{W}$, except for a set of probability no more than ϵ. Compared to the BtG-MPC, Eqs. (4.28g) and (4.28h) are added to reflect the line limits, and Eq. (4.14) is added to impose the bounds on reserve and flexibility scheduling. Note that imposing network balance constraints in Eq. (4.28) is not possible, due to the dependency of the equality on the uncertain parameter $P_w(k)$.

4.4.5 Formulating the chance constrained w-BtG-MPC

Combining the modified formulations of the preceding sections, we are now able to formulate the w-BtG-MPC. The new problem formulation consists of the modified predictive dynamics

in Eqs. (4.3) and (4.4) (using wind power forecast P_w^f), all operating constraints of the w-BtG-MPC (including line limits), and the new probabilistic constraint in Eq. (4.28). The complete w-BtG-MPC is then formulated as follows:

$$\underset{\mathcal{X}_w}{\text{minimize}} \qquad J_w\big(x_t, \{x_d^i\}_{i\in\mathcal{D}}, \mathcal{X}_w\big) \tag{4.29a}$$

Subject to, $\forall k \in \mathcal{K}$:

1. **Wind-integrated TSO/DSO/BLD/storage Dynamics.** The system is subject to the forecasted discretized dynamics (denoted by subscript $_f$) of all physical areas of the network. For TSO, wind-integrated dynamics of Eq. (4.3) are applied:

$$x_{t_f}(k+1) = f_t\big(x_{t_f}(k), P_{\text{GR}}(k+1), P_{\text{IMP}}(k+1), P_{\text{BL}}(k+1), P_w^f(k+1)\big), \tag{4.29b}$$
$$x_{d_f}^i(k+1) = f_d^i\big(x_{d_f}^i(k), P_{\text{IMP}}^i(k+1), P_{\text{BD}}^i(k+1), P_{\text{BL}}^i(k+1)\big), \qquad \forall i \in \mathcal{D} \tag{4.29c}$$
$$x_{b_f}(k+1) = f_b(x_{b_f}(k), P_{\text{hvac}}(k+1), w_g(k+1)) \tag{4.29d}$$
$$x_{s_f}(k+1) = \zeta x_{s_f}(k) + h\eta P_{\text{stor}}(k+1). \tag{4.29e}$$

2. **Wind-integrated TSO network balance.** To achieve power balance in the TSO network, the wind-integrated balance constraint is imposed:

$$\Big[\Gamma P_{\text{GR}}(k+1) + \underbrace{\Upsilon P_w^f(k+1)}_{\text{wind power forecast}} - P_{\text{LD}}(k+1) - P_{\text{BL}}(k+1)\Big]^\top \mathbb{1}_{n_t} = 0 \tag{4.29f}$$

3. **TSO and DSO line limits.** Line limits are imposed similarly as in the probabilistic constraints on the forecasted dynamics:

$$L^{\min} \le \tilde{L}^{\text{TSO}}\big[x_{t_f}(k+1)\big] \le L^{\max} \tag{4.29g}$$
$$L^{i,\min} \le \tilde{L}^{\text{DSO},i}\big[x_{d_f}^i(k+1)\big] \le L^{i,\max} \tag{4.29h}$$

4. **Deterministic operating constraints.** All other deterministic operating constraints of the BtG-MPC are imposed, except for the TSO balance constraint (which is modified for the wind-integrated dynamics:

$$\text{Constraints in Eqs. (3.23f), (3.23g) and (3.23i) to (3.23o)} \tag{4.29i}$$

5. **Probabilistic constraints.** The full set of probabilistic constraints is imposed:

$$\text{Constraints in Eq. (4.28)} \tag{4.29j}$$

It is important to note that the probabilistic constraint Eq. (4.28) is non-convex and hard to determine explicitly. Therefore, a tractable framework is developed in the next section, to obtain a probabilistically feasible solution to the w-BtG-MPC.

4.5 Tractable robust MPC reformulation

Following the compact notation introduced in Section 2.5, the chance constraints in Eq. (4.28) can be written as

$$\mathbb{P}\{\ \mathsf{P}_{w_k}\ \mid\ g(\mathsf{X},\mathcal{X},\mathsf{P}_{w_k}) \leq 0\ \} \geq 1-\epsilon, \tag{4.30}$$

where we introduced concatenated state variable $\mathsf{X} = [x_t, \{x_d^i\}_{i\in\mathcal{D}}, x_b, x_s]_{k\in\mathcal{K}}$, which includes all TSO-DSO-BLD-storage states within the MPC prediction horizon. We approximate the proposed probabilistic constraints in Eq. (4.30) using the following robust reformulation:

$$g(\mathsf{X},\mathcal{X},\mathsf{P}_{w_k}) \leq 0, \quad \forall \mathsf{P}_{w_k} \in \mathbb{W}, \tag{4.31}$$

where $\mathbb{W}$ is a bounded uncertainty set compared to $\mathcal{W}$, which is an unbounded and unknown uncertainty set in Eq. (4.30). Note that the proposed constraint in Eq. (4.31) is a robust constraint, since it should be satisfied for all $\mathsf{P}_{w_k} \in \mathbb{W}$. It follows that any feasible solution to Eq. (4.31) with $\mathsf{P}_{w_k} \in \mathbb{W}$, implies that $g(\mathsf{X},\mathcal{X},\mathsf{P}_{w_k}) \leq 0$, where $\mathsf{P}_{w_k} \in \mathcal{W}$. Therefore, by choosing $\mathbb{W}$ that covers a $1-\epsilon$ content of P_{w_k}, i.e., $\mathbb{W}$ satisfies $\mathbb{P}\{\mathsf{P}_{w_k} \in \mathbb{W}\} \geq 1-\epsilon$, any feasible solution to Eq. (4.31) must also satisfy Eq. (4.30) (Hong et al., 2017). In other words, we conclude that, any feasible solution for Eq. (4.31) using a $(1-\epsilon)$-content of $\mathbb{W}$, is also a feasible solution to the probabilistic constraint in Eq. (4.30).

Let us now introduce the bounded set $\mathbb{W} \subseteq \mathbb{R}^{n_w=1}$, i.e. we assume the presence of only one uncertain input (one wind farm in the network). In line with (Rostampour et al., 2019a), it is assumed that $\mathbb{W}$ is an axis-aligned hyper-rectangular set, with $\mathbb{W} := [-\omega, \omega]$ as an interval, where vector $\omega \in \mathbb{R}^{n_w}$ defines the hyper-rectangle bounds. Consider now the following optimization problem that aims to determine the set $\mathbb{W}$ with minimal volume:

$$\begin{cases} \min\limits_{\omega\in\mathbb{R}^{n_w}} & \|\omega\|_1 \\ \text{s.t.} & \mathsf{P}_{w_k}^n \in [-\omega,\omega]\ ,\ \forall\, n = 1,\cdots,N_s \end{cases}, \tag{4.32}$$

where N_s is a finite number of independent and identically distributed samples $\mathsf{P}_{w_k}^n \in \mathcal{W}$. In the scope of this study, samples are extracted from the Markov Chain wind power model. Denote by $\mathbb{W} = [-\tilde{\omega}, \tilde{\omega}]$ the optimal solution of Eq. (4.32). As proven by Calafiore and Campi (2006) and further discussed by Rostampour et al. (2019a), then the following proposition dictates the number of samples N_s required for the probabilistic constraint with N^d decision variables to be satisfied:

Proposition 1. *Fix* $\epsilon \in (0,1)$, $\beta \in (0,1)$, *determine* $N_s \geq [\frac{2}{\epsilon}(\ln \frac{1}{\beta} + N^d]$, *and solve Eq. (4.32) to obtain its optimal solution* $[-\tilde{\omega}, \tilde{\omega}]$. *Then it must hold that:*

$$\mathbb{P}\{\mathsf{P}_{w_k} \in \mathcal{W} \ : \ \mathsf{P}_{w_k} \notin [-\tilde{\omega}, \tilde{\omega}] = \mathbb{W}\} \leq \epsilon. \tag{4.33}$$

The proof is based on the fact that the proposed optimization problem in Section 4.4.5 is a convex program, with the number of decision variables directly related to the number of uncertain variables, $n_w = 1$. A more detailed discussion of the proof is provided by Calafiore and Campi (2006). Finally, note that in the scope of the current problem, the number of uncertain variables also depends on the number of time steps within the MPC optimization program.

The proposed robust reformulation, the Chance Constrainted Program (CCP) in Eq. (4.28) is reformulated as a Chance Constrainted Program (CCP) in equivalent form to Eq. (2.22) provided in Section 2.5. We consider trajectories generated by the Markov Chain wind power model as the set of extractions in the scenario approach optimization:

$$\mathbb{W} = \{P_w^1, \ldots, P_w^{N_s}\}, \tag{4.34}$$

where P_w^i are wind power trajectories extracted from the model.

4.6 Simulation study and test results

4.6.1 Simulation setup

To demonstrate the grid regulative capacity of (a) reserve scheduling, (b) building HVAC and storage flexibility, and (c) the combination of the two, we consider the following three cases in the simulation study:

1. w-BtG-MPC optimization problem, but with only **reserve** power enabled,
2. w-BtG-MPC optimization problem, but with only **flexibility** power enabled,
3. w-BtG-MPC optimization problem, with both **reserve** and **flexibility** power enabled.

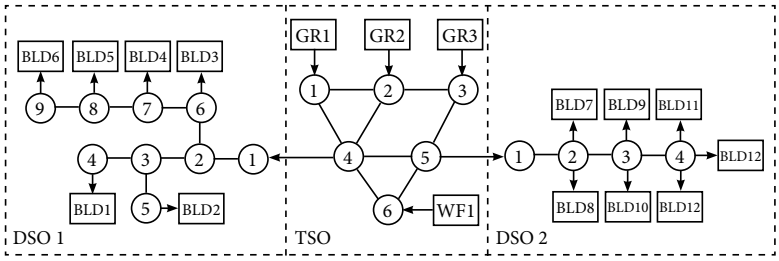

Figure 4.2: Network topology of the MPC problem, indicating the grid structure, generators (GR) buildings (BLD) and wind farm (WF).

The power network topology is described in Figure 4.2, and extends the topology in Figure 3.3 with a wind farm in the TSO network. The case studies are simulated for $T_{\text{end}} = 24$ hours with the prediction horizon $T_p = 1$ hour and time resolution $h = 5$ minutes. The Markov Chain model introduced in the preceding section was used to generate a data set of $100,000$ wind power trajectories, from which the elements for $\mathbb{W}$ were extracted. Following Proposition 1 and similar to Rostampour (2012), $\epsilon = 0.05$ and $\beta = 10^{-4}$. Each MPC iteration, two decision variables are associated for each of the $T_p/h = 12$ time steps, so following Proposition 1 and Eq. (2.24) yields $N_s = 1328 \geq \left\lceil \frac{2}{\epsilon}(2 \times 12 + \ln \frac{1}{\beta}) \right\rceil$. Thereafter, Eq. (4.32) is solved to obtain the bounded set $\mathbb{W}$ at each sampling time k.

The associated cost parameters are $Q_t = Q_d = 1000\,\$/\text{rad}^2$, power generation and consumption are valued at $Q_{\text{GR}} = Q_{\text{hvac}} = 0.1\,\$/\text{MW}^2$, and reserve and flexibility scheduling at $q_R = q_S = 1000\,\$/\text{MW}$. Note that we consider to have the same cost coefficients for both *reserve* and *flexibility* deployment in the cost function. Building storage limits are set equivalent to four Tesla Model S batteries Tesla (2018), i.e. $P^{\text{min}}_{\text{stor}} = -2\,\text{MW}$, $P^{\text{max}}_{\text{stor}} = 2\,\text{MW}$, $x^{\text{min}}_s = 2\,\text{kW h}$, and $x^{\text{max}}_s = 400\,\text{kW h}$.

Simulations were implemented in MATLAB, with Yalmip as interface (Lofberg, 2004) and Gurobi as solver (Gurobi Optimization, LLC, 2019). Building parameters and non-controllable loads were adopted from (Taha et al., 2019), and grid parameters were obtained from MatPower IEEE 5-bus power system (Zimmerman et al., 2011), and scaled appropriately for the current simulation studies.

Similar to the case study in Chapter 3, a stacked equivalent to MPC procedure 1 is formulated for implementation in the MATLAB code. As discussed in Appendix B, this greatly improves computational performance of the code, by replacing its iterative nature with a direct approach. The full overview of simulation parameters is listed in Appendix C.

4.6.2 Simulation results

In this section, the main results to the simulation study are presented. First, grid frequency deviations, storage utilization and average building loads are discussed. Then, the power dispatch for all three cases is presented, and the demand/supply mismatch caused by wind power errors is examined. Finally, the distribution between reserve and flexibility deployment is reviewed, and

Table 4.1: Key results of simulating w-BtG-MPC cases. $\sum(J)$ is the sum of all MPC objective values, and $\omega(x_t + x^i_d)^2$ is the sum of squared grid frequency deviation of the simulation. Differences are calculated relative to Case 1.

Case	$\sum \omega(x_t + x^i_d)^2$ [rad^2]	$\sum(J)$ [\$]
1	0.17992	5,908,659
2	0.12685 (-29.50%)	5,833,499 (-1.27%)
3	0.13119 (-27.08%)	5,833,449 (-1.27%)

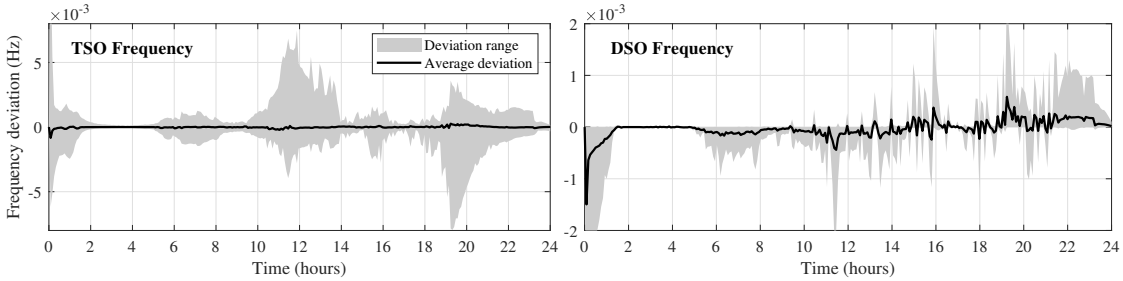

Figure 4.3: Case 3 - Frequency deviations in the TSO and DSO networks.

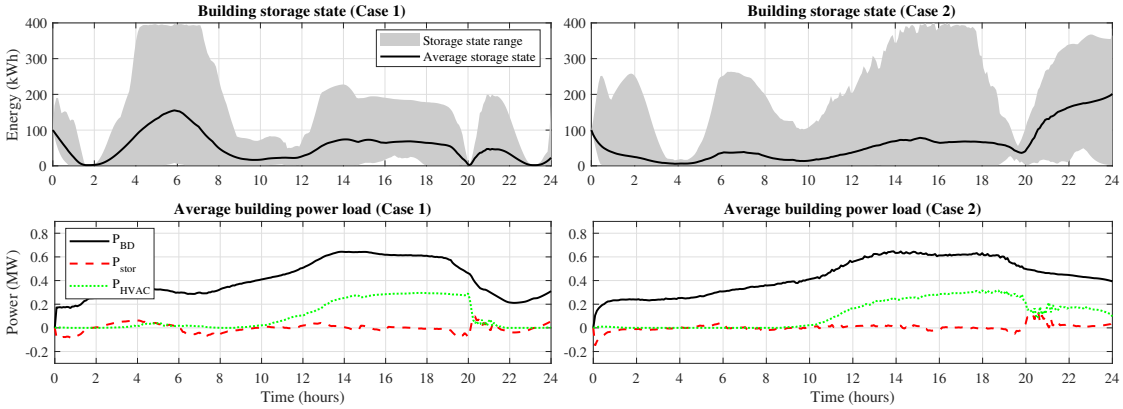

Figure 4.4: Case 1 and 2 - Building storage state, average total building load (P_{BD}), and specific storage (P_{stor}) and HVAC (P_{hvac}) loads.

the differences between the corresponding schedules and actual dispatch are discussed.

Frequency response, storage utilization, and building load

The frequency deviations in the TSO and DSO networks over the simulation horizon of 24 hours for Case 3 are depicted in Figure 4.3. As observed, frequency deviations are kept well below allowable limits for Case 3, and similar results are obtained for Case 1 and 2. As shown in Table 4.1, enabling building-side flexibility results in a reduction of 29.50% in cumulative squared frequency deviation for the total network. As a result of flexibility deployment, Case 3 shows spikes in the DSO frequency deviation, but also fast stabilization afterwards, as illustrated in Figure 4.3. Due to the storage flexibility deployment, building storage units are also used more extensively in Case 2 than for Case 1, as shown in Figure 4.4.

Generator dispatch and demand/supply mismatch

The main results of the deployment of reserve and flexibility in all three cases are presented in Figure 4.5 (Case 1), 4.6 (Case 2), and 4.7 (Case 3). Each figure accumulates power production of individual generators and wind power, and also shows total power demand.

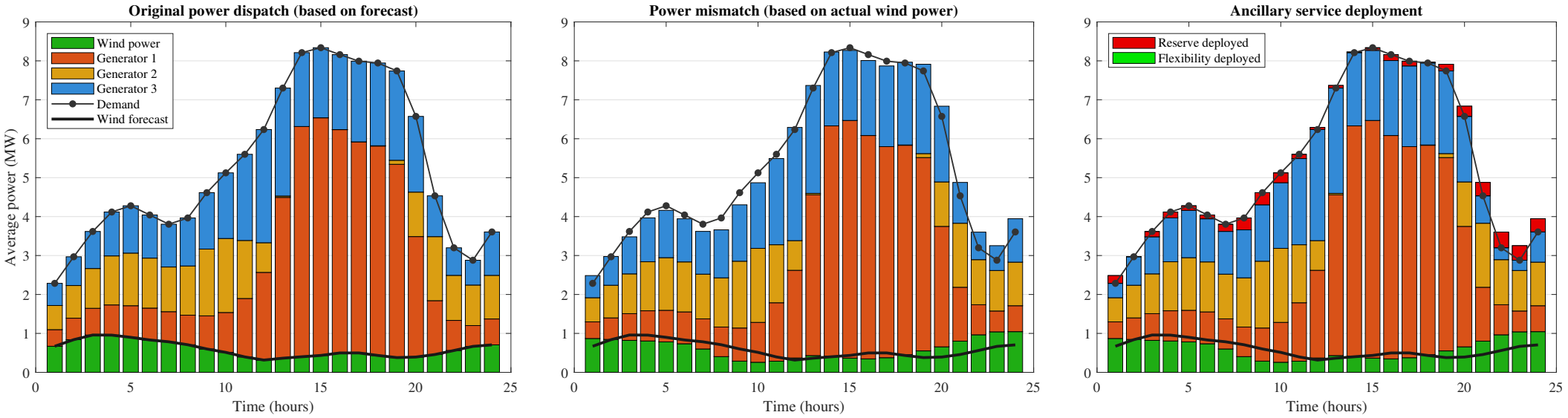

Figure 4.5: Case 1 - Power dispatch (left), power mismatch (middle), and ancillary service deployment (right)

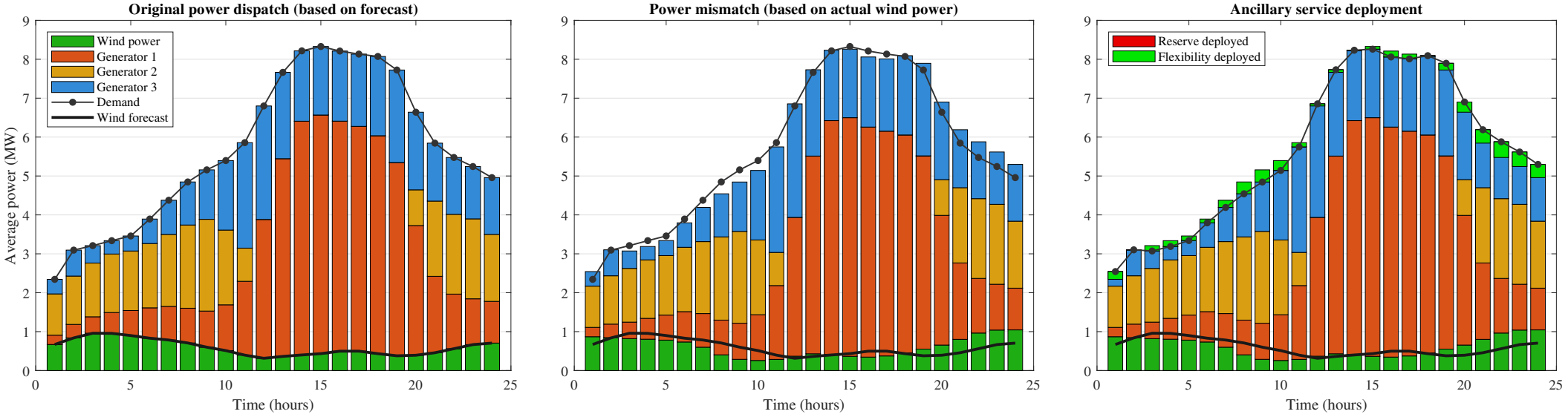

Figure 4.6: Case 2 - Power dispatch (left), power mismatch (middle), and ancillary service deployment (right)

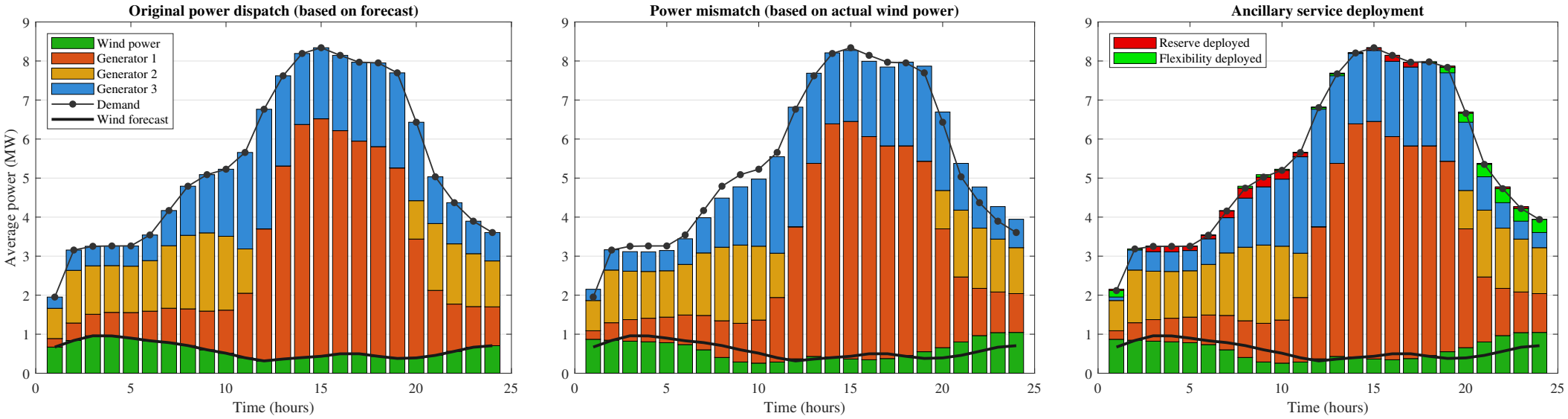

Figure 4.7: Case 3 - Power dispatch (left), power mismatch (middle), and ancillary service deployment (right)

In the left figure for each case, the original power dispatch is shown, which is based on the wind power forecast. It is observed that for all three cases, power supply/demand is well-balanced. Differences in the original dispatch between the cases are a result of the history of reserve and/or flexibility deployment earlier in the day. First of all, the minimum down-spinning reserve scheduling requirement, which is scheduled by Eq. (4.14), leads to higher dispatch at the start of the day (0:00 - 7:00). As power generation cannot be negative ($P_{\text{GR}}(k) \geq 0$), and the operating point with reserve scheduled should still be feasible ($P_{\text{GR}}^{\text{min}} \leq P_{\text{GR}}(k) + R_{\text{GR}}(k) \leq P_{\text{GR}}^{\text{max}}$), the minimum power generation is equal to the reserve scheduling requirement, i.e. $P_{\text{GR}}(k) \geq R_{\text{GR}}^{\text{ds}}(k)$. Furthermore, the deployment and scheduling of reserve or flexibility leads to different trajectories of the state variables (for reserve, generator output is altered; for flexibility, the storage or HVAC usage is affected). Consequently, the next MPC iteration is performed with different initial conditions for the three cases. This implies that also the resulting optimal power dispatch can be different, even though the deterministic optimization problem formulation is equal for all three cases (with the exception of the initial conditions).

In the middle figures, the actual wind power is plotted next to the original dispatch, resulting in a mismatch between power supply and demand for all three cases. Note that, as the same wind power data is used for each case, the demand/supply mismatch is equal for all three cases.

In the right figures, the deployment of reserve (Case 1), flexibility (Case 2) or a combination of the two (Case 3) is shown. The main goal of the deployment of these ancillary services is to cancel the mismatch caused by errors in the wind power forecast, in order to restore the balance between power supply and demand. In Case 1 (Figure 4.5) reserve power is deployed to alter generator output, such that the accumulated generation matches the total demand. On the contrary, in Case 2 (Figure 4.6) flexibility is deployed to alter the power demand, such that it matches the accumulated generation. Finally, in Case 3 (Figure 4.7) a combination of reserve and flexibility is deployed to cancel the supply/demand mismatch. In particular, it is observed that reserve is mainly used if demand was higher than generation (negative mismatch), whereas flexibility is primarily deployed if an increase of demand is required (positive mismatch).

Although not considered in the current simulation study, different costs can be attributed to positive and negative reserve and flexibility. Suppose that costs for up-spinning reserve are higher than for decreased-demand flexibility, and simultaneously, increased-demand flexibility is also more costly than down-spinning reserve. Then, the w-BtG-MPC tends to prefer (down-spinning) reserve over flexibility if the wind power error is positive, but prefers (decreased-demand) flexibility if the actual wind power is lower than predicted. Although it is up to the user whether this distribution would be beneficial, this example illustrates the versatility of the w-BtG-MPC.

Addressing the artificial nature of decreased-demand HVAC flexibility

From Figure 4.5 and 4.6, it is also observed that total energy consumption is higher when flexibility is deployed, compared to reserve. Although the term *decreased-demand* flexibility suggests a reduction in electricity consumption, the opposite is in fact true. For example, between 6:00 - 11:00, decreased-demand flexibility is scheduled and deployed for Case 2, while the demand/-

supply balance in the original power dispatch is higher than for Case 1. This results from the fact that the required HVAC load is required to be at least the minimum power required to remain within the thermal comfort level, i.e. $\hat{P}_{\text{hvac}}(k) \leq P_{\text{hvac}}(k) \leq P_{\text{hvac}}^{\max}$, where $\hat{P}_{\text{hvac}}(k) \geq 0$ is the minimal HVAC load requirement to satisfy the thermal comfort level constraints. However, as scheduling decreased-demand flexibility cannot result in an operating point outside the feasible solution set, we also require $\hat{P}_{\text{hvac}}(k) \leq P_{\text{hvac}}(k) + S_{\text{hvac}}^{\text{dd}}(k) \leq P_{\text{hvac}}^{\max}$, where $S_{\text{hvac}}^{\text{dd}} \geq 0$. As a result, it is required that the original HVAC load is at least the sum of the cooling requirement and the flexibility scheduling requirement, i.e. $P_{\text{hvac}}(k) \geq \hat{P}_{\text{hvac}}(k) + S_{\text{hvac}}^{\text{dd}}(k)$. As $\hat{P}_{\text{hvac}}(k)$ is directly defined by the building state variable x_b, higher flexibility scheduling requirements automatically imply an artificial increase of the original HVAC load, to accommodate for this buffer.

One possible solution for this issue is to allow the building thermal comfort bounds to be flexible. As a results, the minimum HVAC requirement ($\hat{P}_{\text{hvac}}$) is reduced, and no artificial increase of the original HVAC load is required anymore. Imposing flexible temperature bounds can be achieved by modifying the constraint in Eq. 3.23k as follows:

$$x_b^{\min}(k+1) - \Delta x_b^{\min}(k+1) \leq x_b(k+1) \leq x_b^{\max}(k+1) + \Delta x_b^{\max}(k+1), \tag{4.35}$$

where $\Delta x_b^{\min} \geq 0$ and $\Delta x_b^{\max} \geq 0$ are flexible contributions (relaxations) to the temperature bounds of individual buildings. The flexible relaxations can be calculated explicitly, by relating them to the flexibility scheduling requirements, or can be minimized by imposing costs in the objective function:

$$\overline{J}_w\big(x_t, \{x_d^i\}_{i\in\mathcal{D}}, \mathcal{X}_s, \Delta x_b^{\min}, \Delta x_b^{\max}\big) = J_w\big(\cdots\big) + \sum_{k\in\mathcal{K}} q_{\Delta x_b}\big[\Delta x_b^{\min} + q_{\Delta x_b}\Delta x_b^{\max}\big], \tag{4.36}$$

where J_w is the original objective as defined in Eq. 4.23. The imposed costs on the flexible temperature bounds minimize the deviations from the original bounds, while allowing them to be relaxed if required for scheduling demand-side flexibility. Although further implementation of such a flexible temperature bound is outside the scope of the current study, we highlight this work-around as a possibility for future research.

Reserve/flexibility scheduling and deployment

The wind power error together with the reserve and flexibility distribution for Case 3 is presented in Figure 4.8. It is shown that the wind power error is perfectly compensated by the sum of flexibility and reserve deployment. As reserve and flexibility are valued at the same cost in the objective function, the distribution indicates that both mechanisms are well-performing at the TSO to meet the power balance. Total flexibility dispatch accounts for 44.37% of the total compensation for the wind power error over the 24h simulation time. In agreement with the observations of Figure 4.5 - 4.7, it is observed that in the case of positive wind power error, flexibility dispatch is promoted over reserve, while reserve is mainly chosen otherwise.

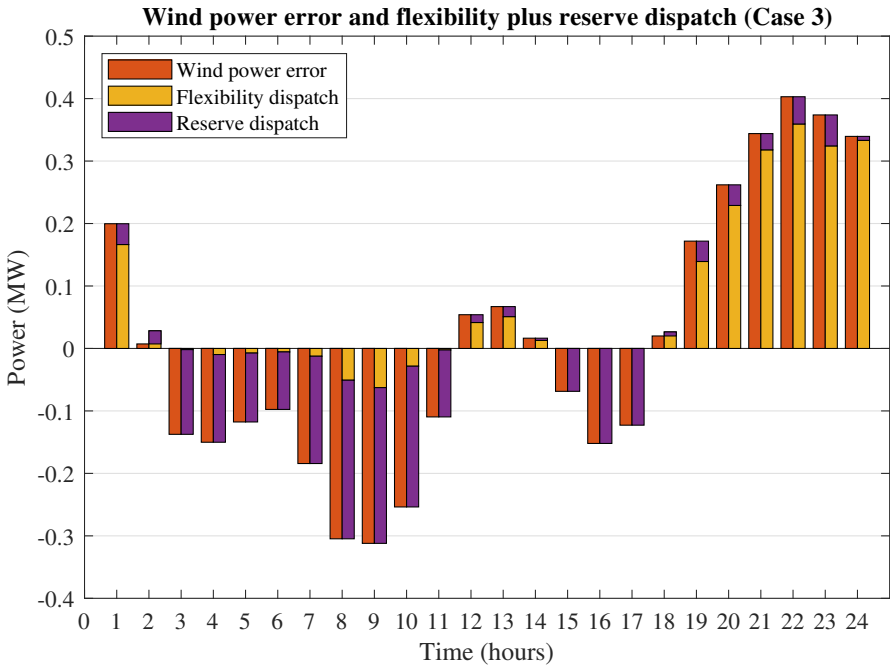

Figure 4.8: Wind power error for Case 3, and distribution of reserve and flexibility dispatch. In order to restore power balance, wind power error always equals the sum of reserve and flexibility dispatch.

The scheduled reserve for Case 1 is compared to the actual reserve dispatch in Figure 4.9. As observed, only a relatively small portion of the schedule is required to compensate for the wind power error. Hence, it is clear that higher reserve deployment is possible within the constraints of the system.

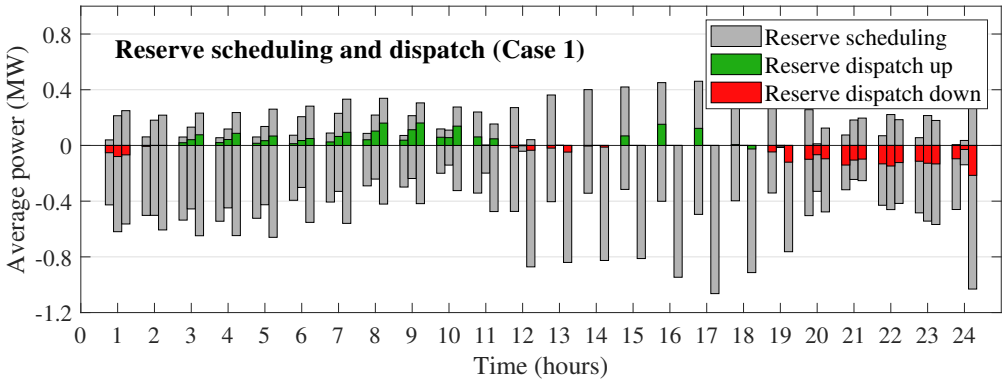

Figure 4.9: Case 1 - Overview of average reserve dispatch per hour compared to the reserve scheduled.

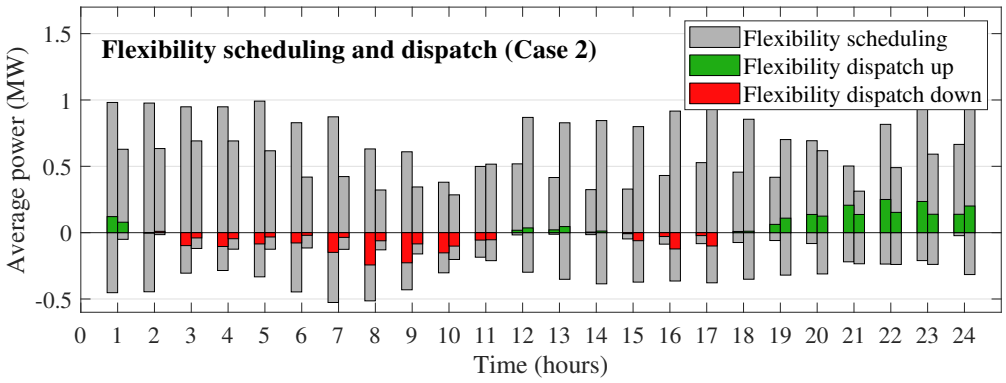

Figure 4.10: Case 2 - Overview of average flexibility dispatch per hour compared to the flexibility scheduled.

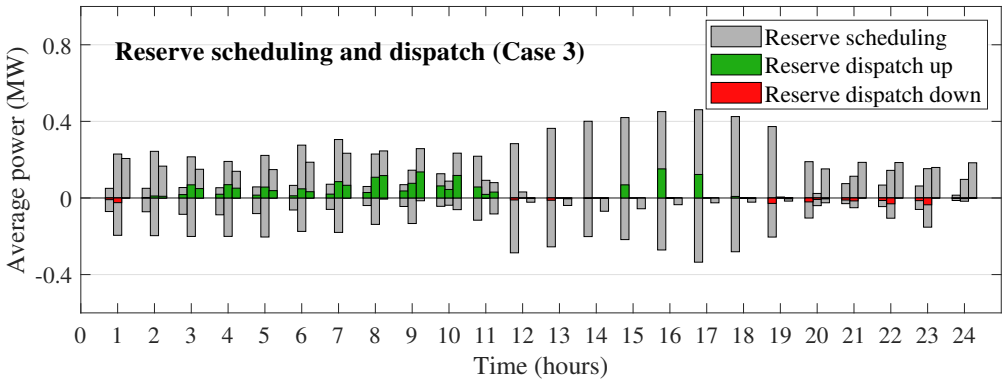

(a) Average reserve scheduling and dispatch per hour

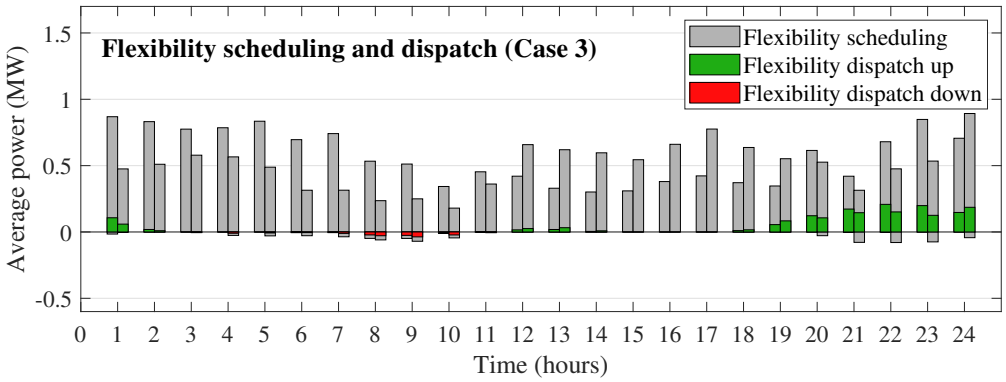

(b) Average flexibility scheduling and dispatch per hour

Figure 4.11: Case 3 - Overview of average reserve and flexibility dispatch per hour compared to the reserve and flexibility scheduled.

Similarly, the scheduled flexibility for Case 2 is compared to the actual dispatch in Figure 4.10. As Case 1 and 2 both compensate for the same wind power error, the sum of reserve dispatch in Case 1 is equal to the sum of flexibility deployment in Case 2. Considering the wind power trajectories in Figure 4.1, the scheduled flexibility is capable of compensating even the largest wind power forecast errors of $\pm 0.5\,\mathrm{MW}$. Hence, building-side flexibility capacity is sufficient to compensate realistic wind power errors without violation of system constraints.

The reserve and flexibility scheduling is compared to the actual dispatch in more detail in Figure 4.11. In agreement with Figure 4.8, up-spinning reserve is promoted over decreased-demand flexibility, while increased-demand is favored over down-spinning reserve. Furthermore, it is observed that reserve and flexibility capacity scheduled (and thus also the amount that is, at least, available) is always significantly higher than the actual reserve or flexibility dispatch (i.e. the portion of the capacity that is implemented in the operational decision-making). This suggests that the current network can potentially also deal with wind power penetration levels significantly higher than the current 10%.

4.7 Monte Carlo study

4.7.1 Monte Carlo setup

The theory of the scenario approach dictates that, if the number of scenarios is chosen such that Eq. (2.24) is satisfied, the specified confidence level is achieved, and the expected probability for any wind power trajectory to violate the imposed constraints is below ϵ. We conduct an a-posteriori analysis by performing Monte Carlo simulations, to validate that the confidence level observed in the experiments is indeed below the expected probability.

In particular, the constraints prone to violation are the line limits in the TSO network. As the wind power directly appears in the dynamics of the TSO network, wind power errors can result in higher or lower voltage angles at the buses than was predicted in the w-BtG-MPC. This can lead to violation of the line limits, potentially causing congestion of the power network (Pillay et al., 2015).

In the Monte Carlo simulations, the optimal control input generated by the w-BtG-MPC for the full simulation length (24 hours) is injected in a simulator. By simulating the system under optimal control input with N^{MC} different wind power scenarios for each case, it is tested a-posteriori if the theoretical maximum violation level is indeed satisfied.

The optimal control inputs generated for the tree cases defined in the previous section were tested in the Monte Carlo simulations with $N^{\mathrm{MC}} = 10,000$. A benchmark case where reserve and flexibility are both disabled was also included. By means of counting the number of trajectories that violate any of the constraints, the empirical violation level is determined for all cases.

4.7.2 Monte Carlo results

The results of the Monte Carlo study are presented in Figure 4.12 for all 3 cases, along with a benchmark case in which no reserve or flexibility is used. As the majority of violations are

observed during peak load hours, only this time span is presented in the figure. For the case with no reserve or flexibility, empirical violation levels are extremely high, as any wind power trajectories almost exclusively results in violation of the line limits. For Case 1 and 3, maximum empirical violation levels are around 0.1%, whereas for Case 2, no violations were observed. In all three cases, the empirical violation level is well below the theoretical limit of $\varepsilon = 0.05$. Hence, the observed empirical violation level is indeed congruent with the probabilistic certificate provided in Proposition 1.

4.8 Conclusion

In this chapter, *research questions 4 and 5* were addressed, and two new developments for the BtG framework were presented. First of all, the existing models were extended to integrate uncertain generation from wind farms, by explicitly formulating the interactions between TSO, DSOs, and buildings. Second, a unified BtG framework was developed to handle the uncertain generation (wind power), by formulating the demand-side flexibility of individual buildings together with the traditional reserve scheduling. Using the unified BtG model, a finite-horizon stochastic control problem was formulated, and a tractable robust reformulation with probabilistic feasibility certificates was provided. As such, we addressed one of the main limitations of the BtG framework developed by Taha et al. (2019), which only pertained to normal grid

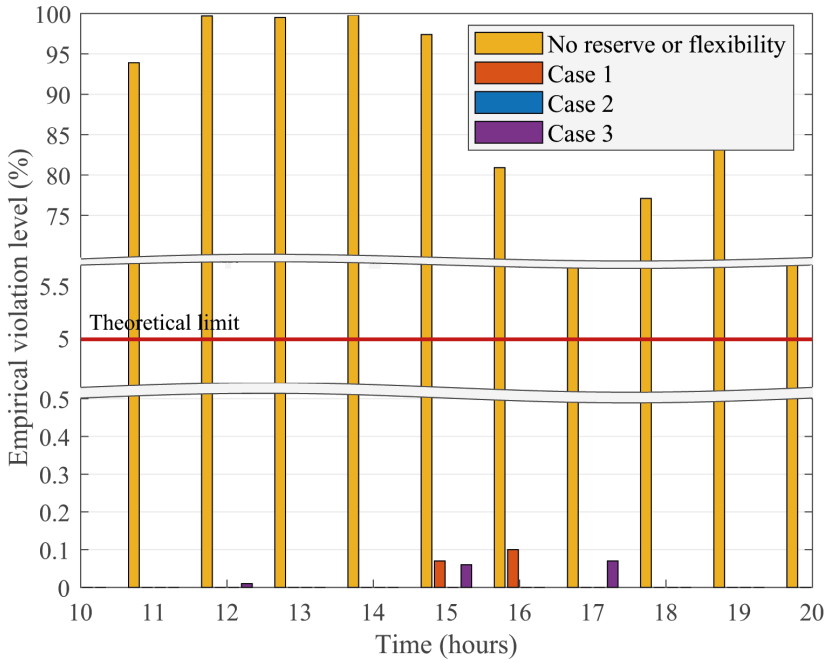

Figure 4.12: Monte Carlo empirical violation levels, and the theoretical limit of $\epsilon = 0.05$ (note the double break in the Y-axis and the limited time span of the plot).

operation. Consequently, the models did not deal with contingencies (such as the uncertain generation considered in our formulation), and corresponding reserve scheduling requirements for grid operators.

When flexibility and reserve scheduling were both enabled (Case 3), flexibility dispatch accounted for 44.37% of the total wind power error compensation, whereas reserve power accounted for the remaining 55.63%. It is, therefore, postulated that the use of building-side flexibility (provided by flexible HVAC and storage control) provides an adequate means of demand response, and can be used in collaboration with (or even instead of) traditional reserve scheduling for providing grid security. This is highly beneficial for the deployment of wind power and other volatile renewables, as the increasing penetration of distributed RES requires operators to schedule larger buffers, to compensate for their inherent variability and unpredictability (Halamay et al., 2011; Lymperopoulos et al., 2015).

Finally, it is concluded that the demand-side flexibility can substitute the traditional reserve scheduling technique in power systems in the presence of wind power generation, without losing stability properties of the power grid, or violating the buildings thermal comfort of occupants. In recent studies, demand response and building participation have been proposed widely among the most promising solutions to deal with the increasing penetration of RES (Blum et al., 2017; Kiliccote et al., 2011; Lamadrid et al., 2011; Vardakas et al., 2015). Hence, the conclusions to the current chapter are indeed consistent with the current body of knowledge, and promote building participation as an adequate means for power grid control under uncertain generation.

The contents of this chapter of the thesis are submitted as Rostampour et al. (2019a) for the 2019 Conference on Decision and Control, organized by the IEEE in December 2019, France.

5 Social Incentives for Demand Flexibility Services in Power Systems with Uncertain Generation

5.1 Introduction

In Chapter 3 and 4, all models assumed perfect collaboration between consumers (buildings) and grid operators. In reality, however, consumers are not readily intrinsically motivated or incentivized to contribute to grid operations, and even grid operators can have opposing stakes (Mohammadi et al., 2018). In this chapter, we address this issue by extending the wind-integrated BtG framework proposed Chapter 4 with a social aspect to model the intrinsic incentive of consumers. We refer to this effect as the sociological impact, and we call the corresponding state variable in the model dynamics the *happiness state* [1]. Furthermore, we assume that consumers are the sole operator of buildings, and thus use both words interchangeably.

The main goal of the current chapter is not to derive a fully proven model with a rigorous link to sociological or psychological research. Instead, we develop a first guideline and the corresponding dynamics for such a model, based on qualitative argumentation. Due to the limited time span, verification of the model in terms of sociological validity is outside the scope of the current study. However, our ongoing research is also devoted to this subject, and we anticipate to submit a paper, in which we study the social incentives for demand flexibility services in BtG integration with uncertain generation (Rostampour et al., 2019b).

The remainder of this chapter is organized as follows. First of all, distributed solar power is integrated in the BtG models, and explicit definitions for the HVAC and storage flexibility capacity are derived. The definitions are used to develop sociological dynamics, in order to capture the impact of social incentives on the availability of demand-side flexibility. Although the sociological impact is a social element, it is translated and modelled into the existing model as a technical aspect. An extended optimal control framework, referred to as the ws-BtG-MPC is formulated, and used to investigate the sociological model in the simulation study.

5.2 Distributed solar power integration

In this chapter, we consider distributed solar power generation by consumers as additional source of electricity. To this end, we modify the nodal building power balance in Eq. (3.23j) as follows:

[1] The discussion whether this is in fact a real contribution to happiness goes beyond the scope of the current study. Instead, the term is used to indicate that certain incentives can drive consumers towards specific decisions.

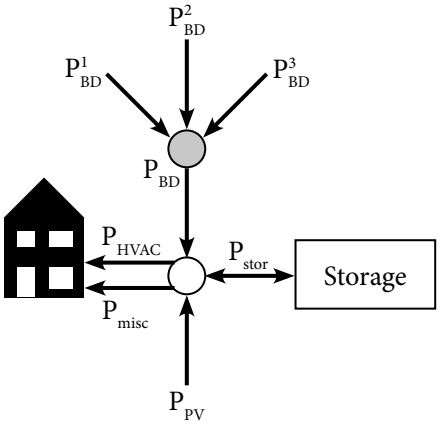

Figure 5.1: Nodal power balance at the building level with solar power integration, with arrows pointing in the positive value of a variable.

$$\sum_{i=1}^{n_d} P^i_{\text{BD}}(k) + \underbrace{P_{\text{pv}}(k)}_{\text{solar power}} = P_{\text{hvac}}(k) + P_{\text{stor}}(k) + P_{\text{misc}}(k), \tag{5.1}$$

where $P_{\text{pv}}(k) \in \mathbb{R}^{n_b}$ is the solar power injection, which is bounded by the actual solar power generation $P_{\text{pv,gen}}(k)$:

$$0 \leq P_{\text{pv}}(k) \leq P_{\text{pv,gen}}(k). \tag{5.2}$$

The bound in Eq. (5.2) implies that in case of a surplus of generation, the injection can be curtailed. In the absence of storage, the power balance is given by

$$\begin{aligned} \sum_{i=1}^{n_d} P^i_{\text{BD}}(k) + P_{\text{pv}}(k) &= P_{\text{hvac}}(k) + P_{\text{misc}}(k) \\ &= P_{\text{tot}}(k), \end{aligned} \tag{5.3}$$

where $P_{\text{tot}}(k)$ is introduced to denote the total instantaneous building load at time k. The modified nodal power balance for each individual building is depicted in Figure 5.1. Real solar power generation curves were adopted from Hodge (2006), and scaled to reflect a realistic wind power penetration level in the lower power system. By small randomization of the average data, the generation curves shown in Figure 5.2 were constructed.

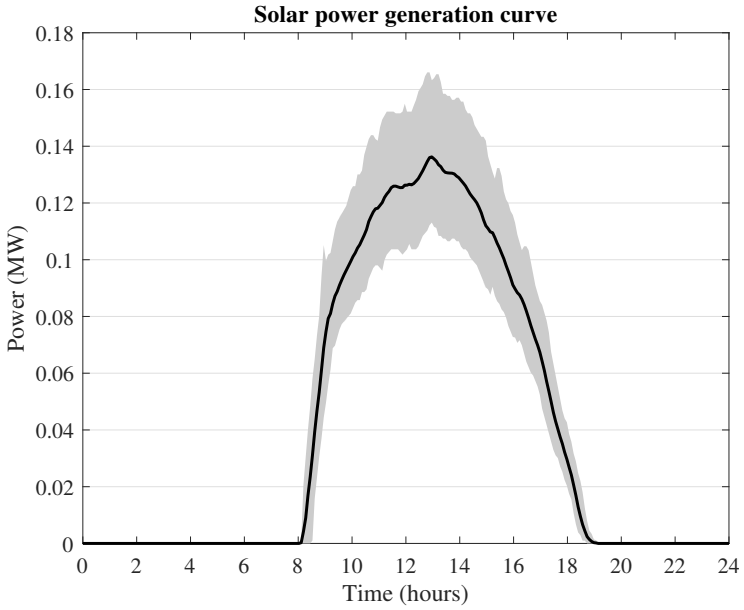

Figure 5.2: Solar power generation curves, used to determine the power generation term, $P_{\text{pv,gen}}(k)$.

5.3 Quantifying building flexibility

As discussed in Chapter 4, we consider (1) *buildings storage systems*, and (2) *building HVAC loads* as the contributions to building flexibility. In this section, explicit definitions for the flexibility capacity of both storage and HVAC are given. These definitions are required to predict power usage and flexibility capability in the sociological dynamics in Eq. (5.7).

5.3.1 Quantifying storage flexibility

Storage flexibility capacity is defined as the margin between the current storage rate ($P_{\text{stor}}(k)$) and the upper and lower bounds, respectively, constrained by the limits on the current buffer level ($x_s(k)$). Taking the storage limit constraints $P_{\text{stor}}^{\max}$ and $P_{\text{stor}}^{\min}$, and the buffer limits $x_s^{\max}$ and $x_s^{\min}$ into account, the storage flexibility capacity of building $l \in \mathcal{B}$ can be formulated as:

$$\begin{aligned} \hat{S}_{\text{stor}}^{\text{id},l}(k) &= \min\Big\{ P_{\text{stor}}^{\max} - P_{\text{stor}}^{l}(k), \quad \frac{x_s^{\max} - x_s^{l}(k)}{h} - P_{\text{stor}}^{l}(k) \Big\}, \\ \hat{S}_{\text{stor}}^{\text{dd},l}(k) &= \max\Big\{ P_{\text{stor}}^{\min} - P_{\text{stor}}^{l}(k), \quad \frac{x_s^{\min} - x_s^{l}(k)}{h} - P_{\text{stor}}^{l}(k) \Big\}, \end{aligned} \tag{5.4}$$

where h is the simulation step width, and $\hat{S}_{\text{stor}}^{\text{id,l}}$ and $\hat{S}_{\text{stor}}^{\text{dd,l}}$ are the increased- and decreased-demand storage flexibility capacity of building l, respectively. As indicated in Figure 5.3, increased-demand storage flexibility is the amount of power with which $P_{\text{stor}}(k)$ can be increased for one

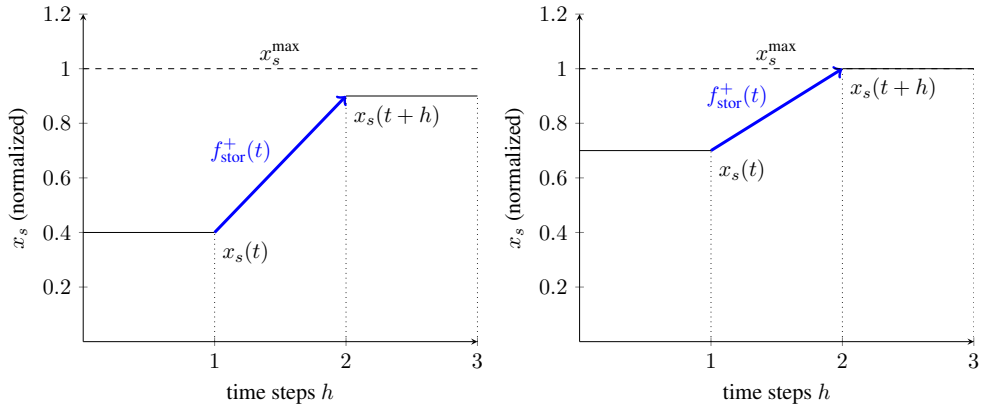

(a) $P^{\max}_{stor}$ is the limiting term

(b) $x_s^{\max}$ is the limiting term

Figure 5.3: Visualization of positive storage flexibility, showing that either the maximum storage rate or the maximum buffer level is the limiting term for positive flexibility f^+_{stor}.

time step h, such that either the upper power limit constraint (Figure 5.3a) or the electricity storage limit is reached (Figure 5.3b).

5.3.2 Quantifying HVAC flexibility

A similar expression is derived for building HVAC flexibility, which is constrained by the HVAC bounds $P^{\min}_{\text{hvac}}$ and $P^{\max}_{\text{hvac}}$, and the allowed power injection $P_{\text{hvac}}(k)$ that still satisfies temperature comfort levels after step width h. For building $l \in \mathcal{B}$, the expressions for HVAC flexibility are given by

$$\begin{aligned}\hat{S}^{\text{id},l}_{\text{hvac}}(k) &= \min\Big\{P^{\max}_{\text{hvac}} - P^{l}_{\text{hvac}}(k), \quad \hat{P}^{\text{id},l}_{\text{hvac}}(k) - P^{l}_{\text{hvac}}(k)\Big\},\\ \hat{S}^{\text{dd},l}_{\text{hvac}}(k) &= -\max\Big\{P^{\min}_{\text{hvac}} - P^{l}_{\text{hvac}}(k), \quad \hat{P}^{\text{dd},l}_{\text{hvac}}(k) - P^{l}_{\text{hvac}}(k)\Big\},\end{aligned} \tag{5.5}$$

where $\hat{S}^{\text{id,l}}_{\text{hvac}}$ and $\hat{S}^{\text{dd,l}}_{\text{hvac}}$ are the increased- and decreased-demand HVAC flexibility capacity of building l, and $\hat{P}^{\text{id},l}_{\text{hvac}}(k)$ and $\hat{P}^{\text{dd},l}_{\text{hvac}}(k)$ are the maximum and minimum HVAC power that still satisfy the comfort level constraints of building l:

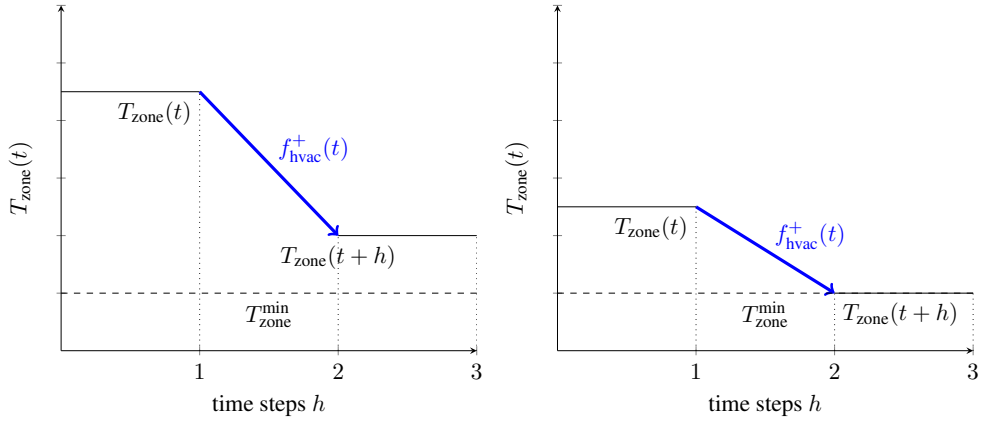

(a) $P^{\max}_{\text{hvac}}$ is the limiting term

(b) $T^{\min}_{\text{zone}}$ is the limiting term

Figure 5.4: Visualization of positive HVAC flexibility, showing that either the maximum cooling power or the comfort level constraint is the limiting term for positive flexibility f^{+}_{hvac}. Note that positive flexibility leads to a temperature decrease, as energy is used to cool the building.

$$\hat{P}^{\text{id},l}_{\text{hvac}}(k) = \frac{T_{\text{wall}} - T_{\text{zone}}}{R_1 \mu_{\text{hvac}}} + \frac{T_{\text{amb}} - T_{\text{zone}}}{R_{\text{win}} \mu_{\text{hvac}}} + \frac{\dot{Q}_{\text{int}}}{\mu_{\text{hvac}}} - \frac{C_{\text{zone}}}{h \mu_{\text{hvac}}} \left[\max \left\{ T^{\min}_{\text{zone}}(k), \quad T^{\min}_{\text{zone}}(k+h) \right\} - T_{\text{zone}}(k) \right], \tag{5.6a}$$

$$\hat{P}^{\text{dd},l}_{\text{hvac}}(k) = \max \left[0, \quad \frac{T_{\text{wall}} - T_{\text{zone}}}{R_1 \mu_{\text{hvac}}} + \frac{T_{\text{amb}} - T_{\text{zone}}}{R_{\text{win}} \mu_{\text{hvac}}} + \frac{\dot{Q}_{\text{int}}}{\mu_{\text{hvac}}} - \frac{C_{\text{zone}}}{h \mu_{\text{hvac}}} \left[\min \left\{ T^{\max}_{\text{zone}}(k), \quad T^{\max}_{\text{zone}}(k+h) \right\} - T_{\text{zone}}(k) \right] \right], \tag{5.6b}$$

where all variables and thermal model parameters are related to building l. Positive HVAC flexibility is visualized in Figure 5.4, showing that the limiting term is either the HVAC power (Figure 5.4a) or the temperature comfort level (Figure 5.4b).

5.4 Integration of sociological dynamics

Consider the state variable $x_h \in \mathbb{R}^{n_b}$ for the level of happiness (i.e. the sociological impact) of consumers. Discrete sociological dynamics proceed according to

$$x_h(k+1) = c_h x_h(k) + (1-\alpha) \underbrace{\left[\tau \frac{P_{\text{pv}}(k)}{P_{\text{tot}}(k)}\right]}_{\text{operating model}} + \alpha \underbrace{\left[\sigma \frac{S^{\text{id}}_{\text{stor}}(k) + S^{\text{dd}}_{\text{stor}}(k) + S^{\text{id}}_{\text{hvac}}(k) + S^{\text{dd}}_{\text{hvac}}(k)}{\hat{S}^{\text{id}}_{\text{potential}}(k) + \hat{S}^{\text{dd}}_{\text{potential}}(k)}\right]}_{\text{market model}}, \tag{5.7}$$

where $\alpha \in (0,1)$ is a parameter indicating the relative influence of the operating and market models, $c_h \in (0,1)$ is the depletion factor, and $\tau, \sigma \geq 0$ are weights for the respective elements. $P_{\text{tot}}(k)$ is the instantaneous total building load as defined in Eq. (5.3), and $\hat{S}^{\text{id}}_{\text{potential}}$ and $\hat{S}^{\text{dd}}_{\text{potential}}$ are estimates of the flexibility capacity. All elements in the numerators are decision variables in the optimization problem.

The first term in Eq. (5.7) represents the consumer *operating model*, and reflects the percentage of power consumption originating from solar energy. As both $P_{\text{PV}}(k)$ and $P_{\text{hvac}}(k)$ are decision variables in the MPC, Eq. (5.7) yields a non-convex problem. In order to render the optimization problem convex, the HVAC power term in Eq. (5.3) is estimated, using its minimal required value, which is given by Eq. (5.6b):

$$\hat{P}_{\text{hvac}}(k) := \min \left\{ P_{\text{hvac}}(k) \;\; : \;\; x_b(k+1) \in \mathbb{X}, P_{\text{hvac}}(k) \in \mathbb{Y} \right\} \approx \hat{P}^{\text{dd}}_{\text{hvac}}(k), \tag{5.8}$$

where $\mathbb{X}$ and $\mathbb{Y}$ denote the feasible sets that satisfy the building thermal comfort and HVAC operating limits, respectively. Hence, variable $P_{\text{hvac}}(k)$ denotes the minimal HVAC power required at time step k, such that the constraints are still satisfied at time $k+1$, and is used to explicitly determine $P_{\text{tot}}(k)$ in Eq. (5.7).

The second term in Eq. (5.7) represents the consumer *market model* of the ancillary services market, and calculates the ratio of scheduled flexibility over the maximum flexibility capacity (both increased- and decreased-demand), given by

$$\begin{aligned} \hat{S}^{\text{id}}_{\text{potential}}(k) &= \max \left[\hat{S}^{\text{id}}_{\text{stor}}(k) + \hat{S}^{\text{id}}_{\text{hvac}}(k) \right], \\ \hat{S}^{\text{dd}}_{\text{potential}}(k) &= \max \left[\hat{S}^{\text{dd}}_{\text{stor}}(k) + \hat{S}^{\text{dd}}_{\text{hvac}}(k) \right], \end{aligned} \tag{5.9}$$

where the contributions denote the estimated flexibility capacity, which are calculated following Eqs. (5.4) and (5.5).

5.4.1 Sociological state boundary conditions

In order to give a physical meaning to the values of the sociological dynamics, we illustrate the following desired boundary situations:

- The lower limit of the happiness is approximately zero[2], i.e. $\min(x_h) \approx 0$. This is inherently achieved by the dynamics in Eq. (5.7), as all terms are positive. In particular, $x_h =$ corresponds to the situation where $P_{\text{pv}} = 0$ and $S^{\text{id}} + S^{\text{dd}} = 0$.
- The upper limit of the happiness is approximately one, i.e. $\max(x_h) \approx 1$. This corresponds to the case where $P_{\text{pv}} = P_{\text{tot}}$ and/or $S^{\text{id}} + S^{\text{dd}} = \hat{S}^{\text{id}}_{\text{potential}} + \hat{S}^{\text{dd}}_{\text{potential}}$, i.e. all power comes from solar energy, and the full potential flexibility is scheduled.

In order to normalize the operating model as desired, we first isolate the operating model dynamics by assuming $\alpha = 0$. Then, the dynamics are written as

$$x_h(k+1) = c_h x_h(k) + \tau \frac{P_{\text{pv}}(k)}{P_{\text{tot}}(k)}. \tag{5.10}$$

The extreme value of the state is characterized by $x_h(k+1) = x_h(k)$. In particular, the minimum state is achieved for $P_{\text{pv}} = 0$. Similarly, in the case of maximum state value, we desire $x_h = 1$, which is achieved for $P_{\text{pv}} = P_{\text{tot}}$:

$$\begin{aligned} x_h(k+1) = c_h x_h(k) + \tau \frac{P_{\text{pv}}(k)}{P_{\text{tot}}(k)} = c_h x_h(k) + \tau = x_h(k), \\ \tau = x_h(k)(1 - c_h) = 1 - c_h. \end{aligned} \tag{5.11}$$

The parameter σ for the market model is more difficult to estimate appropriately. First, it is observed that the m flexibility scheduled is always by the potential flexibility capacity, i.e.

$$\begin{aligned} \hat{S}^{\text{id}}_{\text{potential}}(k) \geq S^{\text{id}}_{\text{stor}}(k) + S^{\text{id}}_{\text{hvac}}(k), \\ \hat{S}^{\text{dd}}_{\text{potential}}(k) \geq S^{\text{dd}}_{\text{stor}}(k) + S^{\text{dd}}_{\text{hvac}}(k). \end{aligned} \tag{5.12}$$

However, as the potential flexibility is calculated based on the theoretical maximum, the actual flexibility available to be scheduled is typically lower. As the market model should exhibit approximately the same strength of influence as the operating model, it is necessary to determine the appropriate value for σ empirically, based on the outcomes from previous simulations.

5.5 ws-BtG-MPC optimal control framework

In order to integrate solar power generation in the optimal control framework, the set of decision variables defined in Eq. (4.21) is extended as follows:

$$\mathcal{X}_s = \{\mathcal{X}_w, P_{\text{pv}}(k)\} \tag{5.13}$$

[2]Note that we can only define the bounds on the happiness approximately, as the effect of power storage on the nodal power balance in Eq. (5.1) is not taken into account.

At each sampling time, we consider the objective function of the ws-BtG-MPC to be the same as for the w-BtG-MPC, extended with a linear cost term for the sociological impact:

$$J_s\big(x_t, \{x_d^i\}_{i\in\mathcal{D}}, x_h, \mathcal{X}_s\big) := J_w\big(x_t, \{x_d^i\}_{i\in\mathcal{D}}, \mathcal{X}_s\big) - \sum_{k\in\mathcal{K}} q_h^\top x_h, \tag{5.14}$$

where $J_w(\cdot)$ is the objective function defined in Eq. (4.23), and $q_h \in \mathbb{R}^{n_b}$ is the vector of positive cost coefficients related to the sociological impact of different consumers (buildings). As the objective of the MPC is to minimize the cost function, the sociological impact itself is maximized.

By integrating the sociological dynamics, the complete ws-BtG-MPC is then formulated as follows:

$$\underset{\mathcal{X}_s}{\text{minimize}} \qquad J_s\big(x_t, \{x_d^i\}_{i\in\mathcal{D}}, x_h, \mathcal{X}_s\big) \tag{5.15a}$$

Subject to, $\forall k \in \mathcal{K}$:

1. **Solar power integrated nodal power balance.** To capture distributed power generation from solar power, the modified nodal balance and bounds on solar power are imposed:

$$\sum_{i=1}^{n_d} P^i_{\text{BD}}(k) + P_{\text{pv}}(k) = P_{\text{hvac}}(k) + P_{\text{stor}}(k) + P_{\text{misc}}(k) \tag{5.15b}$$

$$0 \le P_{\text{pv}}(k) \le P_{\text{pv,gen}}(k) \tag{5.15c}$$

2. **Complete w-BtG-MPC formulation.** The complete set of constraints, except for the nodal power balance (which is extended with solar power), is imposed:

Constraints in Eqs. (4.29b) to (4.29j), except for nodal building power balance (5.15d)

3. **Sociological dynamics.** The sociological dynamics are imposed as follows:

$$x_h(k+1) = c_h x_h(k) + (1-\alpha)\left[\tau \frac{P_{\text{pv}}(k)}{P_{\text{tot}}(k)}\right] + \alpha\left[\sigma \frac{S^{\text{id}}(k) + S^{\text{dd}}(k)}{S^{\text{id}}_{\text{potential}}(k) + S^{\text{dd}}_{\text{potential}}(k)}\right] \tag{5.15e}$$

4. **Physical boundaries of sociological impact.** The sociological state variable is bounded by

$$x_h \le 1 \tag{5.15f}$$

5.6 Simulation study and test results

5.6.1 Simulation setup

To validate the developed sociological dynamics, and demonstrate the impact of consumer participation in the BtG framework, we consider the following cases in the simulation study:

1. ws-BtG-MPC optimization problem, but with **sociological dynamics disabled** (referred to as the benchmark case). This case is achieved by setting the parameters $\tau = \sigma = 0$, and $q_h = 0$, and serves as benchmark for the other cases.
2. ws-BtG-MPC optimization problem, with **sociological dynamics enabled for different values of** α. The optimization problem is solved for the following set of relative importance parameters: $\alpha = \{0.0, 0.5, 1.0\}$. Hence, the problem is solved for different relative importance values between the operating and market model.

We consider the same power network topology as in Chapter 4 (Figure 4.2), but with the solar power integration. Maximum average solar power input is determined as $\max_{k\in\mathcal{N}} \left[P_{\text{pv,gen}}(k)\right] = 0.8\,\text{MW}$. In contrast to all previous simulation studies, the case studies are simulated for $T_{\text{end}} = 7$ days, as sociological influences are better reflected on a longer time horizon. MPC prediction horizon $T_p = 1$ hour and time resolution $h = 5$ minutes. Parameters for the tractable reformulation of the stochastic MPC are equal to the simulation study in Chapter 4.

To capture the inertial behavior of the sociological impact over time, we choose $c_h = 0.995$ (only a small fraction of information is lost per time step). According to Eq. (5.11), define $\tau = 0.005$, and we empirically determine $\sigma = 0.15$. The associated cost parameters are $Q_t = Q_d = 1000\,\$/\text{rad}^2$ for grid frequency deviations, power generation and consumption are valued at $Q_{\text{GR}} = Q_{\text{hvac}} = 0.1\,\$/\text{MW}^2$, and reserve and flexibility scheduling at $q_R = q_S = 1\,\$/\text{MW}$. Furthermore, the price for conventional is electricity is reflected in $q_{\text{BD}} = 0.1\,\$/\text{MW}$, and the price for solar power is $q_{\text{pv}} = 0.15\,\$/\text{MW}$ (which is a combination of fixed costs amortized over a number of years, and variable costs).

The optimization problem is implemented for the simulation study as the stacked MPC formulation defined in Appendix B, and the full overview of simulation parameters is listed in Appendix C.

5.6.2 Simulation results

In this section, the main results to the simulation study are presented. First, the simulation trajectories of the sociological impact (happiness) states of individual consumers are presented. Then, the average utilization of solar power per hour is compared in relation to the relative importance between the operating and market model. Finally, the impact of the market model for ancillary services on the availability of demand-side flexibility is examined.

Sociological impact and happiness state

As stated in the introduction of the current chapter, the sociological impact is reflected by the *happiness state*. The happiness state trajectories for different values of α over the simulation time of 7 days are presented in Figure 5.6. The lines represent the state trajectories of individual buildings (consumers) in the network.

In the case of only operating model ($\alpha = 0$), the sociological dynamics are purely driven by the consumer motivation to maximize the use of solar power. As observed in Figure 5.6 for $\alpha = 0$, the happiness state is increased when solar power is generated (as depicted in Figure 5.2), and decreases overnight. Although it is questionable if the change in happiness is affected on such a short time-scale, the results show that the model dynamics indeed promote consumer incentives to maximize the use of solar power.

In the case of only market model ($\alpha = 1$), the sociological dynamics are purely driven by the consumer incentive to participate on the ancillary services market. Contrary to solar power, demand-side flexibility is available during the full day, and therefore, the resulting happiness state is subject to less volatile oscillations. However, it is observed that the participation level differs heavily between individual consumers, which is a direct consequence of the centralized optimization approach. The imbalance in building participation is visualized in Figure 5.5, showing that participation is only significant for buildings connected near the TSO/DSO interface. However, this also indicates that the flexibility capacity is significantly higher than the requirement for scheduling ancillary services.

The trajectories for the combination of operating and market model ($\alpha = 0.5$) show both the oscillating pattern of the incentive for maximizing solar power usage, and the wide range in happiness value, caused by participation on the ancillary services market. As observed, only one building (number 3 in Figure 5.5) is fully satisfied in happiness state, whereas all others are at a lower level.

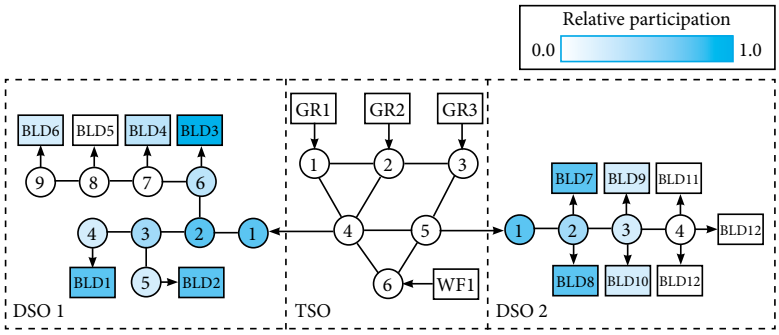

Figure 5.5: Relative participation of individual consumers in providing demand-side flexibility, in case of pure market model dynamics ($\alpha = 1$).

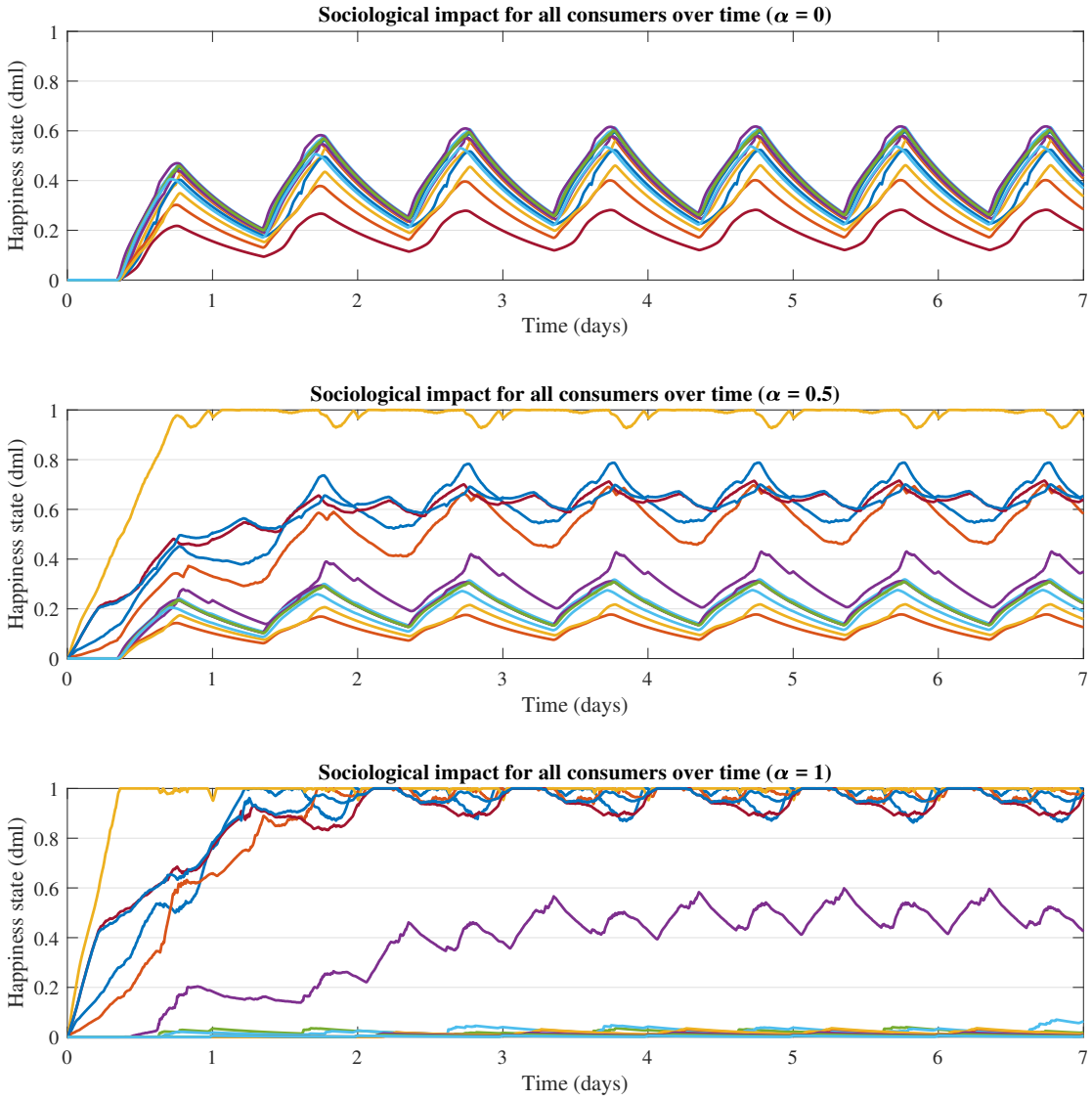

Figure 5.6: Sociological impact and corresponding happiness state of all individual consumers over the simulation horizon of 7 days for different values of α.

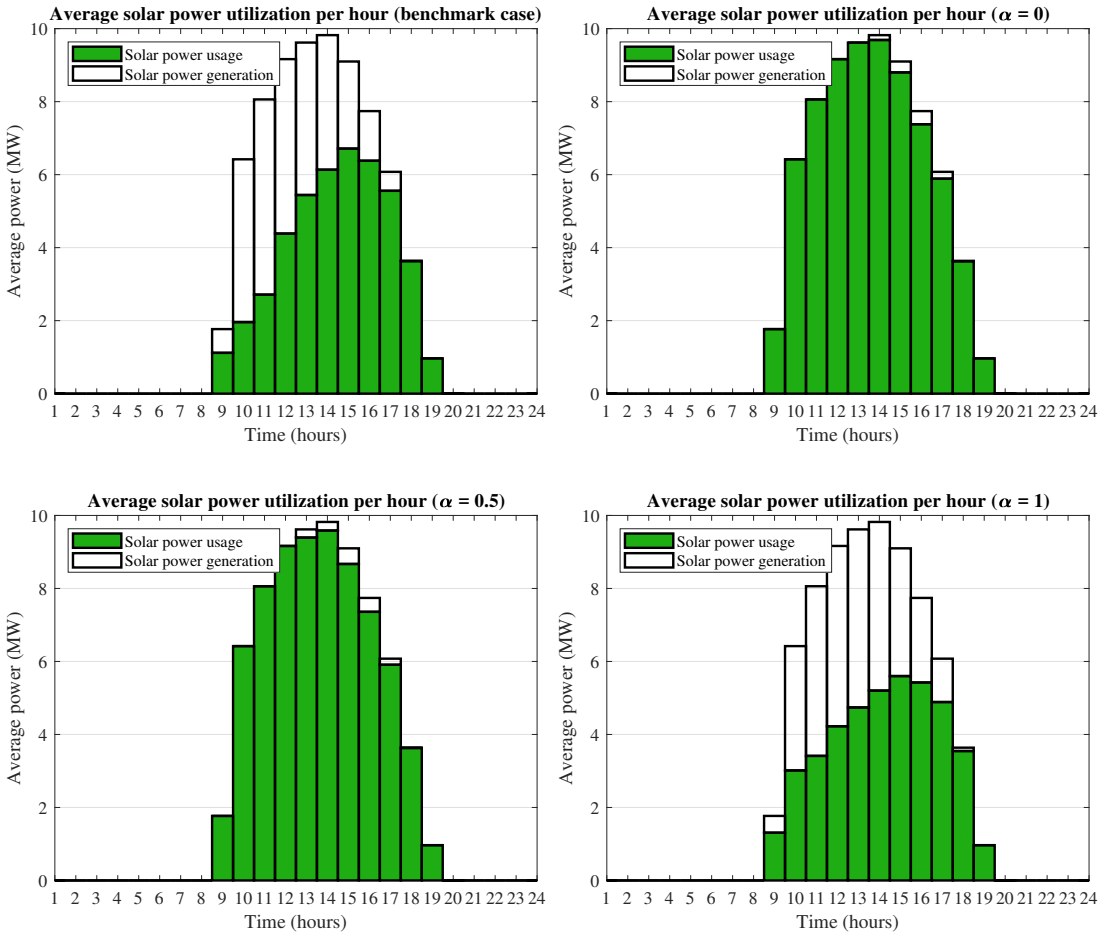

Figure 5.7: Average utilization of solar power per hour (for one day) compared to the total solar power generation for different values of α.

Solar power utilization

The average solar power usage is compared to the total solar power generation over the 24 hour simulation time in Figure 5.7 for all cases. The solar power generation corresponds to the generation curve in Figure 5.2, whereas the usage is the actual injection as defined in Eq. (5.2). It is observed that solar power usage is lowest for case $\alpha = 1$, followed by the benchmark case. Utilization is lower for case $\alpha = 1$, because the increased participation in offering flexibility services obstructs higher levels of solar power efficiency. As dictated by the sociological dynamics, highest solar power utilization is indeed observed for case $\alpha = 0$. Although the price for solar power is higher, the social incentive reflected in this case drives consumers to maximized utilization of solar power.

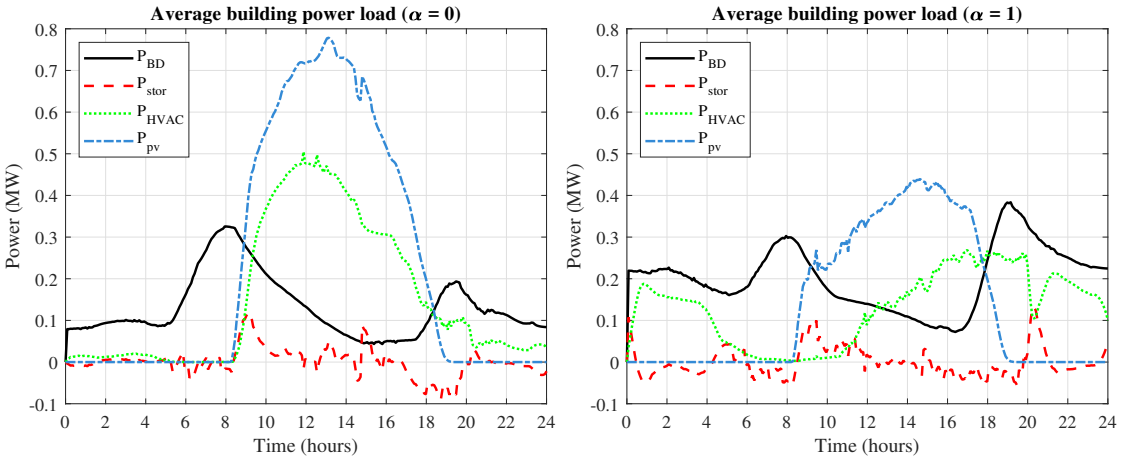

(a) Case $\alpha = 0$ (pure operating model)

(b) Case $\alpha = 1$ (pure market model)

Figure 5.8: Average building power load over the simulation time of 24 hours, showing total grid load (P_{BD}), storage power (P_{stor}), HVAC load (P_{hvac}), and solar power injection (P_{pv}).

The increased solar power penetration for case $\alpha = 0$ compared to $\alpha = 1$ is reflected in more detail in Figure 5.8, which reflects the average nodal power balance in Figure 5.1 over the simulation time. Cumulative solar power injections for one building are $3.26\,\text{MW h}$ per day for case $\alpha = 1$, and $5.49\,\text{MW h}$ per day for case $\alpha = 0$, yielding an increase of 68.65% in solar penetration. The inherent thermal inertia of buildings is used as buffer by increasing the HVAC load between 10:00 - 16:00, in order to deal with the intermittency of solar power. As a result, HVAC load requirements are lower at the and of the day (18:00 - 24:00) for case $\alpha = 0$. Total energy consumption per day for one building is $8.54\,\text{MW}$ for case $\alpha = 0$, $8.94\,\text{MW}$ for $\alpha = 0.5$, and $8.11\,\text{MW}$ for $\alpha = 1$. The total consumption for the benchmark case is $7.6233\,\text{MW}$, indicating that, although the sociological dynamics evoke the intended effects, its implementation is also complemented with higher total electricity consumption.

Availability of demand-side flexibility

Finally, we examine the impact of the sociological dynamics on the availability of demand-side flexibility. The flexibility scheduling and dispatch over time is presented for all cases in Figure 5.9. The benchmark case shows similar deployment of flexibility as the cases in the simulation study in Chapter 4, and case $\alpha = 0$ only shows a minor increase in decreased-demand flexibility between 15:00 - 20:00. For case $\alpha = 0.5$, most ancillary services are already deployed in the form of flexibility, and only a small level of reserve is scheduled. For $\alpha = 1$, this effect is even stronger, and almost all ancillary services are deployed as flexibility, yielding negligible levels of reserves. This behavior clearly shows the effect of the market model for ancillary services, and suggests that only a small relative influence for this model is sufficient to increase the deployment of demand-side flexibility significantly.

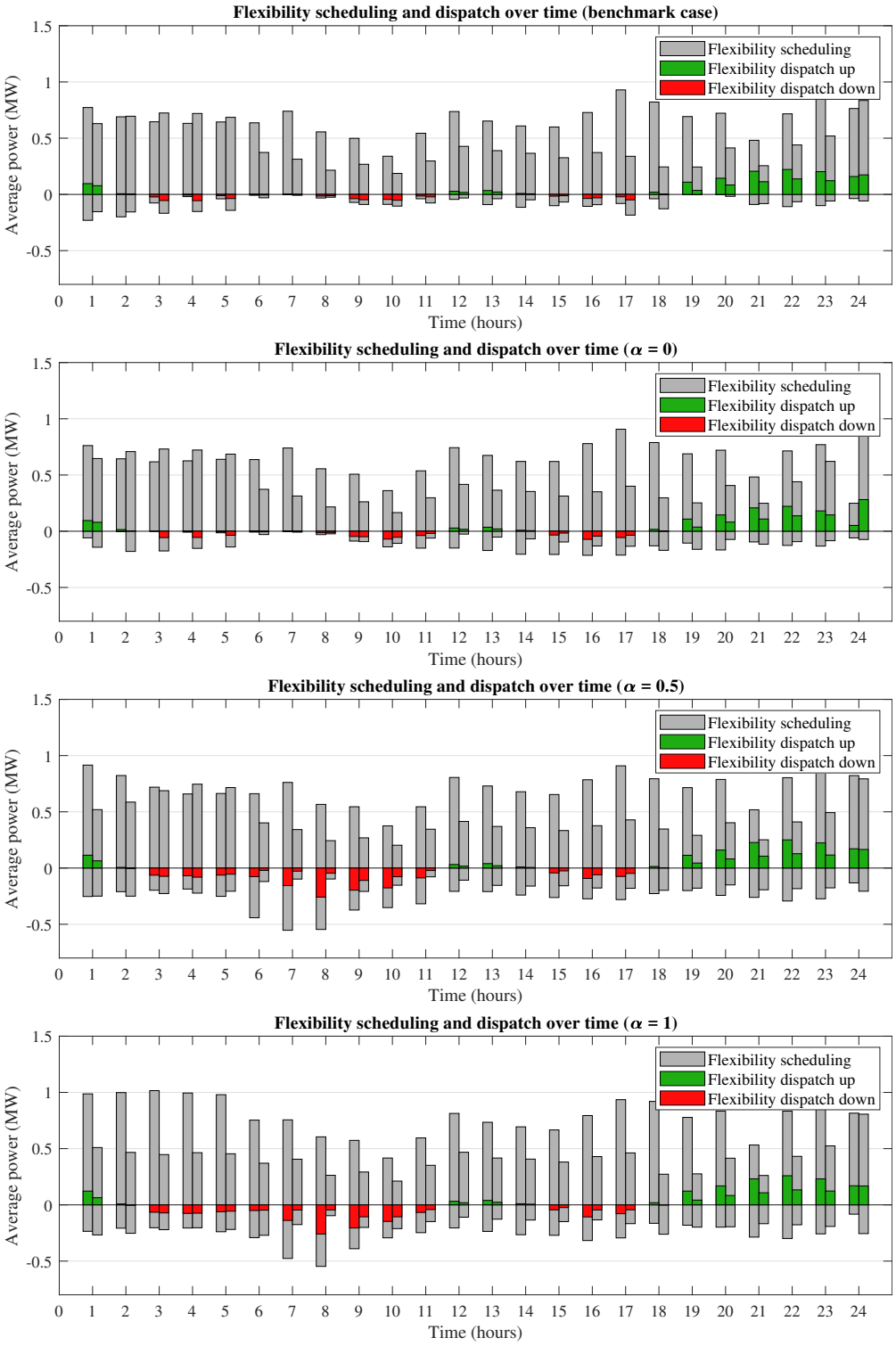

Figure 5.9: Average reserve and flexibility dispatch per hour (for one day) compared to the reserve and flexibility scheduled for different values of α.

5.7 Conclusion

In this chapter, *research questions 6 and 7* were addressed, and a new development for the BtG framework with uncertain generation was presented, by embedding a dynamical model for social incentives for demand flexibility services. As stated in the introduction, the goal was not to develop models that have well-founded roots in sociological or psychological research, but only to introduce a first outline for such a model. First of all, we developed the sociological operating model, to reflect the consumer incentive to maximize utilization of available wind power. Second, we proposed a model to reflect the ancillary services market, with the goal of maximizing consumer participation in providing demand-side flexibility.

From the simulation study, it is concluded that both models have a significant impact on the performance of the system. Intensifying the relative importance of the operating model resulted in an increase of 68.65% in solar power penetration. Furthermore, the market model resulted in enhanced deployment of demand-side flexibility on the ancillary services market, even if consumer incentives for increasing solar power utilization were present as well. However, the centralized optimization approach of the current study prohibits to study social incentives on the level of individual consumers, and also leads to very divided levels of participation of individuals. Although the operating and market model both show the intended effects on the performance of the system, the implementation is paired with an increase of 6.0 - 14.7% in total electricity consumption.

To conclude this chapter, it is postulated that consumer incentives for the utilization of RES, and consumer participation on the ancillary services market can have a significant impact on performance of the power system. However, we stress that the current research is not yet sufficient to draw essential conclusions, as it lacks a rigorous link with sociological research, and is based on many simplifications. Our ongoing research is also devoted to this limitations, and we anticipate to submit a paper to present our future results on the subject (Rostampour et al., 2019b). In the discussion in Chapter 6, it is highlighted how the results presented in this thesis can serve as basis for further research on the topic.

6 Limitations and Further Work

The purpose of this chapter is to discuss the limitations of the current research, and to put them into perspective for further research. First of all, the validity of assumptions made in this study is assessed. Second, limitations and restrictions of the current models are discussed. Finally, the proposed sociological dynamics are reviewed by addressing the lack of a rigorous connection with the theory, and an overview of current and future research directions is provided.

6.1 Validity of current assumptions

In this section, we list the most important assumptions made throughout the current thesis, and assess their validity. In some cases, the rationale behind the assumptions is justified, and recommendations for further research are made.

First of all, cost coefficients were assumed to be constant throughout the horizon of the simulation studies. As this assumption reduces the degrees of freedom of the optimization model, it allows for more direct comparison of the simulated cases. However, electricity prices are generally not constant, and multiple authors have developed bidding mechanisms for the purpose of real-time dispatch, frequency regulation and price-responsive demand (Ilić et al., 2011a; Stegink et al., 2018b). Using such an approach, the different control layers of the power system can potentially be merged, in order to close the gap between long-term system optimization and real-time frequency regulation (Stegink et al., 2018a). By embedding dynamic costs and bidding mechanisms in the simulation studies, this issue can be addressed in a follow-up study.

Second, the cost coefficients used in the current simulation studies were primarily determined such that all individual contributions to the objective were reflected appropriately in the results. However, the current strategy might not reflect actual practice optimally, and better estimates can potentially be made, based on similar case studies in the literature.

Throughout the current study, perfect communication between stakeholders was assumed. Although the social element was reflected in the sociological dynamics in Chapter 5, this still assumed perfect transmission of information, without any miscommunication or lost data. In reality, this assumption is not true, as transmitted data can be incomplete and subject to delays (Mesbahi and Egerstedt, 2010; Mohammadi et al., 2018). In order to improve the accuracy of the current models, the assumptions of total collaboration and complete information-sharing need to be evaluated in more detail.

Finally, most of the parameters used in the current simulation studies, including power load patterns, physical building parameters, and wind and solar power generation curves, were all adopted from other references, such as Taha et al. (2019), Zimmerman et al. (2011) and Rostampour (2012). Due to the limited time span of the current study, validation of the large number of system parameters was not possible. In future research, this could be further investigated,

by theoretical or empirical justification of the parameters and input data for the specific power network structure in the problem formulation.

6.2 Limitations and restrictions of current models

First of all, all models in the current study are based on the DC power flow approximation. Furthermore, all MPC predictive dynamics were linearized, to render the problem convex and improve computational performance. Hence, reactive power flow analysis and the nonlinear nature of real power systems are not considered in the current study. Voltage regulation of distribution networks is one of the main issues in large deployment of decentralized RES (Gill et al., 2014), and is closely related to reactive power management (Qin, 2018). The small-angle approximation in DC power flow is generally not valid for stressed power networks. In emergency conditions, voltage angle differences of up to $\pm 30°$ can occur in heavily loaded transmission lines, leading to a linearization error of 16% in power transfer (Frank and Rebennack, 2016). In a follow-up study, the current BtG framework could, therefore, be extended to nonlinear, AC models, in order to improve accuracy of the predictive dynamics, and to better reflect the real power system, in particular under heavy stress.

Another limitation of the current modeling framework is that all entities involved operate at the same time resolution for control decisions. Although this simplifies formulation of the optimization problems, the assumption of a universal decision-making time resolution cannot be justified in real power system practice (Taha et al., 2019). While grid regulation problems are often reflected in seconds, building HVAC control-decisions are much slower (Dong et al., 2018). A move-blocking strategy was proposed by Taha et al. (2019), to address the time-scale discrepancies between the grid and buildings in a BtG model. By constraining groups of adjacent-in-time predicted inputs to have equal values, a move-blocking scheme can reduce the computational complexity of the MPC problem, and allows to distinguish between different control time scales (Shekhar and Manzie, 2015). In an extension of the current research, a similar strategy can be used to address the issue of time-scale discrepancies.

The network topology considered in all simulation studies was based on the MatPower 5-bus (Case 5) power system, which is a modification of the original PJM 5-bus system (Li and Bo, 2010). Although this specific network is suitable for studies on economic power flow, no other topologies were considered in the current study. Moreover, the DSO networks were designed as generic, radially shaped networks, but were not based on a specific reference. Therefore, conclusions of the current simulation studies need to be verified by considering different or extended networks, such as the IEEE 30-bus system (Li and Bo, 2010) or other MatPower cases (Zimmerman et al., 2011). Furthermore, DSO topologies should be adopted from real distribution networks, to further improve the accuracy of the obtained results.

Following the previous limitation on network size, it must be noted that executing one receding horizon MPC with uncertain generation for the 24 hour simulation time (w-BtG-MPC) can take up to 30 minutes. Therefore, in order to study networks of larger sizes, it is highly recommended to develop distributed MPC formulations, instead of the centralized approach used in the current study. A distributed optimization approach is highly beneficial for scalability of the

control scheme (Doddema, 2015; Halvgaard et al., 2016), and allows for better reflection of the decentralized decision-making nature of individual consumers (Larsen et al., 2013a). For example, the integration of the sociological market model in Chapter 5 resulted in highly scattered levels of demand-side flexibility offered by individual consumers. By adopting a distributed optimization approach, end-users can make individual control decisions based on price incentives, local information, and their own constraints, while still respecting the goal of optimization of the complete power system (Larsen et al., 2014b). Finally, distributed optimization allows to reflect competitive markets, for example by involvement of multiple, non-cooperative DSOs or aggregators that strive for maximization of their own profits (Mohammadi et al., 2018; van der Werf, 2017). Distributed MPC models have been widely proposed in literature (ter Haar, 2016; Halvgaard et al., 2016; Kramer, 2015; Larsen et al., 2013b), and can be used to derive distributed formulations of the centralized optimization problems in a follow-up study.

Finally, the current study primarily focused on technical elements of the power system. Consequently, other perspectives, such as legal aspects, were left outside of the scope. Although research on legal aspects requires different methods and approaches, it is fundamentally important for the applicability of the technical elements addressed in this study. For example, the European Parliament (2012) concluded that legal and regulatory provisions are required to remove barriers for achieving the current climate goals. Contracts between flexible consumers (or aggregators) and the DSO should include requirements that they are obliged to respond to the request of the grid operator (Zegers and Brunner, 2014). To allow the creation of new transparent flexibility services at distribution level, national regulators should properly implement existing and new legislation (Eurelectric, 2013). Although current legislation of some countries allows DSOs to directly procure demand-side flexibility, the overall grid security is generally ensured by the TSO (Silva et al., 2018). Hence, in order to also allow safe operation of the distribution grid, legislation that allows DSOs to procure flexibility should be implemented. It is, thus, important to address the legal aspect in a follow-up study, in order to assess the current (and future) applicability of the conclusions of this thesis.

6.3 Towards a rigorous sociological modeling framework

In Chapter 5, a dynamical model for social incentives for demand flexibility services was proposed, consisting of an operating model to reflect consumer incentives to maximize wind power utilization, and a market model to reflect the ancillary services market. Although the model provides guidelines for the impact on the behavior and performance of the power system, it lacks a rigorous connection with the psychological or sociological theory yet. Therefore, we are not in position to draw strong conclusions from the corresponding simulation study, and can only postulate about potential implications.

In order to develop a more fundamentally rigorous model, it should be linked to the psychological and sociological theory on the subject. Although the limited time span of the current thesis prohibits extensive research on this subject, our ongoing research is also devoted to this. In our ongoing research, we attempt to verify the hypothesized modeling proposed in Chapter 5, by connecting it to the available literature. In the remainder of this section, we provide a prelimi-

nary discussion, to link our proposed model to similar models developed by other authors.

In order to enhance power transmission while considering network congestion, Liu et al. (2008) developed a model for maximizing the so-called *social welfare*, which is defined as the well-being or benefits of various groups, such as customers and producers in the market (Perloff, 2011). Although the social welfare typically focuses on economical aspects, its main idea is similar to the sociological dynamics proposed in the current study. By maximizing the social welfare, real-time regulation of the power system can be achieved, while satisfying the grid capacity limit constraints (Stegink et al., 2017). The concept of social welfare was applied by Kiani et al. (2014) to develop a hierarchical control methodology, with the goal to ensure frequency regulation using optimal allocation of resources in a power grid with uncertain generation. Furthermore, the social welfare was used by Kiani and Annaswamy (2010) as a measure for comparing different cases in a simulation study on the effect of a smart meter on congestion management and stability in a power system market. Chanda and De (2014) developed a price responsive OPF model, which minimizes traditional objectives, while also maximizing social welfare. The authors introduced a *willingness to pay* factor, and successfully validated the model by carrying out simulations on the IEEE 30-bus system. Finally, social welfare maximization in pool-based competitive electricity markets was considered by Singh et al. (2010) to address the problems of reactive power procurement and congestion management.

We stress that the focus of social welfare is typically on economical aspects, whereas the goal of our proposed sociological model is also to capture social consumer incentives, i.e. the maximization of solar power utilization. Nevertheless, the concept of social welfare and its application in the studies mentioned above could potentially provide a good foundation for the envisioned sociological model.

7 Concluding Remarks

The main goal of this study, as determined in Section 1.3, was to develop a holistic power system framework with BtG integration, and to use this framework to explore the potential role of buildings in the regulation and control of power systems with high penetration of RES. In this concluding chapter, it is reviewed if this goal has been achieved, and to what extend.

In the thesis, we proposed a novel Buildings-to-Grid (BtG) modeling framework, which extends the current models in literature on multiple aspects. We successfully integrated demand-side flexibility as alternative to reserve scheduling, introduced uncertain generation from wind power, and developed guidelines for sociological dynamics to capture the impact of social incentives on the system. In the remainder of this chapter, a number of concluding remarks are given, in order to formulate answers to the research questions of the thesis. Based on these points, it is concluded that the research goal has been achieved, and that the corresponding research problem has been addressed in as much detail as possible, within the limitations of the current study.

First of all, in Chapter 3, the potential role of individual buildings in frequency control of the power system was demonstrated, by utilizing their inherent thermal inertia, and introducing electrical storage units for demand-side flexibility. The simulation study showed that building flexibility has significant regulative capacity for the grid, and can reduce grid frequency deviations by up to 64.17%, by reducing power demand ramp up/down and minimizing load fluctuations. Based on this chapter, it is concluded that buildings can play an important role in the (frequency) regulation of power systems, even in the absence of RES or other sources of uncertainty.

Second, a tractable robust reformulation of the stochastic MPC with uncertain wind power generation was developed in Chapter 4. The simulation study showed that demand-side flexibility can substitute reserve scheduling in networks with wind power penetration of at least 20%. With the use of Monte Carlo simulations, it is empirically validated that the given solutions are feasible in the power system with high probability, and that the number of violations of system constraints is negligible. Based on this chapter, it is concluded that demand-side flexibility can substitute the traditional reserve scheduling, without losing stability properties of the grid and violating other constraints.

Finally, social incentives for demand flexibility services were explored in Chapter 5, and the impact of the so-called operating model and market model on the performance of the system were studied. It was concluded that the dynamics for the incentive of using solar power (i.e. operating model) successfully increased the use of solar power by consumers. Furthermore, integrating the ancillary services market model dynamics resulted in increased consumer participation on the ancillary services market. In particular, the deployment of flexibility substituted the use of reserves almost completely. Although it must be stressed that the developed sociological dynamics only provide a first guideline, it is, therefore, postulated that societal elements can have a significant impact on the integration of RES and deployment of demand-side flexibility.

8 Bibliography

Abdi, H., Beigvand, S. D., and Scala, M. L. (2017). A review of optimal power flow studies applied to smart grids and microgrids. *Renewable and Sustainable Energy Reviews*, 71:742–766.

Ahmadimanesh, A. and Kalantar, M. (2017). Two new frameworks for reactive power market considering reactive losses. *International Transactions on Electrical Energy Systems*, 27(10):e2387.

Andersson, G. (2004). *Modelling and Analysis of Electric Power Systems*. ETH Zürich, Zürich.

Anwar, M. B., Cabrera, C. A., Neu, O., O'Malley, M., and Burke, D. J. (2017a). An integrated Building-to-Grid model for evaluation of energy arbitrage value of Thermal Storage. *2016 International Conference for Students on Applied Engineering, ICSAE 2016*, pages 64–69.

Anwar, M. B., O'Malley, M., and Burke, D. J. (2017b). Evaluation of flexibility impacts of thermal electric storage using an integrated building-to-grid model. *2017 5th IEEE International Conference on Smart Energy Grid Engineering, SEGE 2017*, pages 242–247.

Badings, T. S., Rostampour, V., and Scherpen, J. M. A. (2019). Distributed building energy storage units for frequency control service in power systems (accepted). In *2019 IFAC Workshop on Control of Smart Grids and Renewable Energy Sources*.

Beil, I., Hiskens, I., and Backhaus, S. (2016). Frequency Regulation From Commercial Building HVAC Demand Response. *Proceedings of the IEEE*, 104(4):745–757.

Ben-Tal, A. and Nemirovski, A. (1998). Robust Convex Optimization. *Mathematics of Operations Research*, 23(4):769–805.

Bharati, G. R., Razmara, M., Paudyal, S., Shahbakhti, M., and Robinett, R. D. (2016). Hierarchical optimization framework for demand dispatch in building-grid systems. In *2016 IEEE Power and Energy Society General Meeting (PESGM)*.

Blum, D. H. (2016). *Improving the Use of Commercial Building HVAC Systems for Electric Grid Ancillary Services*. PhD thesis, Massachusetts Institute of Technology.

Blum, D. H., Zakula, T., and Norford, L. K. (2017). Opportunity Cost Quantification for Ancillary Services Provided by Heating, Ventilating, and Air-Conditioning Systems. *IEEE Transactions on Smart Grid*, 8(3):1264–1273.

Boyd, S. and Vandenberghe, L. (2004). *Convex Optimization*. Cambridge University Press, Cambridge.

BPA (2014). Energy Imbalance Service - BPA Transmission Business Practice. *Bonneville Power Adiministration*.

Bragard, M., Member, S., Soltau, N., Member, S., Thomas, S., Member, S., and Doncker, R. W. D. (2010). The Balance of Renewable Sources and User Demands in Grids : Power Electronics for Modular Battery Energy Storage Systems. *IEEE Transactions on Power Electronics*, 25(12):3049–3056.

Breeze, P. (2014). *Power generation technologies*. Newnes, Boston, 2nd edition.

Bullo, F. (2018). *Lectures on Network Systems*. CreateSpace, 1 edition. With contributions by J. Cortes, F. Dorfler, and S. Martinez.

Cabadag, R. I., Schmidt, U., and Schegner, P. (2015). The voltage control for reactive power management by decentralized wind farms. *2015 IEEE Eindhoven PowerTech, PowerTech 2015*, pages 1–6.

Calafiore, G. C. and Campi, M. C. (2006). The scenario approach to robust control design. *IEEE Transactions on Automatic Control*, 51(5):742–753.

Camacho, E. and Bordons, C. (2007). *Model Predictive Control*. Springer.

Campi, M. C., Garatti, S., and Prandini, M. (2009). The scenario approach for systems and control design. *Annual Reviews in Control*, 33(2):149–157.

Chanda, S. and De, A. (2014). A multi-objective solution algorithm for optimum utilization of Smart Grid infrastructure towards social welfare. *International Journal of Electrical Power and Energy Systems*, 58:307–318.

Chung, C. Y., Chung, T. S., Yu, C. W., and Lin, X. J. (2004). Cost-based reactive power pricing with voltage security consideration in restructured power systems. *Electric Power Systems Research*, 70(2):85–91.

Conejo, A. J. and Baringo, L. (2018). *Power System Operations*. Springer, Switzerland.

Conte, F., D'Agostino, F., Massucco, S., Palombo, G., Silvestro, F., Bossi, C., and Cabiati, M. (2017). Dynamic equivalent modelling of active distribution networks for TSO-DSO interactions. In *2017 IEEE PES Innovative Smart Grid Technologies Conference Europe (ISGT-Europe)*, pages 1–6.

Corbin, C. D., Makhmalbaf, A., Huang, S., Mendon, V. V., Zhao, M., Somasundaram, S., Liu, G., Ngo, H., and Katipamula, S. (2016). Transactive Control of Commercial Building HVAC Systems. *U.S. Department of Energy*.

Danza, L., Belussi, L., Meroni, I., Salamone, F., Floreani, F., Piccinini, A., and Dabusti, A. (2016). A Simplified Thermal Model to Control the Energy Fluxes and to Improve the Performance of Buildings. *Energy Procedia*, 101:97–104.

Deane, J. P., Ó Gallachóir, B. P., and McKeogh, E. J. (2010). Techno-economic review of existing and new pumped hydro energy storage plant. *Renewable and Sustainable Energy Reviews*, 14(4):1293–1302.

Dentcheva, D. (2006). Optimization Models with Probabilistic Constraints. In Calafiore, G. and Dabbene, F., editors, *Probabilistic and Randomized Methods for Design under Uncertainty*, chapter 2, pages 49–97. Springer, London.

Doddema, L. (2015). *MSc Thesis. Scalability of DMPC Demand Response in the Context of the Universal Smart Energy Framework*. University of Groningen.

Dong, B. (2010). *Integrated Building Heating, Cooling and Ventilation Control*. PhD thesis, Carnegie Mellon University, Pittsburgh, PA.

Dong, B., Taha, A. F., Gatsis, N., Li, Z., and Pipri, A. (2018). Impact of Occupancy-Based Buildings-to-Grid Integration on Frequency Regulation in Smart Grids. In *2018 Annual American Control Conference (ACC)*, pages 5399–5405.

EAC (2018). The Transmission-Distribution Interface - Recommendations for the U.S. Department of Energy. *Electricity Advisory Committee*.

ENTSO-E (2015). Towards smarter grids : Developing TSO and DSO roles and interactions for the benefit of consumers. *European Network of Transmission System Operators for Electricity*.

Eurelectric (2013). Active Distribution System Management A key tool for the smooth integration - findings and recommendations. *Union of the Electricity Industry*.

Eurelectric (2014). Flexibility and aggregation - requirements for their interaction in the market. *Union of the Electricity Industry*.

European Parliament (2012). Directive 2012/27/EU. *Official Journal of the European Union*, L315:1–56.

European Union (2013). A 2030 framework for climate and energy policies (green paper). https://eur-lex.europa.eu/LexUriServ/LexUriServ.do?uri=COM:2013:0169:FIN:EN:PDF.

FERC (2018). Guide to market oversight - glossary. Federal Energy Regulatory Commission, https://www.ferc.gov/market-oversight/guide/glossary.asp.

Ferreira, H. L., Garde, R., Fulli, G., Kling, W., and Lopes, J. P. (2013). Characterisation of electrical energy storage technologies. *Energy*, 53:288–298.

Frank, S. and Rebennack, S. (2016). An introduction to optimal power flow: Theory, formulation, and examples. *IIE Transactions (Institute of Industrial Engineers)*, 48(12):1172–1197.

Freeman, R. E. (2010). *Strategic Management: A Stakeholder Approach*. Pitman Series in Business and Public Policy. Cambridge University Press.

Gear, C. W. (1971). *Numerical Initial Value Problems in Ordinary Differential Equations*. Prentice-Hall, Englewood Cliffs, New Jersey.

Gellings, C. W. (2017). Evolving practice of demand-side management. *Journal of Modern Power Systems and Clean Energy*, 5(1):1–9.

Gill, S., Kockar, I., and Ault, G. W. (2014). Dynamic optimal power flow for active distribution networks. *IEEE Transactions on Power Systems*, 29(1):121–131.

Gržanić, M., Capuder, T., and Krajcar, S. (2018). DSO and Aggregator Sharing Concept for Distributed Battery Storage System. *2018 IEEE International Conference on Environment and Electrical Engineering and 2018 IEEE Industrial and Commercial Power Systems Europe (EEEIC / I&CPS Europe)*, pages 1–6.

Gurobi Optimization, LLC (2019). Gurobi optimizer reference manual.

Halamay, D. A., Brekken, T. K., Simmons, A., and McArthur, S. (2011). Reserve requirement impacts of large-scale integration of wind, solar, and ocean wave power generation. *IEEE Transactions on Sustainable Energy*, 2(3):321–328.

Halvgaard, R., Vandenberghe, L., Poulsen, N. K., Madsen, H., and Jørgensen, J. B. (2016). Distributed Model Predictive Control for Smart Energy Systems. *IEEE Transactions on Smart Grid*, 7(3):1675–1682.

Hirst, E. and Kirby, B. (1996). Electric-Power Ancillary services. *Energy Devision*.

Hodge, B. (2006). Solar power data for integration studies. *National Renewable Energy Laboratory*.

Hong, L. J., Huang, Z., and Lam, H. (2017). Learning-based robust optimization: Procedures and statistical guarantees. *Available on arXiv*.

IFAC (2019). Workshop on Control of Smart Grids and Renewable Energy Sources (CSGRES 2019), Korea.

Ilić, M. D., Xie, L., and Joo, J. Y. (2011a). Efficient coordination of wind power and price-responsive demand—Part I: Theoretical foundations. *IEEE Transactions on Power Systems*, 26(4):1875–84.

Ilić, M. D., Xie, L., and Joo, J. Y. (2011b). Efficient coordination of wind power and price-responsive demand - Part II: Case studies. *IEEE Transactions on Power Systems*, 26(4):1885–1893.

Jerez, J. L., Constantinides, G. A., and Kerrigan, E. C. (2011a). An FPGA implementation of a sparse quadratic programming solver for constrained predictive control. In *19th ACM/SIGDA international symposium on Field programmable gate arrays - FPGA '11*, pages 209–218.

Jerez, J. L., Kerrigan, E. C., and Constantinides, G. A. (2011b). A condensed and sparse QP formulation for predictive control. *Proceedings of the IEEE Conference on Decision and Control*, pages 5217–5222.

Jiang, T., Li, Z., Jin, X., Chen, H., Li, X., and Mu, Y. (2018). Flexible operation of active distribution network using integrated smart buildings with heating, ventilation and air-conditioning systems. *Applied Energy*, 226:181–196.

Kargarian, A., Fu, Y., and Wu, H. (2016). Chance-constrained system of systems based operation of power systems. *IEEE Transactions on Power Systems*, 31(5):3404–3413.

Kempton, W., Udo, V., Huber, K., Komara, K., Letendre, S., Baker, S., Brunner, D., and Pearre, N. (2008). A test of Vehicle-to-Grid (V2G) for Energy Storage and Frequency Regulation in the PJM System. *Results from an Industry-University Research Partnership*.

Kiani, A. and Annaswamy, A. (2010). The effect of a smart meter on congestion and stability in a power market. *Proceedings of the IEEE Conference on Decision and Control*, pages 194–199.

Kiani, A., Annaswamy, A., and Samad, T. (2014). A hierarchical transactive control architecture for renewables integration in smart grids: Analytical modeling and stability. *IEEE Transactions on Smart Grid*, 5(4):2054–2065.

Kiliccote, S., Piette, M. A., and Ghatikar, G. (2011). Smart Buildings and Demand Response. In *American Institute of Physics Conference Series*, volume 1401, pages 328–338.

Kirby, B., Hirst, E., and Vancoevering, J. (1995). Identification and definition of unbundled electric generation and transmission services. *Oak Ridge National Laboratory*.

Kramer, W. (2015). *MSc Thesis. The Distribution System Operator in a d-MPC application for USEF*. University of Groningen.

Kwatny, H. G. and Miu-Miller, K. (2016). *Power System Dyanamics and Control*. Birkhäuser, New York.

La Bella, A., Farina, M., Sandroni, C., and Scattolini, R. (2018). Design of aggregators for the day-ahead management of microgrids providing active and reactive power services. *Available from arXiv*, pages 1–13.

Lamadrid, A. J., Mount, T. D., and Thomas, R. J. (2011). Scheduling of Energy Storage Systems with geographically distributed renewables. *Proceedings - 9th IEEE International Symposium on Parallel and Distributed Processing with Applications Workshops, ISPAW 2011 - ICASE 2011, SGH 2011, GSDP 2011*, pages 85–90.

Lampropoulos, I., Baghină, N., Kling, W. L., and Ribeiro, P. F. (2013). A predictive control scheme for real-time demand response applications. *IEEE Transactions on Smart Grid*, 4(4):2049–2060.

Larsen, G. (2014). *Distributed Control of a Network with Multiple Electricity Producers and Consumers*. PhD thesis, University of Groningen.

Larsen, G. K., Van Foreest, N. D., and Scherpen, J. M. (2013a). Distributed control of the power supply-demand balance. *IEEE Transactions on Smart Grid*, 4(2):828–836.

Larsen, G. K., Van Foreest, N. D., and Scherpen, J. M. (2014a). Distributed MPC applied to a network of households with Micro-CHP and heat storage. *IEEE Transactions on Smart Grid*, 5(4):2106–2114.

Larsen, G. K., van Foreest, N. D., and Scherpen, J. M. (2014b). Power supply-demand balance in a Smart Grid: An information sharing model for a market mechanism. *Applied Mathematical Modelling*, 38(13):3350–3360.

Larsen, G. K. H., Pons, J., Achterop, S., and A, S. J. M. (2013b). Distributed mpc applied to power demand side control. In *Proceedings of the 2013 European Control Conference (ECC)*, pages 3295–3300.

Lawrence, T. M., Boudreau, M. C., Helsen, L., Henze, G., Mohammadpour, J., Noonan, D., Patteeuw, D., Pless, S., and Watson, R. T. (2016). Ten questions concerning integrating smart buildings into the smart grid. *Building and Environment*, 108:273–283.

Lee, D., Nguyen, H. D., Dvijotham, K., and Turitsyn, K. (2018). Convex Restriction of Power Flow Feasibility Set. *Available from arXiv*.

Li, F. and Bo, R. (2010). Small test systems for power system economic studies. In *IEEE PES General Meeting*, pages 1–4.

Lin, Y., Barooah, P., and Mathieu, J. L. (2015). Ancillary services to the grid from commercial buildings through demand scheduling and control. In *2015 American Control Conference (ACC)*, pages 3007–3012. American Automatic Control Council.

Lin, Y., Barooah, P., and Mathieu, J. L. (2017). Ancillary Services Through Demand Scheduling and Control of Commercial Buildings. *IEEE Transactions on Power Systems*, 32(1):186–197.

Liu, H., Shen, Y., Zabinsky, Z. B., Liu, C. C., Courts, A., and Joo, S. K. (2008). Social welfare maximization in transmission enhancement considering network congestion. *IEEE Transactions on Power Systems*, 23(3):1105–1114.

Liu, Y., Yu, N., Wang, W., Guan, X., Xu, Z., Dong, B., and Liu, T. (2018). Coordinating the operations of smart buildings in smart grids. *Applied Energy*, 228(July):2510–2525.

Lofberg, J. (2004). Yalmip : a toolbox for modeling and optimization in matlab. In *2004 IEEE International Conference on Robotics and Automation (IEEE Cat. No.04CH37508)*, pages 284–289.

Löfberg, J. (2012). Oops i cannot do it again: Testing for recursive feasibility in MPC. *Automatica*, 48(3):550–555.

Lund, P. D., Lindgren, J., Mikkola, J., and Salpakari, J. (2015). Review of energy system flexibility measures to enable high levels of variable renewable electricity. *Renewable and Sustainable Energy Reviews*, 45:785–807.

Lymperopoulos, I., Qureshi, F. A., Nghiem, T., Khatir, A. A., and Jones, C. N. (2015). Providing ancillary service with commercial buildings: The Swiss perspective. *IFAC-PapersOnLine*, 28(8):6–13.

Ma, O., Alkadi, N., Cappers, P., Denholm, P., Dudley, J., Goli, S., Hummon, M., Kiliccote, S., MacDonald, J., Matson, N., Olsen, D., Rose, C., Sohn, M. D., Starke, M., Kirby, B., and

O'Malley, M. (2013). Demand response for ancillary services. *IEEE Transactions on Smart Grid*, 4(4):1988–1995.

Macdonald, J., Cappers, P., and Callaway, D. (2012). Demand Response Providing Ancillary Services A Comparison of Opportunities and Challenges in the US Wholesale Markets. In *Grid-Interop Forum 2012*, Irving, TX.

MacDougall, P., Roossien, B., Warmer, C., and Kok, K. (2013). Quantifying flexibility for smart grid services. In *2013 IEEE Power Energy Society General Meeting*, pages 1–5. IEEE.

Machowski, J., Dong, Z. Y., Member, S., and Zhang, P. (2008). *Power System Dynamics: Stability and Control*. John Wiley & Sons, Ltd., Chichester, 2nd edition.

Maciejowski, J. M. (2002). *Predictive control: with constraints*. Pearson education.

Mallada, E., Zhao, C., and Low, S. (2017). Optimal Load-Side Control for Frequency Regulation in Smart Grids. *IEEE TRANSACTIONS ON AUTOMATIC CONTROL*, 62(12):6294–6309.

Margellos, K., Goulart, P., and Lygeros, J. (2014). On the road between robust optimization and the scenario approach for chance constrained optimization problems. *IEEE Transactions on Automatic Control*, 59(8):2258–2263.

Margellos, K., Haring, T., Hokayem, P., Schubiger, M., Lygeros, J., and Andersson, G. (2012). A Robust Reserve Scheduling Technique for Power Systems with High Wind Penetration. *Proceedings of PMAPS*, pages 870–875.

McCalley, J. (2012). The dc power flow equations - steady-state analysis.

Mesbahi, M. and Egerstedt, M. (2010). *Graph Theoretic Methods in Multiagent Networks*. Princeton University Press, New Jersey, 1st edition.

Mirakhorli, A. and Dong, B. (2016). Occupancy behavior based model predictive control for building indoor climate—A critical review. *Energy and Buildings*, 129:499–513.

Mohammadi, A., Mehrtash, M., and Kargarian, A. (2018). Diagonal Quadratic Approximation for Decentralized Collaborative TSO+DSO Optimal Power Flow. *IEEE Transactions on Smart Grid*, 3053(c).

Molder, E., Bailey, V., Hoecker, J., Massey, W., and Santa, J. D. (1996). Order No. 888 - Final Rule. Technical report, USA Federal Energy Regulatory Commission.

NERC (2010). Potential reliability impacts of emerging flexible resources. *North American Electric Reliability Corporation*.

NGK (2008). Clean energy action project. rokkasho-futumata wind farm (the largest nas station stabilizes 51mw wind power). *NGK Insulators, ltd.*

Nguyen, D. B., Scherpen, J. M. A., and Bliek, F. (2017). Distributed Optimal Control of Smart Electricity Grids with Congestion Management. *IEEE Transactions on Automation Science and Engineering*, 14(2):494–504.

Papaefthymiou, G. and Klöckl, B. (2008). MCMC for wind power simulation. *IEEE Transactions on Energy Conversion*, 23(1):234–240.

Papaefthymiou, G., Schavemaker, P. H., van der Sluis, L., Kling, W. L., Kurowicka, D., and Cooke, R. M. (2006). Integration of stochastic generation in power systems. *International Journal of Electrical Power and Energy Systems*, 28:655–667.

Papalexopoulos, A. D. and Andrianesis, P. E. (2014). Performance-based pricing of frequency regulation in electricity markets. *IEEE Transactions on Power Systems*, 29(1):441–449.

Patel, N. R., Risbeck, M. J., Rawlings, J. B., Wenzel, M. J., and Turney, R. D. (2016). Distributed economic model predictive control for large-scale building temperature regulation. In *2016 American Control Conference (ACC)*, pages 895–900.

Pavlak, G. S., Henze, G. P., and Cushing, V. J. (2014). Optimizing commercial building participation in energy and ancillary service markets. *Energy and Buildings*, 81:115–126.

Perloff, J. M. (2011). *Microeconomics (The Pearson Series in Economics)*. Addison-Wesley New York, 2nd edition.

Pillay, A., Prabhakar Karthikeyan, S., and Kothari, D. P. (2015). Congestion management in power systems - A review. *International Journal of Electrical Power and Energy Systems*, 70:83–90.

Pimm, A. J., Garvey, S. D., and Drew, R. J. (2011). Shape and cost analysis of pressurized fabric structures for subsea compressed air energy storage. *Proceedings of the Institution of Mechanical Engineers, Part C: Journal of Mechanical Engineering Science*, 225(5):1027–1043.

Poonpun, P. and Jewell, W. T. (2008). Analysis of the Cost per Kilowatt Hour to Store Electricity. *IEEE Transactions on Energy Conversation*, 23(2):529–534.

Prékopa, A. (1970). on Probabilistic Constrained Programming. In *Princeton Symposium on Mathematical Programming*, pages 113–138. Princeton University Press.

Qin, N. (2018). *Voltage Control in the Future Power Transmission Systems*. PhD thesis, Aalborg University.

Rabiee, A., Shayanfar, H., and Amjady, N. (2009). A New Framework for Reactive Power Market Considering Power System Security. *Iranian Journal of Electrical and Electronic Engineering*, 5(3):196–204.

Razmara, M., Bharati, G. R., Hanover, D., Shahbakhti, M., Paudyal, S., and Robinett, R. D. (2017a). Building-to-grid predictive power flow control for demand response and demand flexibility programs. *Applied Energy*, 203:128–141.

Razmara, M., Bharati, G. R., Hanover, D., Shahbakhti, M., Paudyal, S., and Robinett, R. D. (2017b). Enabling Demand Response programs via Predictive Control of Building-to-Grid systems integrated with PV Panels and Energy Storage Systems. In *2017 American Control Conference (ACC)*, pages 56–61.

Razmara, M., Bharati, G. R., Shahbakhti, M., Paudyal, S., and Robinett, R. D. (2018). Bilevel optimization framework for smart building-to-grid systems. *IEEE Transactions on Smart Grid*, 9(2):582–593.

Rebours, Y. and Kirschen, D. (2005). What is spinning reserve? *University of Manchester*.

Reinders, J., Morren, J., and Slootweg, H. (2017). Comparing probabilistic load flow methods in dealing with uncertainties at TSO/DSO interface. In *2017 52nd International Universities Power Engineering Conference (UPEC)*, pages 1–5.

Rene, A. S. (2016). *MSc Thesis. Model Predictive Control of District Heating Systems*. Norwegian University of Science and Technology.

Riffonneau, Y., Bacha, S., Barruel, F., and Ploix, S. (2011). Optimal power flow management for grid connected PV systems with batteries. *IEEE Transactions on Sustainable Energy*, 2(3):309–320.

Rodríguez, A. G. G., Rodríguez, A. G., and Payán, M. B. (2007). Estimating Wind Turbines Mechanical Constants. *Renewable Energies and Power Quality Journal*, 1(5):697–704.

Roossien, B. (2011). Mathematical quantification of near real- time flexibility for Smart Grids. *Energy research Centre of the Netherlands*.

Rostampour, V. (2012). *MSc Thesis. Tractable Reserve Scheduling Formulations for Power Systems with Uncertain Generation*. Politecnico di Milano, Milan.

Rostampour, V., Badings, T. S., and Scherpen, J. M. A. (2019a). Buildings-to-grid integration with high wind power penetration (submitted). In *2019 IEEE Conference on Decision and Control*.

Rostampour, V., Badings, T. S., and Scherpen, J. M. A. (2019b). Social incentives for demand flexibility services in buildings-to-grid integration with uncertain generation (under preparation). *IEEE Transactions on Power Systems*.

Rostampour, V. and Keviczky, T. (2017). Energy management for building climate comfort in uncertain smart thermal grids with aquifer thermal energy storage. *IFAC World Congress*, 50:13156–13163.

Rostampour, V. and Keviczky, T. (2018). Probabilistic energy management for building climate comfort in smart thermal grids with seasonal storage systems. *IEEE Transactions on Smart Grid*.

Rostampour, V., Ter Haar, O., and Keviczky, T. (2019c). Distributed stochastic reserve scheduling in ac power systems with uncertain generation. *IEEE Transactions on Power Systems*, 34(2):1005–1020.

Saint-Pierre, A. and Mancarella, P. (2017). Active Distribution System Management: A Dual-Horizon Scheduling Framework for DSO/TSO Interface under Uncertainty. *IEEE Transactions on Smart Grid*, 8(5):2186–2197.

Shampine, L. F. and Gear, C. W. (1979). A User's View of Solving Stiff Ordinary Differential Equations. *SIAM Review*, 21(1).

Shekhar, R. C. and Manzie, C. (2015). Automatica Optimal move blocking strategies for model predictive control. *Automatica*, 61:27–34.

Short, J., Infield, D., and Freris, L. (2007). Stabilization of Grid Frequency Through Dynamic Demand Control. *IEEE Transactions on Power Systems*, 22(3):1284–1293.

Siemens (2011). High Voltage Direct Current Transmission - Proven Technology for Power Exchange. Technical report, Siemens AG, Germany.

Silva, J., Sumaili, J., Bessa, R. J., Seca, L., Matos, M. A., Miranda, V., Caujolle, M., Goncer, B., and Sebastian-Viana, M. (2018). Estimating the Active and Reactive Power Flexibility Area at the TSO-DSO Interface. *IEEE Transactions on Power Systems*, 33(5):4741–4750.

Simon, D. (2017). *Fighter Aircraft Maneuver Limiting Using MPC Theory and Application*. PhD thesis, Linköping University.

Sincovec, R. F., Erisman, A. M., Yip, E. L., and Epton, M. A. (1981). Analysis of Descriptor Systems Using Numerical Algorithms. *IEEE Transactions on Automatic Control*, 26(1):139–147.

Singh, K., Padhy, N. P., and Sharma, J. D. (2010). Social welfare maximization considering reactive power and congestion management in the deregulated environment. *Electric Power Components and Systems*, 38(1):50–71.

Stegink, T., Cherukuri, A., De Persis, C., Van der Schaft, A., and Cortes, J. (2018a). Hybrid interconnection of iterative bidding and power network dynamics for frequency regulation and optimal dispatch. *IEEE Transactions on Control of Network Systems, to be published*.

Stegink, T., Cherukuri, A., de Persis, C., van der Schaft, A., and Cortes, J. (2018b). Stable interconnection of continuous-time price-bidding mechanisms with power network dynamics. In *2018 Power Systems Computation Conference (PSCC)*, pages 1–6. Power Systems Computation Conference.

Stegink, T., De Persis, C., and Van Der Schaft, A. (2017). A Unifying Energy-Based Approach to Stability of Power Grids with Market Dynamics. *IEEE Transactions on Automatic Control*, 62(6):2612–2622.

Stock, D. S., Sala, F., Berizzi, A., and HOfmann, L. (2018). Optimal Control of Wind Farms for Coordinated TSO-DSO Reactive Power Management. *Energies*, 11(173).

Strang, G. and Moler, C. (2016). Learn differential equations: Up close with gilbert strang and cleve moler (lecture notes).

Swaminathan, B. P. (2018). *Operational Planning of Active Distribution Networks*. PhD thesis, University of Grenoble-Alps.

Swilling, M., Robinson, B., Marvin, S., Hodson, M., and Hajer, M. (2013). City-level decoupling: urban resource flows and the governance of infrastructure transitions. a report of the working group on cities of the international resource panel. *United Nations Environment Programme (UNEP)*.

Taha, A. F., Gatsis, N., Dong, B., Pipri, A., and Li, Z. (2019). Buildings-to-Grid Integration Framework. *IEEE Transactions on Smart Grid*, 10(2):1237–1249.

ter Haar, B. (2016). *MSc Thesis. Modeling and Optimization of USEF ' s Market Mechanisms*. University of Groningen.

Tesla (2018). Website support - tesla model s specifications.

Trip, S., Bürger, M., and De Persis, C. (2016). An internal model approach to (optimal) frequency regulation in power grids with time-varying voltages. *Automatica*, 64:240–253.

Tuohy, A., Kaun, B., and Entriken, R. (2014). Storage and demand-side options for integrating wind power. *Wiley Interdisciplinary Reviews: Energy and Environment*, 3(1):93–109.

Unicef (2012). The state of the world's children 2012: children in an urban world.

United Nations (2015). Un sustainable development goals. https://www.un.org/sustainabledevelopment/sustainable-development-goals/.

USEF (2015). *USEF: The Framework explained*. Universal Smart Energy Framework Foundation.

Van Den Bergh, K., Delarue, E., and D'haeseleer, W. (2014). DC power flow in unit commitment models. *TME Working Paper - Energy and Environment, KU Leuven Energy Institute*.

van der Werf, H. (2017). *MSc Thesis. A non-cooperative market model extension for USEF*. University of Groningen.

Vardakas, J. S., Zorba, N., Verikoukis, C. V., and Member, S. (2015). A Survey on Demand Response Programs in Smart Grids : Pricing Methods and Optimization Algorithms. *IEEE Communications Surveys & Tutorials*, 17(1):152–178.

Wan, Y., Milligan, M., and Kirby, B. (2007). Impact of Energy Imbalance Tariff on Wind Energy. *AWEA WindPower 2007 Conference Los*.

Wang, J., Liu, C., Ton, D., Zhou, Y., Kim, J., and Vyas, A. (2011). Impact of plug-in hybrid electric vehicles on power systems with demand response and wind power. *Energy Policy*, 39(7):4016–4021.

Wieringa, R. J. (2014). *Design science methodology for information systems and software engineering*. Springer, Heidelberg.

Yahiaoui, A., Hensen, J., and Paassen, D. V. (1996). Model Based Optimal Control for Integrated. *Building*, pages 6–7.

Zegers, A. and Brunner, H. (2014). TSO-DSO interaction : An Overview of current interaction between transmission and distribution system operators and an assessment of their cooperation in Smart Grids (Discussion Paper Annex 6, Task 5). *International Smart Grid Action Network (ISGAN)*.

Zhao, C., Mallada, E., and Dorfler, F. (2015). Distributed frequency control for stability and economic dispatch in power networks. *Proceedings of the American Control Conference*, 2015-July:2359–2364.

Zhu, J. (2009). *Optimization of Power System Operation*. John Wiley & Sons, Inc., Hoboken, New Jersey.

Zimmerman, R. D., Murillo-Sánchez, C. E., and Thomas, R. J. (2011). MATPOWER: Steady-state operations, planning, and analysis tools for power systems research and education. *IEEE Transactions on Power Systems*, 26(1):12–19.

Appendices

A Discretization of BtG Dynamics

In this appendix, a full derivation of the discretization of BtG dynamics is provided. Congruent with Taha et al. (2019) and Dong et al. (2018), we utilize a discretization based on Gear's method; a backward differentiation routine for stiff Differential-Algebraic system of Equations (DAE). First, we provide a general definition of Gear's method. Thereafter, we apply the method to discretize the continuous-time BtG dynamics described in Chapter 3.

A.1 Gear's discretization method for stiff problems

Consider a general DAE of the form

$$E\dot{y}(t) = Ay(t) + Bg(t), \quad y(t_0) = y_0, \tag{A.1}$$

with matrices $E, A \in \mathbb{R}^{n\times n}$ and $B \in \mathbb{R}^{k\times k}$. This problem is called *stiff* if no solution component is unstable, and at least one component is extremely stable (Shampine and Gear, 1979). If, for simplicity, we take $E = I_n$, this implies that A has no eigenvalues with positive real part, and at least one eigenvalue with very large negative part. Calculating numerical solutions to stiff problems involves very high computational effort, and can result in large round-off errors (Kwatny and Miu-Miller, 2016). In order to derive adequate solutions to stiff problems, very small integration step size is generally required (Strang and Moler, 2016). As most physical systems, including typical power network analyses, involve stiff problems (Sincovec et al., 1981), it is natural to consider these disadvantages.

Another way to deal with stiff problems of DAEs is the use of specialized integration methods. Gear (1971) proposed such a technique based on an implicit Euler method, which is generally referred to as *Gear's method* in this study. As discussed by Sincovec et al. (1981), the general form of Gear's method of order s for the system in Eq. (A.1) is given by

$$y_n = (E - h\beta_0 A)^{-1}\Big[\sum_{i=1}^{s} \alpha_i E y_{n-i} + h\beta_0 B g_n\Big], \tag{A.2}$$

where

$$\beta_0 = \Big(\sum_{i=1}^{s} \frac{1}{i}\Big)^{-1} \quad \text{and} \quad \alpha_i = (-1)^{i+1}\beta_0 \sum_{j=i}^{s} \frac{1}{j}\binom{j}{i}.$$

The order of convergence for the global error of Gear's method of order s with integration step size h is $\mathcal{O}(h^s)$ (Sincovec et al., 1981). Although higher order Gear's method can result in faster

convergence of the global error, it also increases the related computational effort. Similar to Taha et al. (2019), this study is limited to using 1st order Gear's method for all discretization purposes. Note that for 1st order, $s = 1$ and the parameters account to $\beta_0 = 1$ and $\alpha_1 = 1$, and the method itself reduces to an implicit Euler method.

A.2 Discretization of BtG dynamics

Similar to Taha et al. (2019), we utilize 1st order Gear's method Eq. (A.2) to discretize TSO, DSO, and building dynamics. Storage dynamics were initially proposed as discretized system, so no discretization is needed for this part of the framework.

According to the general DC power flow assumptions, we linearized the nonlinear part of the TSO swing equation in Eq. (3.5), yielding the following expression:

$$E_t \dot{x}_t(t) = A'_t x_t(t) + B_{\text{GR}} P_{\text{GR}}(t) - B\big(P_{\text{LD}}(t) + P_{\text{BL}}(t)\big), \tag{A.3}$$

where we introduced the auxiliary matrix A'_t to embed the linearization of $\Psi(\delta(t))$, which is defined as

$$A'_t = \begin{bmatrix} \mathbb{0}_{n_t \times n_t} & \mathrm{I}_{n_t} \\ -\Psi' & -D \end{bmatrix}. \tag{A.4}$$

Here, we introduced the weighted Laplacian matrix $\Psi' \in \mathbb{R}^{n_t \times n_t}$, with entries given by

$$\psi'_{k,j} = \begin{cases} \sum_{\substack{m=1 \\ m \neq j}}^{n_t} b_{km} & \text{if } k = j, \\ -b_{kj} & \text{if } k \neq j \text{ and } j \in \mathcal{T}_k^n, \\ 0 & \text{otherwise.} \end{cases} \tag{A.5}$$

Following the general Gear's method in Eq. (A.2), the discretization of A.3 is now written as follows:

$$\text{TSO} \begin{cases} x_t(t+h) & = f_t\big(x_t(t), P_{\text{GR}}(t+h), P_{\text{IMP}}(t+h), P_{\text{BL}}(t+h)\big) \\ & = \big(E_t - hA'_t\big)^{-1}\Big[E_t x_t(t) + h\big(B_{\text{GR}} P_{\text{GR}}(t+h) - B_t(P_{\text{LD}}(t+h) + P_{\text{BL}}(t+h))\big)\Big]. \end{cases} \tag{A.6}$$

By rewriting Eq. (A.6), we obtain the difference equation

$$E_t \frac{x_t(t+h) - x_t(t)}{h} = A'_t x(t) + B_{\text{GR}} P_{\text{GR}}(t+h) - B_t\big(P_{\text{LD}}(t+h) + P_{\text{BL}}(t+h)\big), \tag{A.7}$$

which is indeed the standard backward (implicit) Euler method, as stated before.

Similarly, the discrete form of the dynamics of DSO i in Eq. (3.11) are written as

$$\text{DSO}\begin{cases} x_d^i(t+h) & = f_d^i\big(x_d^i(t), P_{\text{IMP}}^i(t+h), P_{\text{BD}}^i(t+h), P_{\text{BL}}^i(t+h)\big) \\ & = \big(E_d^i - hA_d^{\prime i}\big)^{-1}\Big[E_d^i x_d^i(t) + hB_d^i\big(P_{\text{LD}}^i(t+h) - P_{\text{BD}}^i(t+h) - P_{\text{BL}}^i(t+h)\big)\Big], \end{cases} \tag{A.8}$$

with auxiliary matrix $A_d^{\prime i}$ and the corresponding Laplacian matrix $\Psi^{\prime i} \in \mathbb{R}^{n_d^i \times n_d^i}$ defined as follows:

$$A_d^i = \begin{bmatrix} \mathbb{0}_{n_d^i \times n_d^i} & \mathrm{I}_{n_d^i} \\ \mathbb{0}_{n_d^i \times n_d^i} & -D^i \end{bmatrix}, \qquad \psi_{k,j}^{i\prime} = \begin{cases} \sum_{\substack{m=1 \\ m \neq j}}^{n_t} b_{km}^i & \text{if } k = j, \\ -b_{kj}^i & \text{if } k \neq j \text{ and } j \in \mathcal{D}_k^{n,i}, \\ 0 & \text{otherwise.} \end{cases} \tag{A.9}$$

Finally, the discrete form of the building dynamics in Eq. (3.15) are written as

$$\text{BLD}\begin{cases} x_b(t+h) & = f_b\big(x_b(t), u_b(t), w_b(t)\big) \\ & = \big(I_{2n_b} - hA_b\big)^{-1}\Big[x_b(t) + h\big(B_{u_b}u_b(t+h) + B_{w_b}w_b(t+h)\big)\Big]. \end{cases} \tag{A.10}$$

In the discrete building dynamics, matrix E is simply the identity matrix, and is therefore replaced with I_{2n_b}.

B Stacked MPC implementation in MATLAB

In this appendix, the MATLAB implementation of the MPC procedures proposed in this study is discussed in more detail. In particular, a stacked MPC implementation is formulated, in order to improve computational performance in MATLAB. First, we describe the main algorithm applied to the iterative MPC formulation, which is in the same format as the MPC procedures in the main text of the thesis. Thereafter, a stacked alternative formulation of the problem is proposed, which eliminates the iterative nature of the original implementation.

Define h_{sim} as the prediction time resolution (sample time), k_{sim} as the number of control steps that are implemented after each optimization, and t_{end} as the end time of the simulation (generally set at 24 hours). Furthermore, $x(k)$ denotes the internal prediction state variable, whereas $\tilde{x}(m)$ is the real simulated state of the system. Finally, $N = T_p/h_{sim}$ is the number of optimization steps that are enclosed in the prediction horizon, and is calculated using the prediction horizon T_p.

The MPC formulations provided in the main text of the thesis are of iterative nature. That is, within one optimization iteration, the state of the system is predicted step by step till the MPC prediction horizon is reached. The main iterative MPC implementation is described in Algorithm 1. By defining $\mathbb{N}$ as the set of natural numbers, line 2 ensures that a new MPC iteration is started each multiplicate of $h_{sim}k_{sim}$. At each prediction iteration, the next state of the system is generally given by

$$x(k+1) = Ax(k) + Bu(k) + Cw(k), \tag{B.1}$$

Algorithm 1 Iterative MPC implementation

1: **for** $m = 1 : h_{sim} : t_{end}$ **do**
2: **if** $m - (\epsilon h_{sim} k_{sim}) = 1, \forall \epsilon \in \mathbb{N}$ **then**
3: $x(1) = \tilde{x}(m)$
4: **for** $k = 1 : N$ **do**
5: $x(k+1) = f\big(x(k), u(k), \delta(k) \cdots\big)$
6: $\underline{x} \leq x(k) \leq \overline{x}$
7: $\underline{u} \leq u(k) \leq \overline{x}$
8: **end for**
9: Minimize cost function $J = f\big(x, u, \cdots\big)$
10: Save optimal control decisions $u = u^*$
11: **end if**
12: $\tilde{x}(m+1) = f\big(x(m), u^*(k), w(k)\big)$
13: **end for**

where x is the state variable, u is the control variable, and w is an (uncertain) external input. The advantage of this structure is that is comprehensible, and that the system dynamics and constraints are easily implemented. However, the main drawback is that the $k = 1 : N$ for-loop requires high computational effort. Compiling the optimization problem causes the majority of computational complexity, rather than actually solving it (Lofberg, 2004). Hence, the computational effort can be reduced significantly if the state trajectory is calculated directly over the complete prediction horizon.

In order to improve computational performance, a stacked implementation of the MPC formulations developed in the main thesis is proposed. Instead of calculating the state trajectory iteratively, the trajectory is directly calculated over the complete prediction horizon. To this end, define the stacked state variable $X = [x(1), x(2), \ldots, x(N)]^T$, where N represents the prediction horizon (Löfberg, 2012). Similarly, define the stacked input vector U and stacked vector of uncertain inputs W. Following the approach of Jerez et al. (2011b), the stacked dynamics of the system in Eq. (B.1) are given by $X = A^* x_0 + B^* U + C^* W$, where the system matrices are defined as

$$A^* = \begin{bmatrix} A \\ A^2 \\ \vdots \\ A^N \end{bmatrix}, \quad B^* = \begin{bmatrix} B & & & \\ AB & B & & \\ \vdots & \ddots & \ddots & \\ A^{N-1}B & \cdots & AB & B \end{bmatrix}, \quad C^* = \begin{bmatrix} C & & & \\ AC & C & & \\ \vdots & \ddots & \ddots & \\ A^{N-1}C & \cdots & AC & C \end{bmatrix}.$$

The stacked MPC implementation is described in Algorithm 2. The new implementation eliminates the for-loop in the MPC predictions, which contributes to computational performance of the overall procedure. Although the system matrices are typically sparse, the stacked problem formulation can require big matrix definitions if the problem network is big, leading to significant memory requirements. For a problem with α states, β inputs, and γ external inputs, the dimensions of the system matrices are $A^* \in \mathbb{R}^{N\alpha \times \alpha}$, $B^* \in \mathbb{R}^{N\alpha \times N\beta}$, and $C^* \in \mathbb{R}^{N\alpha \times N\gamma}$, implying that the problem grows exponentially with the network size (Jerez et al., 2011a). However, as the new system matrices are only determined once in the problem definition, the stacked MPC exhibits much better computational performance than the iterative implementation.

Algorithm 2 Stacked MPC implementation

for $m = 1 : t_{end}/h_{sim}$ **do**
  if $m - (\epsilon h_{sim} k_{sim}) = 1, \forall \epsilon \in \mathbb{N}$ **then**
    $x_1 = \tilde{x}(m)$
    $X = A^* x_1 + B^* U + C^* \delta$
    $\underline{X} \leq X \leq \overline{X}$
    $\underline{U} \leq U \leq \overline{U}$
    Minimize cost function $J = f\big(x, u, \cdots\big)$
    Save optimal control decisions $u = u^*$
  end if
  $\tilde{x}(m+1) = f\big(x(m), u^*(k), w(k)\big)$
end for

C Simulation Study Parameters

This appendix provides a full list of parameters used in the dynamics and constraints of the simulation studies in the thesis. If appropriate, references for the adopted values are mentioned. Note that storage and sociological parameters are only relevant if the corresponding element is enabled in the simulation.

Table C.1: Simulation time parameters

Parameter	Value	Units	Description or source
T_{end}	24	h	End time of simulation
T_p	3600	s	MPC receding horizon time
h	300	s	Simulation time resolution
MVA_{base}	1	MW	Base MVA power unit

Table C.2: TSO network parameters

Parameter	Value	Units	Description
M	0.06	MWs^2	Inertia coefficient (Rodríguez et al., 2007)
D	4.50	MW s	Damping coefficient (Rodríguez et al., 2007)
$\hat{D}$	0.00	MW s	Frequency sensitive load
P_{BL}	0.01	MW	Base load
$P_{\text{GR}}^{\text{min}}$	0	MW	Minimum power generation
$P_{\text{GR}}^{\text{max}}$	100	MW	Maximum power generation
$P_{\text{GR}}^{\text{ramp,dw}}$	-1	MW	Maximum generator ramp down
$P_{\text{GR}}^{\text{ramp,up}}$	1	MW	Maximum generator ramp up

Table C.3: DSO network parameters

Parameter	Value	Units	Description
M^i	0.06	MW/s^2	Inertia coefficient, interface (Rodríguez et al., 2007)
D^i	4.50	MW s^{-1}	Damping coefficient, interface (Rodríguez et al., 2007)
$\hat{D}^i$	0.00	MW s^{-1}	Frequency sensitive load
P_{BL}^i	0.01	MW	Base load

Table C.4: Building parameters; mostly adopted from Taha et al. (2019)

Parameter	Value	Units	Description
R_1	5.8	$^\circ\mathrm{C}\,\mathrm{MW}^{-1}$	Outer wall resistance
R_2	11.6	$^\circ\mathrm{C}\,\mathrm{MW}^{-1}$	Inner wall resistance
R_{win}	655	$^\circ\mathrm{C}\,\mathrm{MW}^{-1}$	Window resistance
C_{zone}	21.1×10^3	$\mathrm{MJ}\,^\circ\mathrm{C}^{-1}$	Zone thermal capacity
C_{wall}	11.3×10^2	$\mathrm{MJ}\,^\circ\mathrm{C}^{-1}$	Wall thermal capacity
μ_{hvac}	3	*unitless*	HVAC coefficient of performance
$T^{\text{min}}_{\text{day}}$	21.5	$^\circ\mathrm{C}$	Minimum temperature during day
$T^{\text{max}}_{\text{day}}$	23.0	$^\circ\mathrm{C}$	Maximum temperature during day
$T^{\text{min}}_{\text{night}}$	21.5	$^\circ\mathrm{C}$	Minimum temperature during night
$T^{\text{max}}_{\text{night}}$	25.0	$^\circ\mathrm{C}$	Maximum temperature during night
$t^{\text{start}}_{\text{day}}$	8	h	Start time of day
$t^{\text{end}}_{\text{day}}$	20	h	End time of day
$P^{\text{min}}_{\text{hvac}}$	0	MW	Minimum HVAC power
$P^{\text{max}}_{\text{hvac}}$	1	MW	Maximum HVAC power
$P^{\text{ramp,dw}}_{\text{hvac}}$	-0.1	MW	Minimum HVAC ramp down
$P^{\text{ramp,up}}_{\text{hvac}}$	0.1	MW	Maximum HVAC ramp up

Table C.5: Storage parameters (in case storage is enabled)

Parameter	Value	Units	Description
x^{min}_s	0.5	MW	Minimum buffer level
x^{max}_s	100	MW	Maximum buffer level
$P^{\text{min}}_{\text{stor}}$	-0.5	MW	Minimum storage rate
$P^{\text{max}}_{\text{stor}}$	0.5	MW	Maximum storage rate
ζ	1	*unitless*	State efficiency parameter
η	1	*unitless*	Input efficiency parameter

Table C.6: Sociological parameters (in case social dynamics are enabled)

Parameter	Value	Units	Description
c_h	0.8	*unitless*	State efficiency parameter
τ	1	*unitless*	Operating model weight
σ	30	*unitless*	Market model weight